AGU ADVANCING EARTH AND SPACE SCIENCES

Reviews of Geophysics

REVIEW ARTICLE
10.1029/2023RG000832

Age of Stratospheric Air: Progress on Processes, Observations, and Long-Term Trends

H. Garny[1], F. Ploeger[2,3], M. Abalos[4], H. Bönisch[5], A. E. Castillo[6], T. von Clarmann[5], M. Diallo[2], A. Engel[7], J. C. Laube[2], M. Linz[6], J. L. Neu[8], A. Podglajen[9], E. Ray[10,11], L. Rivoire[6,12], L. N. Saunders[13], G. Stiller[5], F. Voet[2,3], T. Wagenhäuser[7], and K. A. Walker[13]

[1]Institut für Physik der Atmosphäre, Deutsches Zentrum für Luft und Raumfahrt (DLR), Oberpfaffenhofen, Germany, [2]Institute for Energy and Climate Research: Stratosphere (IEK-7), Forschungszentrum Jülich, Jülich, Germany, [3]Institute for Atmospheric and Environmental Research, University of Wuppertal, Wuppertal, Germany, [4]Earth Physics and Astrophysics Department, Universidad Complutense de Madrid, Madrid, Spain, [5]Karlsruhe Institute of Technology, Institute of Meteorology and Climate Research - Atmospheric Trace Gases and Remote Sensing (IMK-ASF), Karlsruhe, Germany, [6]Department of Earth and Planetary Sciences, School of Engineering and Applied Sciences, Harvard University, Cambridge, MA, USA, [7]Goethe-Universität Frankfurt am Main, Frankfurt am Main, Germany, [8]Jet Propulsion Laboratory (JPL), California Institute of Technology, Pasadena, CA, USA, [9]Laboratoire de Météorologie Dynamique/IPSL, Ecole Polytechnique, Institut Polytechnique de Paris, ENS-PSL, CNRS, Paris, France, [10]Cooperative Institute for Research in Environmental Sciences, University of Colorado Boulder, Boulder, CO, USA, [11]Chemical Sciences Division, Earth Systems Research Laboratory, NOAA, Boulder, CO, USA, [12]Department of Earth, Atmospheric, and Planetary Sciences, Massachusetts Institute of Technology, Cambridge, MA, USA, [13]Department of Physics, University of Toronto, Toronto, ON, Canada

Abstract Age of stratospheric air is a well established metric for the stratospheric transport circulation. Rooted in a robust theoretical framework, this approach offers the benefit of being deducible from observations of trace gases. Given potential climate-induced changes, observational constraints on stratospheric circulation are crucial. In the past two decades, scientific progress has been made in three main areas: (a) Enhanced process understanding and the development of process diagnostics led to better quantification of individual transport processes from observations and to a better understanding of model deficits. (b) The global age of air climatology is now well constrained by observations thanks to improved quality and quantity of data, including global satellite data, and through improved and consistent age calculation methods. (c) It is well established and understood that global models predict a decrease in age, that is, an accelerating stratospheric circulation, in response to forcing by greenhouse gases and ozone depleting substances. Observational records now confirm long-term forced trends in mean age in the lower stratosphere. However, in the mid-stratosphere, uncertainties in observational records are too large to confirm or disprove the model predictions. Continuous monitoring of stratospheric trace gases and further improved methods to derive age from those tracers will be crucial to better constrain variability and long-term trends from observations. Future work on mean age as a metric for stratospheric transport will be important due to its potential to enhance the understanding of stratospheric composition changes, address climate model biases, and assess the impacts of proposed climate geoengineering methods.

Plain Language Summary Transport strongly influences the composition of the stratosphere, the layer at around 10–50 km altitude. Air masses are transported upward into the stratosphere in the tropics, and get distributed globally by a hemisphere-wide overturning circulation. Stratospheric age of air is a measure of the transport times along this circulation. This metric is a crucial measure of the circulation strength, deducible from observations of certain stratospheric gases. Over the past two decades, scientific progress has been made in three main areas. First, we now understand better which processes influence transport times. Second, we have good knowledge on the global average distribution of age of air, thanks to more observational data and improved methods to deduce this metric. Third, a large focus has been on climate-change related trends in age of air. While it is well established and understood that global models predict an accelerating stratospheric circulation, the related decrease in age of air can only be confirmed observationally in the lower stratosphere. Continuous monitoring of stratospheric trace gases will be crucial to constrain circulation trends throughout the stratosphere. This is essential for understanding climate change effects, improving climate models, and assessing potential climate intervention strategies.

Key Points:

- Understanding of how individual processes impact stratospheric age of air has been improved through development of dedicated diagnostics
- The global age of air climatology is now well constrained by observations thanks to improved data records and age calculation methods
- Observed age trends confirm lower stratospheric model predictions but are too uncertain to confirm or dismiss middle stratospheric trends

Supporting Information:

Supporting Information may be found in the online version of this article.

Correspondence to:

H. Garny,
hella.garny@dlr.de

Citation:

Garny, H., Ploeger, F., Abalos, M., Bönisch, H., Castillo, A. E., von Clarmann, T., et al. (2024). Age of stratospheric air: Progress on processes, observations, and long-term trends. *Reviews of Geophysics*, *62*, e2023RG000832. https://doi.org/10.1029/2023RG000832

Received 28 JAN 2024
Accepted 11 SEP 2024

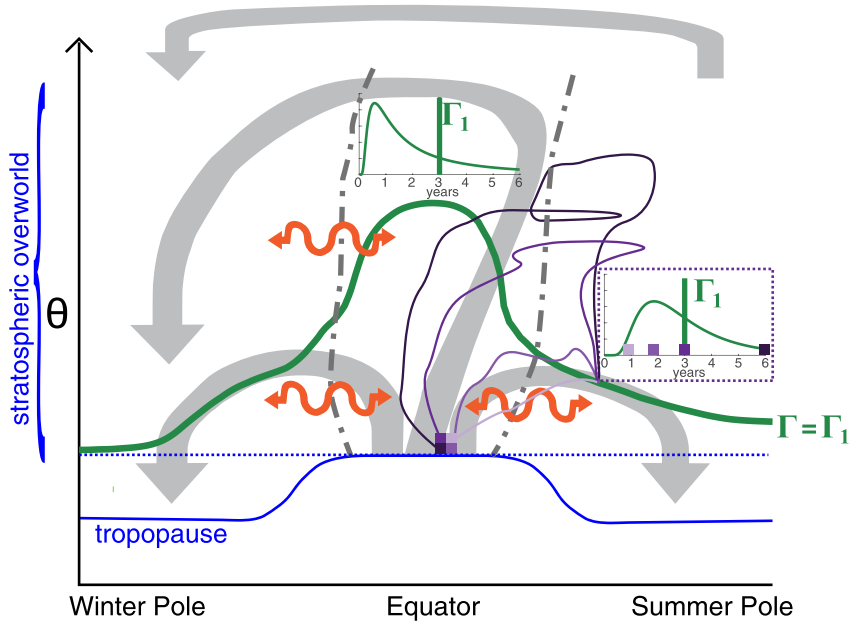

Figure 1. Schematic of the stratospheric circulation and age of air. The schematic displays the stratospheric circulation processes at solstice as a function of latitude and height (here with potential temperature as vertical coordinate): the mean stratospheric overturning circulation (diabatic circulation in isentropic coordinates) is shown as thick gray arrows, including also the global mesospheric circulation (thin gray arrow). The dash-dotted gray lines indicate the edges of the tropical pipe (lines of zero diabatic velocity), with squiggly orange arrows indicating adiabatic mixing across these edges. The tropopause is shown as solid blue line, and the "stratospheric overworld" is indicated to lie above the isentrope intersecting the tropical tropopause in dashed blue. A contour of constant mean age is shown as thick green line. The inset panels show examples for tropical and mid-latitude age spectrum, which poses different shapes despite having the same mean age. In purple, four trajectories are traced from their entry at the tropical tropopause to the location in the mid-latitudes whose age spectrum is shown in the right inset panel (shortest trajectory in lightest purple, longest trajectory in darkest purple).

1. Introduction

While merely around 10% of the atmospheric mass is situated above the tropopause, the composition of the stratosphere, spanning from approximately 10–50 km, significantly influences the global climate system through its chemical and radiatively active trace gas species. Variations in the stratospheric content of water vapor (Solomon et al., 2010), ozone (Forster & Shine, 1997), aerosol (Solomon et al., 2011; Vernier et al., 2011) and other trace gases (e.g., Prather et al., 2023) can substantially alter the global radiation budget and cause climate feedbacks (e.g., Banerjee et al., 2019; Charlesworth et al., 2023). In global climate models, small uncertainties in simulated stratospheric trace gas distributions can imply significant radiative effects (Riese et al., 2012). Hence, understanding of the relevant processes that control stratospheric composition is crucial to comprehend and model the coupled climate system and future changes therein.

A key factor controlling the chemical composition of the stratosphere is the stratospheric overturning circulation, the Brewer-Dobson circulation (Brewer, 1949; Butchart, 2014; Holton et al., 1995). Brewer (1949) had postulated the existence of such a circulation to explain measured distributions of water vapor. However, it was not until a few decades later that the stratospheric transport circulation had been fully recognized and understood. Today, the common conceptual picture of the Brewer-Dobson circulation (BDC) consists of global-scale circulation cells in each hemisphere with slow upward motion (upwelling) in the tropics, poleward flow, and downwelling in the extratropics (Figure 1, gray arrows). This overturning circulation is driven primarily by momentum deposition through the breaking and dissipation of planetary-scale waves (Haynes et al., 1991). The wave breaking also leads to strong horizontal stirring and subsequent mixing of air masses (in the following referred to as (two-way) "eddy mixing"), which causes no net mass transport but influences transport of trace constituents in the stratosphere (Figure 1, red wiggly arrows). The combined effect of slow overturning and eddy mixing shapes the distribution of stratospheric trace gases. For example, the stratospheric ozone column (i.e., vertically integrated concentrations) maximizes in the extratropics despite strongest chemical production in the tropics. This can be understood

from the poleward and downward transport of air masses by the stratospheric transport circulation (here used interchangeably with BDC).

A common way to diagnose the strength of the overall transport circulation in the stratosphere is by the mean transport time from a reference surface, typically taken to be the tropical tropopause, to any given point in the stratosphere (Hall & Plumb, 1994; Waugh & Hall, 2002). Those mean transport times are referred to as the mean age of stratospheric air. This diagnostic of the strength of the BDC has a number of advantages, as will be elaborated in the following: (a) Age of air measures the full transport circulation as experienced by stratospheric trace gases, incorporating all processes, and is as such relevant to interpret observed tracer concentrations and their changes over location or time. (b) Age of air can be directly derived from observables, namely measurements of specific trace gases. This is opposed to the velocities of the slow overturning circulation, which are on the order of millimeters per second, and thus cannot be directly observed. (c) Age of air is based on a solid theoretical framework, with a general mathematical description of transport that has been developed and applied for various systems (e.g., the ocean).

In the overall conceptual picture of stratospheric transport, as depicted in Figure 1, the regions of upwelling in the tropics and of downwelling in the extratropics are separated from the tropics by a transport barrier (gray dash-dotted line in Figure 1). The wintertime extratropics are well mixed due to strong wave breaking, termed "surf zone" region (McIntyre & Palmer, 1984). The subtropical transport barrier is associated with the zero westerly wind line, equatorward of which planetary-scale waves cannot propagate. The region of suppressed mixing within the subtropical transport barriers is known as the "tropical pipe" (Neu & Plumb, 1999). The relatively well separated regions of upwelling and downwelling lead to relatively young air masses in the tropics, with a steep gradient toward older air masses in the extratropics, as depicted by a typical age contour line in Figure 1 (green line). A certain air volume on this age contour is, however, not characterized by a single time scale, but by a distribution of transit times, called the "age spectrum." One can envision the air volume to consist of individual fluid elements (Schoeberl et al., 2000) that have traveled different pathways through the atmosphere (depicted as purple trajectories in Figure 1), making up the age spectrum. The "mean age of air" at a given location in space and time then represents the average of the age spectrum. Age spectra in the tropics and extratropics typically differ even if corresponding to the same mean age value (Figure 1, which illustrates the different nature of transport to those locations). This emphasizes that age is an integrated measure of all different transport processes like the overturning (residual) circulation advection, eddy-mixing and turbulent diffusion. Hence, age is a measure of the net transport circulation.

In the lowermost stratosphere, below about 380 K potential temperature (see dashed blue line in Figure 1), tracers are strongly influenced by mixing across the extratropical tropopause, in addition to transport via the BDC from the deep stratosphere (e.g., Bönisch et al., 2009; Hauck et al., 2020). This somewhat complicates the concept of age of air in this region due to the multiple entry points, and in this review we mostly focus our attention to levels above the lowermost stratosphere, which is often referred to as the "stratospheric overworld" (Holton et al., 1995, see Figure 1).

Application of age of air as a diagnostic for the stratospheric circulation has a history of several decades. In an early attempt to estimate stratospheric age of air, Kida (1983) calculated the age spectrum from the motion of a large number of Lagrangian air parcels to investigate transport by the Brewer-Dobson circulation. Subsequent work has deduced age of air as lag time between stratospheric and tropospheric mixing ratios for trace gas species with systematically increasing tropospheric concentrations (Bischof et al., 1985; Schmidt et al., 1991). However, ambiguities in these calculations have been pointed out related to seasonal and interannual fluctuations in tropospheric concentrations (Hall & Prather, 1993). In a seminal paper, Hall and Plumb (1994) solved these issues and presented a precise mathematical theory relating age of air to the boundary propagator (Green's function) of the transport operator. This theory made it clear that equality between mean age and tracer lag time exists only for species with linearly increasing concentrations in the troposphere. For deducing mean age from other species, information on the age spectrum needs to be included. Soon thereafter, a rigorous calculation of mean age from a trace gas with a quadratic tropospheric increase was carried out by Volk et al. (1997), and since then numerous studies have used this method to derive mean age of air from stratospheric trace gas measurements, such as CO_2 and SF_6.

Age of air derived from observations as well as diagnosed in global models has proven valuable in understanding and quantifying the stratospheric transport circulation in many ways. Comparisons between observed and

modeled age of air are used to evaluate the ability of global models to simulate stratospheric transport (e.g., Abalos et al., 2021; Dietmüller et al., 2018; Waugh & Hall, 2002). Understanding the past evolution of the stratospheric ozone layer and assessment of the expected progress of its recovery hinges on knowledge of how ozone depleting substances (ODS) are transported from the troposphere to the stratosphere. Estimation of the ozone-depletion potential of halocarbons (e.g., Engel et al., 2018; Newman et al., 2007), largely relies on calculating fractional release factors which include information on the amount of a halocarbon that is released to its inorganic form, that is, the species that are directly involved in catalytic ozone destruction cycles. These calculations, in turn, relate the measured stratospheric mixing ratio to the air parcel's tropospheric mixing ratio lagged by the stratospheric age.

Age of air has gained particular attention as a circulation measure in view of potential long-term trends in the stratospheric circulation (e.g., Waugh, 2009). Answering the question whether the stratospheric circulation is increasing in a future climate is highly relevant when assessing and projecting impacts of climate change. Models predict an acceleration of the stratospheric circulation in response to rising greenhouse gases (GHG) (Butchart, 2014), with impacts on the transport of stratospheric ozone to Earth's surface (Hegglin & Shepherd, 2009) and on the distribution, and thus radiative forcing, of ozone and water vapor. The fact that age can be derived from tracer observations provides one of the few ways to verify this model prediction. To date, observationally-based age records confirm model simulated age trends only in the lower stratosphere (Ray et al., 2014), while in the middle stratosphere past studies suggested a discrepancy between models and observations (Engel et al., 2009, 2017). This has been the motivation for many studies over the past years to better understand the processes leading to age of air changes, as well as uncertainties in deriving age of air from observations.

As age is based on a general mathematical framework it can be applied also to other geophysical circulations beyond the stratosphere. Recently, age theory has been applied to estimate tropospheric transport time scales from the surface to the tropopause and lowest stratosphere (Luo et al., 2018; Ray et al., 2022). In this regard, age can be applied as a diagnostic for rapid convective transport, but needs to take into account regional aspects of the reference surface (e.g., Holzer & Hall, 2008; Orbe et al., 2013). Also for ocean circulation the age theory is frequently applied to investigate transport time scales (e.g., Haine & Hall, 2002). In this case the ocean or water age is defined based on when the water was last in contact with the surface ocean, and in the ocean interior it is significantly higher (decades to centuries or even millennia) compared to stratospheric age of air which usually ranges from months to years.

More than two decades have passed since the publication of the last review article on age of stratospheric air by Waugh and Hall (2002), and numerous research activities have been undertaken and led to new results and insights into stratospheric transport and age. Therefore, we consider it to be the right time for a new, updated age of air review paper. First, research on the question whether the stratospheric circulation is changing with increasing GHG has substantially enhanced our knowledge of the stratospheric circulation and stratospheric age of air. Nevertheless, the key question whether there is a significant circulation trend remains unanswered, and here we provide a new age trend assessment based on a synthesis of most recent results. Second, new age-based diagnostics which are dedicated to disentangling the effect of different processes, like the residual circulation, eddy mixing, or vertical mixing have been developed over recent years. Third, satellite trace gas observations have become available which allow the deduction of global age of air distributions from measurements. Also, new in situ observation capabilities have been set-up enabling local estimates of stratospheric age with high precision. In particular in view of these new observational capabilities it appears critical to consolidate on a method of how to calculate stratospheric age of air from observations which identifies and reduces the uncertainties inherent in these calculations. Such a "consolidated recipe" to calculate stratospheric age from realistic, measurable trace gas species, including all current knowledge of related methodological uncertainties, is provided in this review article.

The structure of this review article is as follows. First, Section 2 provides the theoretical background with special emphasis on the aspects relevant to calculate age from observations and in models. Thereafter, Section 3 discusses the relation between age and various transport processes, first within an idealized model framework and then based on global age distributions, and reviews recently developed age-based diagnostics for particular transport processes. Section 4 presents an overview of available measurements for stratospheric age calculation, both based on satellite and in situ balloon and aircraft data. This section also provides a review on how age has been deduced from tracer observations, including the consolidated recipe for age calculation we suggest here. In Section 5, we review how most recent model simulations represent age, both compared to each other and compared to

observations. Section 6 reviews our knowledge on variability and trends in age, and provides a synthesis of most recent findings on this subject leading to a new assessment of stratospheric age trends. Finally, Section 7 points out the main conclusions from this review and summarizes our subjective view of most urgent open issues regarding stratospheric age.

2. Theory of Age of Air in Geophysical Fluids

Transit time is frequently used as a diagnostic of circulation, both for the circulation in the ocean and in the stratosphere. In the stratosphere, the transit time of air to a given location has been termed the "age of stratospheric air" (in the following the "stratospheric" is dropped in many instances for brevity). In the following we review the general theory of age of air, with a special focus on those aspects relevant for the calculation of age of air from realistic, measurable tracers, which will be later introduced in Section 4.

2.1. The Transit Time Distribution or Age Spectrum

Without the existence of atmospheric mixing processes (including molecular diffusion), an air parcel would remain intact during its travel through the stratosphere and would be characterized by a single transit time and constant composition (for a chemically passive gas). However, as mixing processes on a wide range of different scales, eventually cascading down to molecular diffusion, are present in the real atmosphere, such an air parcel will undergo changes in its composition on the way through mixing with other air parcels. Thus, it can be considered as a mixture of "fluid elements," which traveled different paths for different durations to end at the same time t and location $\mathbf{x}$ (see Figure 1). The statistical distribution of the transit times of these fluid elements (often termed "irreducible," e.g., Schoeberl et al., 2000) making up a given air parcel is termed its *age spectrum*. Mathematically, this description was formalized by Hall and Plumb (1994) based on the transport equation of a conserved and passive tracer, that is,

$$\frac{\partial \chi}{\partial t} + \mathcal{L}(\chi) = 0. \tag{1}$$

Here, χ is the tracer mixing ratio and $\mathcal{L}$ the transport operator, which is assumed to be linear for the trace gas species under consideration. As for many fluid-dynamical application, in the case of stratospheric tracer transport, $\mathcal{L}$ may be represented as an advection-diffusion operator (e.g., Holzer & Hall, 2000). Since the operator $\mathcal{L}$ is linear, the general solution to Equation 1 subject to a time-varying homogeneous boundary condition χ_0 on a given reference surface S_0 can be expressed using a form of Green's function $\mathcal{G}(\mathbf{x},t;S_0,t')$, which depends on both the given stratospheric sampling location $\mathbf{x}$ and the reference source surface S_0, as well as the time t and source time t'. The Green's function can be re-written as a function of transit time or age $\tau = t - t'$ instead of source time, $G(\mathbf{x},t;S_0,\tau) = \mathcal{G}(\mathbf{x},t;S_0,t')$, such that the general solution to Equation 1 is given by

$$\chi(\mathbf{x},t) = \int_0^t \chi_0(t')\,\mathcal{G}(\mathbf{x},t;S_0,t')\,\mathrm{d}t' = \int_0^t \chi_0(t-\tau)G(\mathbf{x},t;S_0,\tau)\,\mathrm{d}\tau. \tag{2}$$

Specifically, $\mathcal{G}(\mathbf{x},t;S_0,t_0)$ is the solution to Equation 1 satisfying the boundary condition $\chi_0(t) = \delta(t-t_0)$ and initial condition $\chi(\mathbf{x},0) = 0$. Because it effectively propagates the boundary condition through the whole domain, $\mathcal{G}$ is sometimes referred to as the *boundary propagator* (for a rigorous presentation, see Holzer & Hall, 2000). When written in terms of transit time, $G(\mathbf{x},t;S_0,\tau)$ is termed the "age spectrum" of stratospheric air (e.g., Hall & Plumb, 1994). In the more general case of inhomogeneous boundary conditions, the general solution (Equation 1) includes a spatially dependent boundary propagator integrated over the boundary surface (e.g., Holzer & Hall, 2000).

As G represents a distribution of transit times, the choice of the reference surface S_0 is of particular importance. In general, S_0 can be chosen as any surface where the flow enters the domain, but usual choices are the tropical tropopause or the tropical or global surface. If the Earth's surface is chosen as reference, the transit time also includes the time scale of tropospheric transport which, however, can usually be assumed to be much smaller (days to weeks) than the stratospheric transport time scale (months to years). The only necessary condition for the reference surface is that the considered trace gas mixing ratio is homogeneous on that surface (but allowed to be time-varying), so that it can be written as $\chi_0(t')$ in Equation 2. For most trace gases, the tropical tropopause

fulfills this condition, because the troposphere is well-mixed, and can be considered as "single entry point" into the stratospheric overworld (above about 380 K, see Figure 1). In the lowermost stratosphere, however, this single entry point assumption generally does not hold as a substantial amount of air originates from the extratropical tropopause where the tracer entry mixing ratio differs (e.g., Hauck et al., 2020, and discussion in Section 4).

Assuming a sufficiently long time passed since starting to release a tracer with a constant boundary condition ($\chi_0 = 1$) at the reference surface, this constant mixing ratio propagates to the whole domain ($\chi(\mathbf{x},t) = 1$). In this limit ($t \to \infty$), Equation 2 leads to the normalization condition of the age spectrum:

$$\int_0^{+\infty} G(\mathbf{x},t;\tau)\mathrm{d}\tau = 1. \tag{3}$$

Here and in the following, we have dropped the reference to the source surface for compactness. The normalization to unity reflects the property of the age spectrum to be the probability distribution of transit times for an air parcel.

2.2. Mean Age of Air

Of particular interest for investigations of stratospheric transport is the first moment of the transit time distribution G, which is termed the *mean age* Γ and is defined as

$$\Gamma(\mathbf{x},t) = \int_0^{\infty} \tau\, G(\mathbf{x},t;\tau)\mathrm{d}\tau. \tag{4}$$

For a tracer whose mixing ratio is linearly growing at the boundary according to $\chi_0 = a\ t$ (where a is the constant growth rate), mean age can be calculated without knowledge of the age spectrum, as in this case Equation 2 reduces to the simple relation

$$\chi(\mathbf{x},t) = \chi_0(t - \Gamma(\mathbf{x},t)) = a\ (t - \Gamma(\mathbf{x},t)) \tag{5}$$

Hence, for such a particular tracer the mean age is nothing but the lag time between the given stratospheric mixing ratio and the occurrence of that mixing ratio in the tropospheric reference time series. Note that this relation is valid for any age spectrum but only for a tracer linearly increasing at S_0, although useful approximations exist for periodic and exponentially growing tracers (Hall & Plumb, 1994).

It is also illustrative to consider the transport equation Equation 1 in the absence of mixing. In this case, Equation 1 is solvable along Lagrangian trajectories (the characteristics of the equation), and $\mathcal{G}(\mathbf{x},t;t') = \delta(t' - \Gamma(\mathbf{x},t))$ and $\chi(\mathbf{x},t) = \chi_0(t - \Gamma(\mathbf{x},t))$. Hence, in this case, the mean age $\Gamma(\mathbf{x},t)$ corresponds to the actual, unique transit time from the boundary to $(\mathbf{x},t)$.

By construction, mean age has a number of specific properties which make it especially appealing to characterize transport. Considering the transport equation for a linearly increasing tracer, hence inserting Equation 5 into Equation 1 shows that this definition is mathematically equivalent to that of the "ideal age," that is a tracer with source of one unit per unit time in the interior of the domain, whose evolution is governed by

$$\frac{\partial \Gamma}{\partial t} + \mathcal{L}(\Gamma) = 1, \tag{6}$$

with $\Gamma = 0$ at the boundary S_0 (Neu & Plumb, 1999). As $\mathcal{L}$ includes all transport processes (i.e., advection, mixing, diffusion), mean age measures the full transport circulation as seen by a tracer and is as such a useful measure of the net transport circulation.

2.3. Moments of the Age Spectrum

It is instructive to consider also higher-order moments $\mathcal{M}_n$ of the age spectrum, which can be defined similarly to the definition of mean age Γ as

$$\mathcal{M}_n(\mathbf{x},t) = \int_0^{+\infty} \tau^n G(\mathbf{x},t;\tau)\mathrm{d}\tau. \tag{7}$$

These higher-order moments can be related to tracers with a boundary condition evolving as a polynomial function of time t and of order N, given by $\chi_0(t-\tau) = \chi_0(t) + \sum_{n=1}^{N} \alpha_n \tau^n$, where the α_n are the coefficients of the polynomial. Inserting this boundary mixing ratio timeseries into Equation 2 yields

$$\chi(\mathbf{x},t) - \chi_0(t) = \sum_{n=1}^{N} \alpha_n \mathcal{M}_n(\mathbf{x},t). \tag{8}$$

A particular case of such tracers with polynomial boundary condition are linearly increasing tracers, where $N = 1$, $\alpha_1 < 0$, and $\chi_0(t-\tau) = \chi_0(t) + \alpha_1 \tau$.

The second order moment of the age spectrum is of particular interest as it is used to define the width Δ of the spectrum

$$\Delta^2(\mathbf{x},t) = \frac{1}{2}\int_0^{+\infty} (\tau - \Gamma(\mathbf{x},t))^2 G(\mathbf{x},t,\tau)\mathrm{d}\tau = \frac{\mathcal{M}_2(\mathbf{x},t) - \Gamma(\mathbf{x},t)^2}{2}. \tag{9}$$

A related parameter that is frequently used to parameterize stratospheric age of air spectra is the *ratio of moments*, which is defined as the ratio of spectrum width squared and mean age $\frac{\Delta^2}{\Gamma}$.

It should be stressed that moments of the age spectrum are very sensitive to aged air, that is, the tail of the age spectrum. This statement is already valid for mean age and holds even more so for higher-order moments. From theoretical considerations of the linear transport operator presented in Prather (1996) and Ehhalt et al. (2007), and from model studies (e.g., Diallo et al., 2012; Ploeger & Birner, 2016; Scheele et al., 2005), it may be argued that the decay of the tail of the age spectrum may be approximated as an exponential function of transit time ($G(\mathbf{x},t,\tau) \simeq A(\mathbf{x},t)\exp(-\lambda(\mathbf{x},t)\tau)$. The contribution of the tail to the age spectrum moment of order n, denoted $\delta\mathcal{M}_n$, can be readily estimated in the case of an exponential tail as

$$\delta\mathcal{M}_n(\mathbf{x},t) = \int_{\tau_{\max}}^{+\infty} \tau^n A(\mathbf{x},t)\exp(-\lambda(\mathbf{x},t)\tau)\ \mathrm{d}\tau, \tag{10}$$

and the expression is nothing but the incomplete gamma function of order $n + 1$.

2.4. Insights From Conceptual Models of Stratospheric Transport

To gain understanding on the stratospheric transit time distribution and its sensitivity to processes, it is enlightening to consider idealized models of stratospheric transport (Waugh & Hall, 2002). As a simplified model of stratospheric transport, the global diffusor model has been introduced by Plumb and Ko (1992). This model assumes very rapid horizontal mixing compared to the much slower overturning circulation, such that mean transport in this model reduces to a 1D-diffusion equation

$$\frac{\partial\chi}{\partial t} + \frac{\kappa}{\rho}\frac{\partial}{\partial z}\left(\rho\frac{\partial\chi}{\partial z}\right) = 0 \tag{11}$$

with H the density scale height $\left(\rho = \rho_0 \exp\left(-\frac{z}{H}\right)\right)$. Strictly, the vertical coordinate in the global diffusor model is the reference height of isopleths of a long-lived tracer.

Assuming a constant diffusivity κ, the analytical solution to the transit time distribution (Hall & Plumb, 1994) in this model corresponds to the Wald, or inverse Gaussian function

$$G(\tau) = \sqrt{\frac{\Gamma^3}{4\pi\Delta^2\tau^3}}\exp\left(-\frac{\Gamma(\tau-\Gamma)^2}{4\Delta^2\tau}\right), \tag{12}$$

which is completely parameterized by its first two moments (mean age and width). The mean age Γ follows from using this explicit form of the age spectrum in Equation 4 and is given by $\Gamma = \frac{H}{\kappa}z$, and similarly the age spectrum width by $\Delta = \frac{\sqrt{H^3 z}}{\kappa}$. Consequently, the ratio of moments is given by $\frac{\Delta^2}{\Gamma} = \frac{H^2}{\kappa}$. Note that the ratio of moments in that model is independent of z.

The canonical form of the transit time distribution as an inverse Gaussian function, as given in Equation 12, is frequently used as a first guess for stratospheric age spectra. Using a single age spectrum of this shape for stratospheric transport inherently assumes a single entry point for transport into the stratosphere. As discussed above, in the lowermost stratosphere this assumption does not hold and additional adjustments are necessary (see also Section 4).

The global diffusor model only provides an imperfect conceptual picture of stratospheric transport. In particular, it does not account for mixing barriers at the edge of the polar vortex and the subtropics. Another conceptual picture that does account for mixing barriers is the tropical pipe model (Plumb, 1996), which represents stratospheric transport with three coupled vertical profiles corresponding to the isolated tropics and the horizontally well-mixed extratropical surf-zones. However, it was soon acknowledged that while the tropics are relatively well isolated, horizontal mixing between the tropical upwelling region and the extratropics is crucial for a more complete conceptual picture of stratospheric transport, leading to the formulation of the tropical *leaky* pipe (TLP) model (Neu & Plumb, 1999). The TLP model will be used later in Section 3.1 to illustrate the sensitivity of age of air with respect to different transport processes.

3. Transport Processes and Diagnostics

Stratospheric age of air is affected by the interplay of a variety of different transport processes (e.g., residual circulation transport, eddy, and turbulent mixing; see Figure 1) and integrates the effects of these processes along the air parcel's pathway. In general, it is not straightforward to interpret a given age of air change in terms of either residual circulation or mixing changes. First, mean age is a non-local and non-instantaneous measure of circulation, essentially integrating the transport processes in space and time. Second, dynamical processes driving residual circulation and eddy mixing can be tightly related (e.g., breaking of atmospheric waves), so that their relative effect on mean age is not immediately clear. Conceptual models can be used to gain understanding on the role of different processes for mean age and the age spectrum, as will be demonstrated in the next Section 3.1. To quantify the role of different transport processes for age of air and its changes from global comprehensive model or observational data, sophisticated diagnostics have been developed based on theoretical understanding, as will be reviewed in Section 3.2.

3.1. Insights on Effects of Different Processes on Age of Air From a Conceptual Model

The TLP model represents stratospheric transport with three coupled vertical profiles corresponding to the relatively isolated tropics and the horizontally well-mixed extratropical surf-zones of each hemisphere (see Text S4 in Supporting Information S1 for equations and details). This conceptual model includes mean advection, vertical diffusion in each of the three columns and horizontal mixing between the tropics and extratropics. Analytical and numerical solutions for the age spectrum and mean age in idealized TLP model settings with constant vertical velocities have been presented in Neu and Plumb (1999) and Hall (2000) and highlight the role of different transport processes. First considering only the advective part of the circulation, the tropical pipe age spectrum is characterized by a pronounced mode responding to the bulk advection with tropical upwelling velocity. The mid-latitude column naturally exhibits a long tail resulting from the downwelling of air detrained from the tropics at different levels. Including the mixing term between the tropics and extratropics generates recirculation loops and tends to introduce a tail in the tropical spectrum and to increase the tail in the mid-latitude spectrum. The TLP model allows independent variation of residual circulation upwelling and eddy mixing, and thus is ideally suited to demonstrate how different processes affect mean age and the age spectrum, as will be described in the following.

3.1.1. Mean Age

A set of idealized TLP model simulations demonstrate the sensitivity of residual circulation, eddy mixing and vertical diffusion on mean age. The TLP model equations were solved with particle trajectories and

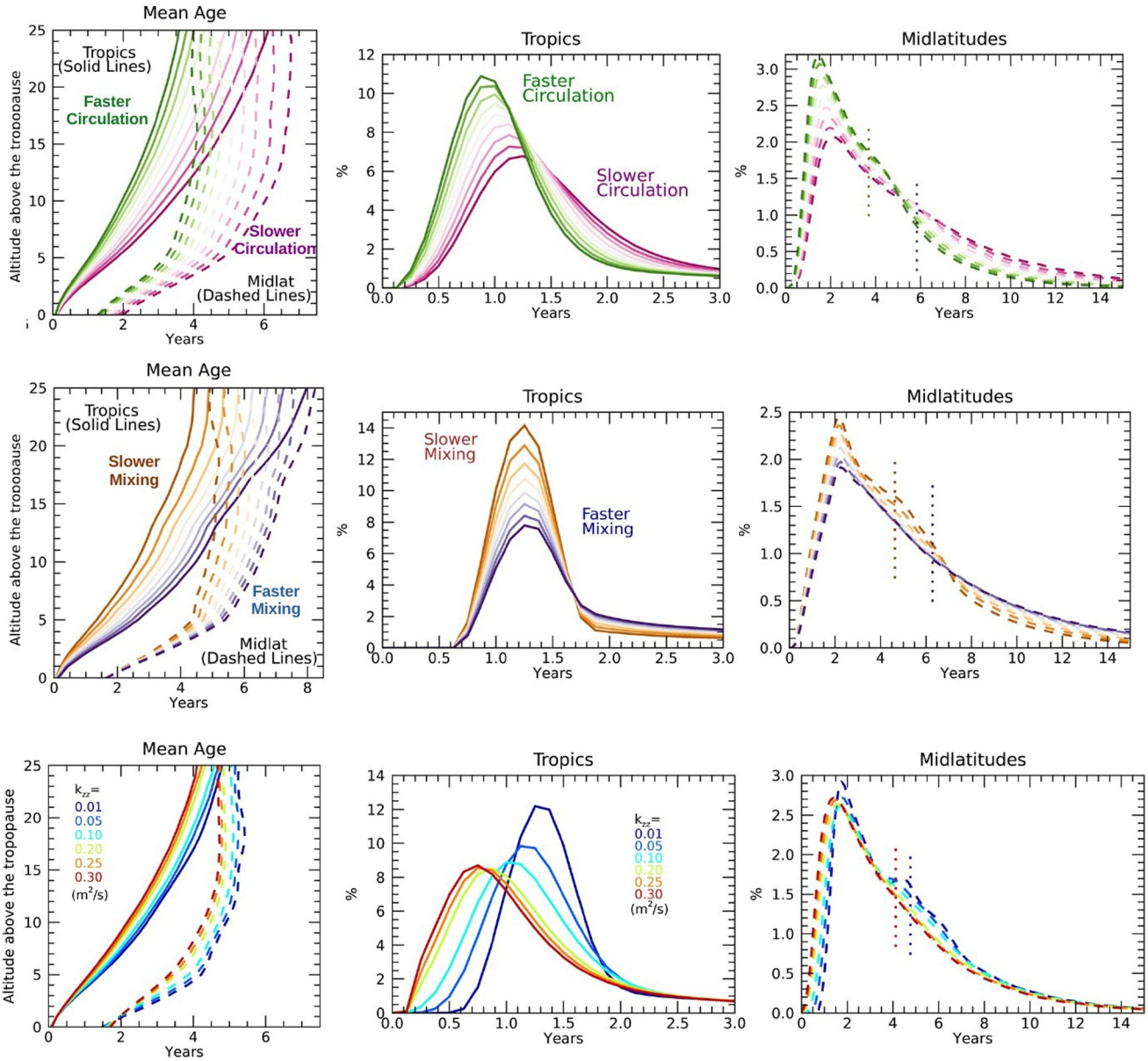

Figure 2. Idealized tropical leaky pipe model results demonstrating sensitivity of mean age (left) and age spectra in tropics (middle) and mid-latitudes (right) to different processes: Top row shows sensitivity to mean circulation changes, the middle row sensitivity to mixing time scale changes and the bottom plot sensitivity to vertical diffusion. Solid lines are tropical profiles, dashed lines mid-latitude profiles. The spectra are averaged over 8–10 km above the tropopause in each region. The oldest and youngest mean ages for the midlatitude spectra are shown by the vertical dotted lines.

photochemistry as in Ray et al. (2016). The reference state vertical velocity and horizontal mixing time scale profiles are also similar to previous studies (Ray et al., 2014, 2016) and based on MERRA reanalysis (see Figure S9 in Supporting Information S1 for the profiles). Figure 2 shows TLP model output sensitivity to mean circulation strength, horizontal mixing time scales and vertical diffusion. The mean circulation in the runs is varied by ±20% around the reference profile. The response of mean age to residual circulation changes is straightforward to interpret: mean age decreases with faster circulation both in the tropics and mid-latitudes, with changes by 30%–40% at all levels.

The sensitivity to horizontal mixing time scales between the mid-latitudes and tropics is shown by varying the value of the mixing efficiency parameter ϵ and holding the mean circulation strength constant (see Text S4 in Supporting Information S1) for details on the relation of the mixing efficiency and mixing time scale, and Figure

S9 in Supporting Information S1 shows the mean age (see Figure 2, left middle row) increases by roughly the same amount in both the tropics and mid-latitudes at all levels greater than ∼5 km above the tropopause in response to faster mixing. This effect of horizontal eddy mixing leading to a global increase in mean age above the level of mixing can be directly derived from the TLP model (see Neu and Plumb (1999)), and can be conceptually understood in the following way: horizontal eddy mixing transports relatively young air from the tropics to the mid-latitudes and old air from mid-latitudes to tropics. This might lead to the expectation that age of air would decrease in the extratropics due to mixing; however the old air mixed into the tropics will travel upward in the tropical pipe, and eventually be advected to the extratropics, where the air parcel sinks to the initial mixing level (see example trajectories shown in Figure 1). Thus, this air parcel contributes to "aging" in the extratropics which can be shown to overcompensate the initially mixed younger air (see e.g. Garny et al., 2014). This process is sometimes referred to as "re-circulation." The response of mean age to mixing changes is nonlinear in the sense that mixing time scale changes from the shortest mixing times result in relatively larger mean age changes compared to mixing time scale changes from the longest mixing times.

One fact to note is that increases in mixing strength amount to similar increases in mean age in tropics and in mid-latitudes. A faster residual circulation, on the other hand, decreases mean age more strongly in the extratropics than in the tropics. This fact revealed from the conceptual model can be generalized and used to infer circulation strength from the difference of mean age between tropics and mid-latitudes (see Section 3.2.1).

The sensitivity to vertical diffusion is shown by varying the value of the vertical diffusivity constant k_{zz} from 0.01 to 0.3 m^2/s in both the tropical and mid-latitude regions while holding the mean circulation and horizontal mixing fixed at the base profile values. In general, the stronger the vertical diffusion the younger the mean age in both regions and at all altitudes, consistent with previous studies (e.g., Dietmüller et al., 2018). For the largest values of k_{zz} the sensitivity of mean age decreases, suggesting a saturation of the effect of vertical diffusion. The effect of vertical diffusion on mean age can be understood as essentially an additional "effective" vertical velocity, and appears to have similar effects on mean age as a faster residual circulation. Therefore, it is not trivial to judge based on mean age alone which process is responsible for mean age changes or differences among models (see e.g. Gupta et al., 2021). In the following it will be discussed that the age spectrum does show distinct responses to changes in the individual processes, demonstrating the usefulness of the age spectrum for understanding transport processes.

3.1.2. Age Spectrum

The age spectra sensitivity to various processes is shown in Figure 2 (middle and right panels) based on the same TLP model runs discussed above. The Lagrangian particle trajectory technique of these TLP runs allows age spectra to be calculated in vertical bins for each region (Ray et al., 2014). The mean circulation strength affects the timing of the mode as well as the shape and the tail of the spectra. A slower circulation results in a mode at an older transit time, concomitant with a flattening of the peak. This response is roughly linear, as can be seen most clearly in the tropics. The mid-latitude spectra clearly show the difference in the tail beyond 6 years where there is significantly higher probability for the slower circulation runs. The ratio of moments (see Section 2.3) increases both in the tropics and mid-latitudes for a slower circulation, thus the broadening of the spectrum dominates over the increasing mean age.

The mixing sensitivity is different to that of the mean circulation in that the timing of the spectrum mode does not change but the shape of the tail does such that faster mixing results in a higher probability of transit times older than seven (two) years in mid-latitudes (tropics). The change in the slope of the tail does affect the amplitude of the mode as expected since the spectra are normalized. In the mid-latitudes, the spectrum tail appears to become insensitive to horizontal mixing, in particular for the fastest mixing time profiles. Faster mixing leads to an increase in the ratio of moments, similar to a slower circulation.

The age spectrum sensitivity to vertical diffusion is unique from either of the other two processes in that the diffusion changes both the mode timing and the shape of the tail but in the opposite sense to the mean circulation changes. A larger vertical diffusion moves the mode to a shorter transit time (in the tropics), while also increasing the probabilities in the tail of the spectra. These age spectrum sensitivities demonstrate how diffusion acts to spread air parcels and essentially flattens the distribution of ages. Given the younger mean age, and broader age spectrum, the ratio of moments increases for enhanced vertical diffusion.

3.2. Transport Diagnostics Based on Global Age and Tracers

As demonstrated in the previous Section 3.1, interpreting age of air changes in terms of processes is challenging as an interplay of residual circulation advection, eddy mixing and vertical diffusion affects age of air in non-unique ways. To quantify the role of those transport processes individually in the atmosphere or in complex models it is necessary to apply sophisticated transport diagnostics to unambiguously interpret actual age of air changes. Over recent years, two new diagnostic frameworks have been established and applied to model and observational age data. Both diagnostic frameworks essentially target to separate the role of the mean advective circulation on age of air from the effects of quasi-horizontal eddy mixing. The former (Section 3.2.1) uses a rigorous formulation in isentropic coordinates, and allows to estimate the strength of the mean diabatic circulation from the age difference between tropics and extratropics. As such, it only requires global data of mean age on isentropes, providing the unique opportunity to diagnose the strength of the overturning circulation from observational data. The second framework (Section 3.2.2) explicitly calculates the contribution of residual circulation advection and mixing to mean age of air, and can be applied to model data upon knowledge of the mean age and the 3-D winds. This separation between residual circulation and mixing proved particularly useful to better understand the impact of those processes on local age of air (changes), as well as model differences.

3.2.1. Diabatic Mass Flux Strength From Age Difference

A process diagnostic that can be derived from mean age and that has been developed further over the recent years is the difference of mean age between tropics and extratropics, which can be related theoretically to the total mass flux (or the diabatic circulation), thus separating the advective part of the circulation from effects of eddy mixing.

As age is a record of the Lagrangian history of a parcel, it has a useful relationship with mass transport, as pointed out by Neu and Plumb (1999) and more recently by Linz et al. (2016, 2021). Indeed, considering a general advective-diffusive transport operator $\mathcal{L}(\chi) = \mathbf{u}\nabla\chi + \frac{1}{\rho}\nabla\cdot(\rho\,\kappa\,\nabla\boldsymbol{\chi})$ it can be shown from the continuity and age evolution equations that the *age substance* $\rho\Gamma$ obeys the budget equation:

$$\frac{\partial\rho\Gamma}{\partial t} + \nabla\cdot\mathbf{F}^{\Gamma} = \rho, \tag{13}$$

with the flux of mean age $\mathbf{F}^{\Gamma}$ given by $\mathbf{F}^{\Gamma} = \rho\Gamma\mathbf{u} + \rho\,\kappa\,\nabla\Gamma$. Integrating Equation 13 over a volume V bounded by a closed surface S and assuming steady-state results in a relation between the age flux and mass

$$\int_S \mathbf{F}^{\Gamma}\cdot\mathbf{n}_{\mathbf{S}}\mathrm{d}A = M, \tag{14}$$

with the normal unit vector $\mathbf{n}_{\mathbf{S}}$ pointing outside of the volume. Hence, the total age flux leaving the volume V through the boundary surface S is equal to the mass of air enclosed by that surface. This statement holds for any closed surface, be it a pressure level, or the tropopause. Particularly suitable is a translation of the circulation to isentropic coordinates as it naturally separates the isentropic horizontal mixing from the meridional diabatic circulation and is thus desirable for disentangling the effects of these processes on age, as done in Linz et al. (2016, 2021). The meridional circulation in isentropic coordinates covaries closely with the more traditional residual circulation vertical velocity, especially if the residual circulation is calculated using diabatic heating rates as well (Linz et al., 2019). Hence, we rewrite the relationship between age flux and mass above a surface (Equation 14) in isentropic coordinates:

$$\int_{\theta}\sigma\dot{\theta}\Gamma dA = -M(\theta), \tag{15}$$

where $\sigma = -\frac{1}{g}\frac{\partial p}{\partial\theta}$ is the isentropic density, $\dot{\theta}$ is the diabatic heating (the vertical velocity in isentropic coordinates), $\int_{\theta}$ is the integral over the θ surface and $M(\theta) = \int_V \sigma dV$ is the mass above the θ surface. This relationship has neglected diabatic diffusion, so the extent to which this relationship holds for a model is a measure of the combination of diabatic and numerical diffusion (Gupta et al., 2021).

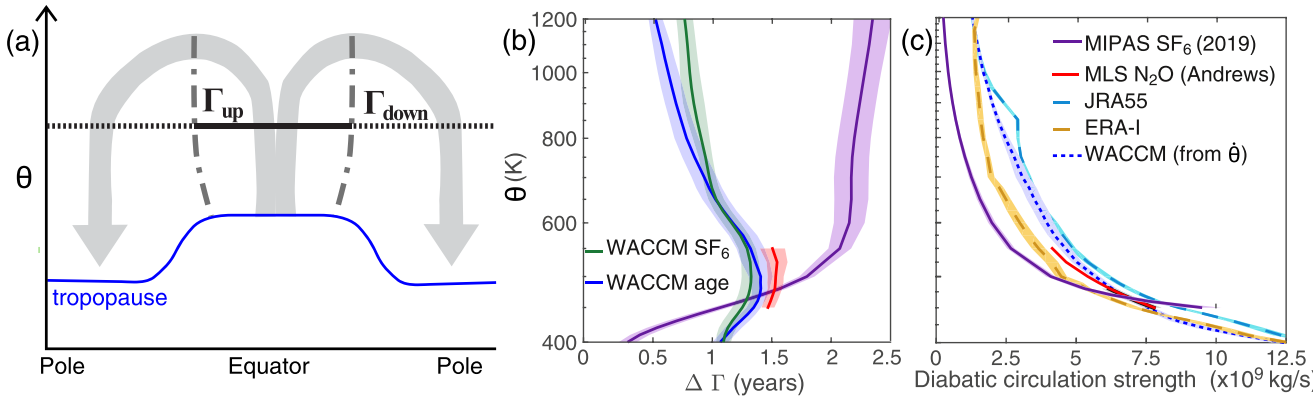

Figure 3. Diagnosing the diabatic circulation strength from the age difference. (a) Schematic of the time-mean (or statistically steady-state) circulation with one isentrope in the stratosphere emphasized in black. The upwelling region is shown in solid black, and the downwelling region is shown in dotted black. (b) Updated from Linz et al. (2017, Figure 2), the age difference between the tropics and extratropics from a model (WACCM) run with ideal age (blue) and an SF_6-based age (green) with no sink correction. Note that the mesospheric sink in this version of WACCM is too weak. Purple shows the age difference calculated from the most recent MIPAS SF_6 retrievals but without the mesospheric sink correction, and red shows the age difference from MLS N_2O using the cubic fit from A. E. Andrews, Boering, et al. (2001). (c) Updated from Linz et al. (2017, Figure 3), the implied diabatic circulation strength from the two age products shown in (b), from two reanalyses based on their radiative heating rates (dashed lines, JRA-55 in teal and ERA-Interim in yellow) and from the radiative heating rates in WACCM (blue dotted line). For more details, see Linz et al. (2017).

To determine the total overturning mass flux through a surface, that surface is divided into upwelling and downwelling regions and the total flux through each is equal and is given by

$$\int_{up} \sigma\dot{\theta} dA = -\int_{\text{down}} \sigma\dot{\theta} dA = \mathcal{M}(\theta). \tag{16}$$

Then,

$$\mathcal{M}\Delta\Gamma = \int_{\theta} \sigma\dot{\theta}\Gamma dA = M, \tag{17}$$

where $\Delta\Gamma = \Gamma_d - \Gamma_u$ is the difference in mass-flux-weighted age averaged over the downwelling region (where $\dot{\theta} < 0$) and over the upwelling region (where $\dot{\theta} > 0$). This is shown schematically in the first panel of Figure 3.

For this relationship to hold identically, it is necessary to know the age and the velocities through the isentrope, as Γ_d and Γ_u are mass-flux weighted, but area-weighting introduces only a small bias (about 10% in an idealized model with seasonal cycle, Linz et al., 2016). Thus, the age, pressure, and isentropic density on an isentropic surface are sufficient to calculate the mass flux through that surface. Note that the total circulation strength is not related to the average of all age above the surface but is related to the *difference in age between upwelling and downwelling through the surface*. The mixing is along the isentrope and affects both regions equally.

This age difference diagnostic was applied to mean age from model as well as satellite data (Linz et al., 2017). These results are shown in Figure 3 in panels (b) and (c). The satellite-based data from MLS N_2O are only valid for a limited region because of the limitations of the translation from N_2O to age. The version of the MIPAS SF_6 age used here has not been corrected for the mesospheric sink. Based on the WACCM model, this sink will start to impact the age difference quite substantially above 700 K, but this version of the WACCM model has too weak a mesospheric sink, and so the comparison is likely invalid even at lower levels (compare also to Garny, Eichinger, et al., 2024). For the region between 450 and 500 K, the different calculations generally agree well for the diabatic circulation strength.

Given this diagnostic can be applied to mean age derived from satellite products, it provides a unique opportunity to estimate the strength of the mean diabatic overturning circulation from observations. With improved methods to derive mean age, and additional data products becoming available (see Section 4), this is a promising avenue

for future research. Ongoing work is using the age from SF_6 with a mesospheric sink correction and from N_2O to calculate the mean circulation strength and trends.

Two notable follow-up papers use this diagnostic framework to address the diabatic mass flux in isentropic coordinates and along-isentropic mixing. Linz et al. (2021) present the hemispheric separation of the diabatic mass flux calculation and describe a metric for along-isentropic mixing into and out of the tropical pipe region based on the vertical gradients of age in the tropics or extratropics. These diagnostics are more limited than the global diabatic mass flux calculation because of assumptions about regions being well mixed: both assume that the tropics are well mixed, and the along-isentropic mixing metric assumes that the extratropical region is well mixed. This latter assumption is not reasonable and leads to nonphysical implied mixing in some cases, which was addressed by a follow up study by Gupta et al. (2023). That study presents the age-isentropic streamfunction that better represents the full picture of the stratospheric mixing and eliminates nonphysical results from Linz et al. (2021). The age-isentropic streamfunction does rely on more than just observed age, however, and so it cannot be calculated directly from observations.

3.2.2. Residual Circulation Transit Times and Aging by Mixing

The effects of different transport processes on age, in particular of the interplay of residual circulation advection and eddy mixing, can be clearly illustrated by consideration of the zonal mean tracer continuity equation (Equation 13). For mean age and in isentropic coordinates, this age budget equation can be written (see also D. G. Andrews et al., 1987; Plumb, 2002)

$$\partial_t \overline{\Gamma} = \underbrace{1}_{\text{Source}} \underbrace{-\frac{\overline{v}^*}{a}\partial_\phi \overline{\Gamma} - \overline{Q}^* \partial_\theta \overline{\Gamma}}_{\text{advection}} + \underbrace{\frac{1}{\overline{\sigma}} \nabla \cdot M^\Gamma}_{\text{mixing}} - \frac{1}{\overline{\sigma}} \partial_t \left(\overline{\sigma' \Gamma'}\right). \tag{18}$$

Here, $\left(\overline{v}^*, \overline{Q}^*\right)$ represent the 2D zonal mean residual circulation, σ the isentropic mass density, a Earth's radius, overbars denote zonal mean quantities and primes the deviations from these. The 2D eddy flux vector components for mean age are given by $M^\Gamma_\phi = -\overline{(\sigma v)' \Gamma'}$ and $M^\Gamma_\theta = -\overline{(\sigma Q)' \Gamma'}$. The first term on the right-hand side represents the unit source of age, the second term the avection by the residual circulation, and the third term represents the effects of eddy mixing. The last term on the right-hand side is generally very small and can be neglected in the budget.

Integration of Equation 18 along air parcel trajectories, the characteristics of the equation, results in a decomposition of mean age into residual circulation transit time (RCTT) and the integrated mixing effect, which has been termed "aging by mixing" (Garny et al., 2014). The RCTT is calculated as the transit time along 2D residual circulation trajectories, and as such requires knowledge of the residual circulation velocities from model or reanalysis data (T. Birner & Bönisch, 2011). The concept of RCTT was used earlier to estimate stratospheric transport timescales (Rosenlof, 1995). More recently, the diagnostic of RCTTs has proven useful to disentangle the effects of residual circulation transport and mixing in reanalysis and global models (Garny et al., 2014; Ploeger et al., 2015). Based on 3D model data, the effects of mixing on age can be calculated explicitly by integrating the eddy mixing tendency in Equation 18 along the residual circulation trajectories (Ploeger et al., 2015). If 3D data is not available (e.g., for observations) the aging by mixing can be calculated to a good approximation as a residual in the age budget (mean age minus RCTT). It should be noted that the aging by mixing term is influenced both by the mixing strength and by the residual circulation strength through recirculation (see Garny et al., 2014, a faster circulation will cause faster re-circulation and thus reduced aging by mixing.).

The stratospheric distribution of mean age, RCTT and aging by mixing is shown in Figure 4 based on a reanalysis-driven transport model. Throughout the stratosphere the contributions of residual circulation and mixing on mean age are of similar magnitude. RCTT is, in general, younger than mean age, except in the polar lower stratosphere. The large latitudinal gradients in RCTT polewards of about 60° indicate the separation between the shallow and deep branches of the Brewer-Dobson circulation (T. Birner & Bönisch, 2011). Compared to the RCTT, mixing causes a significant aging of stratospheric air, in particular in mid-latitudes around 50 hPa. This additional aging by eddy mixing is consistent with the conceptual model results discussed in the previous section, and the aging by mixing diagnostic can in addition reveal the 2D structure of mixing effects. Specifically, aging by mixing is

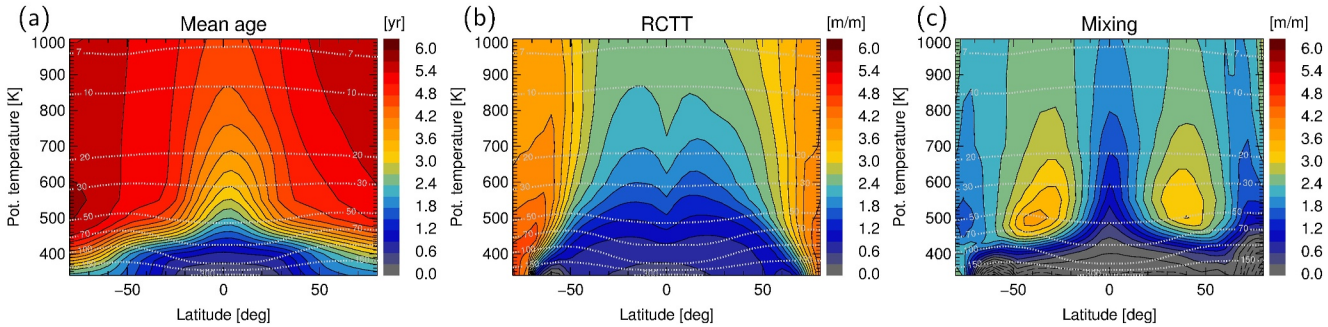

Figure 4. Effects of residual circulation and eddy mixing on age of air. (a) Mean age from ERA5-driven CLaMS model simulation as annual average (contours highlighted in black), with pressure levels shown as gray lines. (b) Same but for residual circulation transit time. (c) Same but for the integrated mixing effect "aging by mixing" (explicitly calculated).

highest in the lower stratosphere in mid-latitudes, where the integrated effect of mixing and re-circulation maximizes, while the tropics and high latitudes are more isolated (for a thorough discussion, see Ploeger et al., 2015; Garny et al., 2014). Furthermore, if the aging by mixing is calculated explicitly from the resolved fluctuations in the 3D fields, the residual from the age budget in Equation 18 can be analyzed for effects of unresolved mixing in models due to numerical diffusion (Dietmüller et al., 2017).

4. Age of Air From Observations

This section presents and discusses the basic principles related to the calculation of mean age of air from observations of long-lived tracers (Section 4.1), the currently available observational data from in situ (Section 4.2) and remote sensing (Section 4.3) methods and the consistency of data from different sources (Section 4.4). Finally, transport diagnostics that can be derived from observed age-related tracers are reviewed in Section 4.5.

4.1. How to Calculate Mean Age From Realistic Tracers

The basic relationship on which all methods to derive mean age of air in the stratosphere rely is Equation 2. This equation states that the mixing ratio of an inert tracer in the stratosphere can be described by the integration backward in time over the representative tropospheric mixing ratios weighted by the transit time distribution. Consequently, the observed mixing ratio in the stratosphere carries information on the transit time distribution and in particular its first moment, the mean age of air (see Equation 4). In the derivation of Equation 2, two fundamental assumptions have to be made. This is first that the tracer is chemically inert, thus it neither is destroyed nor is it produced during the transport process. The second fundamental assumption is that there is a single point of entry from the troposphere into the stratosphere, which in practice is interpreted as a homogeneous region (the tropical tropopause) rather than a single point. The transit time distribution is thus the probability density function for the occurrence of a given transit time from this single point of entry to the given location in the stratosphere for which the mean age of air is sought. This assumption of single entry point is closely related to a second prerequisite, which is that the tropospheric reference time series is a unique function and that the time series of the input mixing ratio to the stratosphere can thus be described correctly using a single time series. The tracers most commonly used in the past to derive mean age of air are SF_6 and CO_2. Other tracers, in particular CH_4 and N_2O, while not being age tracers have also been used in the calculation of mean age and in deriving global age distributions. Available databases for these tracers and other tracers that have been suggested to be used as mean age tracers in the stratosphere are discussed in Sections 4.2 and 4.3.

In Section 4.1.1, we will discuss the reference time series and how these can be derived for several decades into the past. We then discuss in Section 4.1.2 how well the assumption of chemical inert behavior is in reality for the different mean age tracers which have been used, and how deviations from chemical inertness can be corrected for. Finally, it has been shown by Hall and Plumb (1994) that Equation 2 can be solved very easily to derive the mean age of air in case of a linear time series of the mean age tracer. In this ideal case, no information on the shape of the transit time distributions is needed. We will discuss in Section 4.1.3 how well this assumption is met for different tracers and discuss methods used to correct for non-linear behavior. All methods used to correct for non-linear behavior require some knowledge or assumptions on the shape of the transit time distributions. Of

particular importance in this correction is the so-called ratio of moments, that is, the ratio of the squared second moment of the transit time distribution (the width) to the first moment of the transit time distribution (see Section 2.3). This property can be derived from atmospheric transport models but is not a directly observable quantity. Section 4.1.5 finally describes a suggested method to derive mean age of air. Python source code for the numerical implementation of this suggested method is made publicly available (Wagenhäuser et al., 2024; see also Data Availability Statement Section). A number of age data sets have been recalculated with this method and are discussed and inter-compared in Section 4.4.

4.1.1. Reference Time Series

To calculate mean age from tracers, the time-series of the input reference mixing ratios of the age tracer is required (see Equation 2). The reference surface where the age of air is defined as zero has traditionally been considered to be the tropical tropopause for air parcels in the stratospheric overworld (e.g., Kida, 1983). Since there are no regular measurements of trace gases at the tropical tropopause, measurements at the earth's surface have been most commonly used as reference time series. An average of mixing ratios observed at Mauna Loa (19°N) and American Samoa (13°S) have often been used to derive representative entry mixing ratios for the tropical tropopause (e.g., Boering et al., 1996), in some cases with considering a lag between about 26 days (Park et al., 2007) to about 2 month (Boering et al., 1996) to approximate the transport time from the surface to the tropical tropopause. Volk et al. (1997) even used a lag time of 0.8 years based on the observed lag of SF_6 mixing ratios between the global mean surface time-series and the tropical tropopause. Especially for CO_2, which has a strong seasonal cycle in the troposphere, the magnitude of the seasonal cycle could also be dampened during the transport to the tropical tropopause. The amplitude of the seasonal cycle in CO_2 at the tropical tropopause has been estimated at about 3.2 ppm peak-to-peak (A. E. Andrews, Daube, et al., 2001), which is similar to the amplitude of a tropical mean time series (e.g., from the average of Mauna Loa and American Samoa mixing ratios). It should be noted that inaccuracies in the estimate of the input time series will directly influence the derived mean age values. For example, if the input to the stratosphere were more strongly dominated by the Northern Hemisphere (with higher mixing ratios) this would lead to a systematic underestimation of mean age. Also input from the Asian Summer Monsoon could lead to inaccuracies of the assumptions on the input time series. In the course of this review, we have compiled our best estimates of reference of mixing ratios at the tropical Earth's surface from 1945 to 2023 for the mean age tracers SF_6 and CO_2, as well as for CH_4 and N_2O (see Text S1.2 in Supporting Information S1 for details).

4.1.2. Correction for Chemical Sinks and Sources

A perfect age tracer should have neither sources nor sinks in the region in which it is applied as an age tracer. This is not ideally given for either of the two age tracers which have most commonly been used. CO_2 has a chemical source in the stratosphere from the oxidation of methane (Boucher et al., 2009; Shindell et al., 2017), and SF_6 has a chemical sink in the upper stratosphere and lower mesosphere (Reddmann et al., 2001). Some of the alternative mean age tracers suggested for example, by Leedham Elvidge et al. (2018) have probably extremely long life times and no chemical sources in the stratosphere or mesosphere. These tracers are, however, much more challenging to measure with good precision and accuracy in the stratosphere.

In the case of CO_2, the chemical source from the oxidation of methane can contribute to CO_2 mixing ratios by up to about 1.5 ppm, which would lead to an underestimation of mean age by up to a half year at the oldest mean ages (Ray et al., 2017) if not corrected for. Using simultaneous CH_4 measurement, the amount of CO_2 produced from the oxidation of methane can be easily estimated. To account for CH_4 oxidation, the traditional approach has been to subtract the difference between CH_4 stratospheric and global surface mean mixing ratios at the time of measurement from the stratospheric CO_2 mixing ratios (Boering et al., 1996; Daniel et al., 1996). If simultaneous stratospheric CH_4 measurements are unavailable and N_2O measurements are available, then CH_4 can be approximated using the nearly linear N_2O-CH_4 relationship (A. E. Andrews, Daube, et al., 2001; Michelsen et al., 1998).

The correction for the chemical loss of SF_6 is much more difficult. It has long been assumed that the loss is negligible in the middle and lower stratosphere outside the polar vortex, where depleted air is transported downward from the upper stratosphere and mesosphere (e.g., Engel, 2006). However, over the past years the lifetime of SF_6 was found to be lower than previously assumed by a number of studies (Kovács et al., 2017;

Leedham Elvidge et al., 2018; Ray et al., 2017), and it was acknowledged that the chemical sink can induce substantial biases in mean age throughout the stratosphere (Leedham Elvidge et al., 2018; Loeffel et al., 2022). Since the calculation of mean age relies on absolute differences in tracer concentrations, a chemical sink with constant depletion rates induces a larger bias on mean age for higher absolute abundances. Thus, with a monotonically increasing tracer, an apparent positive trend in mean age is induced by a chemical sink (Loeffel et al., 2022; Schoeberl et al., 2000). Recently, a correction scheme for the effects of chemical sinks of SF_6 has been suggested by Garny, Eichinger, et al. (2024), and it was shown that observational mean age estimates based on SF_6 can be reconciled with mean age from other tracers when applying this sink correction (see also Section 4.4). However, the fit parameters of the correction are so far based on global model data. More high-quality observations of mean age and alternative age tracers are necessary to constrain the sink correction by observations.

4.1.3. Correction for Non-Linear Increasing Tracers

For the propagation of an inert tracer into the stratosphere, the age spectrum can be thought of as a weighting function, describing how strongly air with a given transit time contributes to the observed mixing ratio in the stratosphere. Only for a perfectly linearly increasing (or decreasing) chemically inert age tracer, can mean age be simply calculated as the lag time between the reference time-series and abundances at a given location in the stratosphere, as was shown theoretically in Section 2. For such a tracer, no additional knowledge on the age spectrum is needed. While such tracers can be easily implemented in global models, in practice no such perfect linearly increasing tracer exists, so that the calculation of mean age from observations requires knowledge of the age spectrum (see Equation 4). This is of course a circular problem, since if the age spectrum were known, mean age would be directly accessible. Therefore, different approaches have been used in the past to overcome the problem. All of these approaches are based on assumption about the second moment of the age spectrum (see Section 2.3), generally referred to as the width of the age spectrum. There are generally two different approaches. The "fit method" is based on the assumption that the reference time series can be described by a second order polynomial, in which case an analytical solution can be found (Hall & Plumb, 1994; Volk et al., 1997). In the "convolution method" an exact mathematical description of the age spectrum is required and mean age is derived numerically by finding the value of mean age which matches the observed mixing ratio. The methods were tested and illustrated in detail in Fritsch et al. (2020), and in the following they are briefly described.

- *Fit method* In this method it is assumed that the reference time-series can be fitted using an analytical function, most commonly as polynomial of second order. If the time series can be approximated using a second order polynomial the mean age calculation only requires knowledge of the relation of the width of the age spectrum to the mean age, the ratio of moments (see Section 2.3). The general approach was first suggested by Hall and Plumb (1994) and then solved for a second order fit by Volk et al. (1997), and later applied by for example, by Engel et al. (2002, 2009) and follow-up studies. They assumed a fixed ratio of moments, using values between 1.25 years (Volk et al., 1997) and 0.7 years (Engel et al., 2009). Engel et al. (2009) included the uncertainty arising from the unknown ratio of moments in their error estimates of mean age, but as found later this uncertainty does also depend on a second parameter, namely the length of the time-series used to perform the polynomial fit on (Fritsch et al., 2020). Thus, the advantage of this method is that no explicit form for the age spectrum needs to be assumed and that the solution can be solved analytically. The disadvantage is that this method can only be applied to age tracers for which the tropospheric reference time series can be described by a second order polynomial and that additional uncertainty enters through the uncertainty in the polynomial fit, and in choosing the fit interval.
- *Convolution method* If the age spectrum is known, the convolution of the reference time-series and the age spectrum provides an expected tracer mixing ratio (see Equation 2). If the reference time series is monotonic, this relates in a unique relationship between observed mixing ratio and mean age. A common assumption for the age spectrum is the inverse Gaussian function based on the "global diffuser" model (see Section 2, Equation 12). This inverse Gaussian can be parameterized based on a mean age value and on a given ratio-of-moments. Thus, if assuming the ratio-of-moments, the convolution with the reference time-series can be performed for a range of mean age values, resulting in a range of stratospheric tracer concentrations. Subsequently, mean age is estimated to be the age value with the best match to the observed value (either via interpolation from a "look-up" table, or via iteration as in Stiller et al. (2008)). Thus, the advantage of this approach is that it can be used for any behavior of the reference time-series with variable temporal slopes. It is

also possible to use different age spectra in this convolution method, for example, model derived age spectra. The disadvantage is that the explicit shape of the age spectrum needs to be assumed.

4.1.4. Limitations of Methods to Determine Mean Age

For any of the age calculation methods outlined above, the ratio-of-moments is a critical input parameter that needs to be assumed in case of non-linear temporal increase. In addition, information on the temporal evolution of the mean age tracer in the source region as well as chemical loss or production during transport and in case of the convolution method on the exact shape of the age (e.g., an inverse Gaussian) spectrum add to uncertainty in mean age values derived from observations. A rather detailed assessment of the different sources of uncertainty has been given in the supplement to Engel et al. (2009). They concluded that the total uncertainty could add up to about a year (see Table S1 in the supplement to Engel et al., 2009). The main sources of uncertainty are related to the assumptions about the correct description of the tropospheric reference time series of the mean age tracer and to non-linearity related uncertainties. These factors will partly vary over time, as for example, the non-linearity in the time series may change with time. Note that chemical loss of SF_6 was not included in this uncertainty analysis. However, if long-term changes are of interest, different factors may dominate uncertainty. The slope and curvature in the reference time-series may change with time causing systematic changes or biases over time. Interhemispheric gradients and associated uncertainty in how to represent the tropospheric input time series will, however, vary less over time. For example, Fritsch et al. (2020) showed that the same data set used by Engel et al. (2017) yielded different long-term trends when applying different ratios-of-moments and using different methods to calculate mean age (see also Section 6.2). In the past, values for the ratio-of-moments used in observational studies had to rely on model data since this quantity has not been constrained from observations so far. Early estimates of the ratio of moments by Hall and Plumb (1994) report a value of around 0.7 years based on global model simulations. This value has been used widely in mean age calculations (e.g., Engel et al., 2009), but was updated to a larger values based on modern model simulations (Fritsch et al., 2020; Hauck et al., 2019). In particular, it is crucial to account for the long tail for transit times beyond 10 years when calculating the ratio of moments. As outlined in Section 3.1, different transport processes can affect the age spectrum shape, and the ratio-of-moment. It is highly sensitive to the underlying circulation: for example, estimates of the ratio-of-moment in mid-latitudes in the middle stratosphere vary between 0.7 and 1.3 years for two different reanalysis, despite being driven by the same transport model (see Text S1.1 and Figure S1 in Supporting Information S1). This leads us to conclude that the ratio-of-moments is currently not well constrained from neither models nor observations, and thus imposes a major uncertainty in the calculation of mean age and its trends (see Section 6.2.2).

Another uncertainty is imposed by assuming a single entry to the stratosphere, equivalent to a mono-model age spectrum. This assumption is violated most strongly in the lowermost stratosphere, where seasonal entry across the extra-tropical tropopause into this region is known to occur (e.g., Ray et al., 1999). A number of studies have accounted for the multiple entry points into the lowermost stratosphere in order to calculate mean ages in this region from trace gas measurements (e.g., Bönisch et al., 2009; Hauck et al., 2019, 2020; Wagenhäuser et al., 2023). In this study we have focused on age of air in the stratospheric overworld above 380 K where the single entry point assumption is most valid.

Furthermore, age tracers with strong seasonal cycles like CO_2 impose problems to derive mean age close to the entry point at the tropopause, and the derivation of mean ages of less than about 2 years from CO_2 is problematic (A. E. Andrews, Boering, et al., 2001; A. E. Andrews, Daube, et al., 2001). To overcome this problem, A. E. Andrews, Daube, et al. (2001) used correlations of age to N_2O mixing ratios to constrain mean ages. The N_2O-age correlation has also been used more generally to derive mean age from N_2O satellite data (Linz et al., 2017), and this poses a promising method that might, if further developed, be explored to enrich the current satellite-based mean age data sets (see also Section 4.2).

4.1.5. A Consolidated Method to Calculate Mean Age

Based on the above discussion, we suggest here a consolidated method that should be used in the calculation of mean age values in order to yield comparable and consistent results. First, we suggest using the convolution method rather than the fitting method, because it is the most versatile method (see Section 4.1.3). A second advantage of this method is that it can also be used with age spectra deduced from model simulations to derive an

expected tracer mixing ratio. In this way, the seasonalities in troposphere-to-stratosphere transport can be taken into account as well as seasonal cycles in the tropospheric reference time series. This method also eliminates the need to choose an appropriate fitting interval for a tropospheric reference time series, which on the one hand covers the relevant period, yet can be reasonably approximated by a quadratic function (see discussion in Fritsch et al., 2020). As noted above, a mathematical approximation of the age spectrum and the ratio-of-moments need to be chosen in the convolution method. As shown by Ploeger and Birner (2016), the annual mean age spectrum is well described by an inverse Gaussian function. We therefore suggest that this will be a good analytical form for an age spectrum in the convolution method. The ratio-of-moments is needed for our suggested method, as for all other approaches, and may well be the single largest source of uncertainty. Given this quantity is currently not constrained by observations, we suggest to use climatological mean values from transport model simulations with CLaMS, driven by the ERA-interim reanalysis. ERA-Interim is chosen, because mean age driven by this reanalysis was found to compare overall best to observational constraints of mean age and long-term changes (see Supporting Information S1 for more information on the chosen model and data set). Furthermore, the reference time-series as described in Text 4.1.1 and in Supporting Information S1 should be used.

Code for the age calculation and the necessary input (reference time-series, ratio-of-moments climatology) is provided by Wagenhäuser et al. (2024) and Garny, Eichinger, et al. (2024) (see also Data Availability Section). In Section 4.4 we present mean age derived from SF_6 with the method defined here from balloon, aircraft and satellite data, and discuss implications of the new calculation method. We constrain here the method to the trace gas SF_6, because of the complication of the seasonal cycle in CO_2. Future work will be needed to define a consistent and improved method to derive age from CO_2, in particular in the lower stratosphere.

4.2. In Situ Observations

Over the last two decades a large number of stratospheric in situ data sets have become available, many of which are suited for the derivation of mean age of air. This has helped to further our understanding of age of air and the stratospheric overturning circulation in many ways. Perhaps the most obvious contribution was to constrain and improve the detailed picture of the BDC and its representation in models. In addition, a few select examples will be given here.

In terms of their use as indicators of stratospheric circulation variability, CO_2, SF_6, and N_2O have been the most established age tracers for some time (A. E. Andrews, Daube, et al., 2001; Volk et al., 1997). This was underlined by their application to establish, and later improve, the equivalent effective stratospheric chlorine (EESC, Engel et al., 2018; Leedham Elvidge et al., 2018; Newman et al., 2006, 2007; Ostermöller et al., 2017). EESC is the metric of choice for the stratospheric loading of ozone-depleting chlorine and bromine species, and therefore of major importance for tracking the recovery of the ozone layer (Daniel et al., 2022). A more direct age of air application has been the observation-based long-term data set compiled by Engel et al. (2009) and updated in Engel et al. (2017), which did not confirm expectations of the BDC trends from many models. This has sparked multiple scientific debates, some of which are still ongoing. More details on this complex topic can be found in Section 6.2.

As the understanding of transport and processes evolved, so did the expectations on the quality of those data—especially on appropriate precisions and accuracies, as well as a robust characterization of overall uncertainties. We primarily focus on those published data sets that have been used to derive mean ages while at the same time considering such traceability and comparability aspects (Table 1). This specifically includes a comprehensive characterization of the analytical instrumentation, a good link to an established calibration scale (with specific scale years) as well as to a tropospheric time series. For the latter two, long-term trends derived from the two main global observational networks (NOAA Global Monitoring Laboratory, https://gml.noaa.gov/ and AGAGE, https://agage.mit.edu/) have been the most frequently used. On the mean age side, the expectation is that tracer-tracer relationships are compact throughout the profiles, and that their tropospheric end points are close to the corresponding tropospheric background values. Importantly, this does not preclude the use of all the earlier (pre-2000) in situ observations, as for some of them the trace gas data is of sufficient quality (Leedham Elvidge et al., 2018); whereas for others it was possible to remeasure air samples that had been archived at the time (e.g., Engel et al., 2009).

We classify the data sets into three categories, based on (a) the quantity and altitude ranges of available observations, and (b) the suitability of the trace gas as an age tracer (see Section 4.1):

Table 1
Overview of Available High-Altitude Stratospheric In Situ Data Sets for Mean Age Derivation From Priority 1 and 2 Trace Gases

Time period (no. of flights)platform[a]	Latitude range (°)	Altitude range (km)	Trace species	Reference/campaign
1975–2005 (27 B)	32–51 N	5–43	SF_6, CO_2, CH_4	Engel et al. (2009)
12/1989–02/1990 (18 H)	37–81 N	10–21	N_2O	AASE[b]
08/1991–03/1992 (33 H)	21–90 N	10–21	SF_6, N_2O	AASE2[b]
10–11/1992, 04–05/1993, 10/1993 (23 H)	14–60 N	10–21	SF_6, CO_2, N_2O, CH_4	SPADE[b]
01–11/1994 (45 H)	70 S–87 N	10–23	SF_6, CO_2, N_2O, CH_4	ASHOE[b]
03–05, 10–11/1995, 01–02, 07–09, 12/1996, (54 H)	2 S–62 N	10–21	SF_6, CO_2, N_2O, CH_4	STRAT
1996–2000 (8 B)	7 S–68 N	10–34	SF_6, CO_2, N_2O, CH_4	OMS
01/1997, 04–09/1997 (36 H)	3 S–90 N	10–21	SF_6, CO_2, N_2O, CH_4	POLARIS[b]
11/1998, 09/1999, 12/1999–03/2000	11–89 N	10–22	SF_6, CO_2, N_2O, CH_4	SOLVE[b]
02/1999 (1 B)	68 N	9–26	SF_6, CF_4, C_2F_6,	Leedham Elvidge et al. (2018)
06/2008 (1 B)	5 S	14–34	C_3F_8, HFC-23, HFC-125	
10–11/2009 (2 H)	48–54 N	10–20		
01–02/2010 (7 H)	62–77 N	9–19		
12/2011 (2 H)	62–71 N	15–20		
09/2016 (2 H)	33–41 N	10–21		
03–04/1999, 09–10/1999 (20 H)	5–39 N	10–20	SF_6, N_2O, CH_4	ACCENT
05–07/2002 (19 H)	12–39 N	10–19	CO_2, CH_4	CRYSTAL-FACE
01–02/2004 (8 H)	3 S–39 N	10–19	SF_6, CO_2, N_2O, CH_4	Pre-AVE
2002–2004 (3 B)	34 N	10–33	SF_6, CO_2, N_2O, CH_4	BOS
06/2005 (9 H)	18–43 N	10–19	SF_6, N_2O, CH_4	AVE
06/2005–10/2006 (3 B, 5 H)	22 S–44N	12–34	SF_6	Laube et al. (2010)
01–02/2006 (16 H)	1 S–40 N	10–20	SF_6, CO_2, N_2O, CH_4	Costa Rica-AVE
08/2007 (7 H)	1–37 N	10–19	SF_6, CO_2, N_2O, CH_4	TC4
04/2010 (5 H)	12–85 N	10–20	SF_6, N_2O, CH_4	GloPac
10–11/2011 (5 H)	6–37 N	10–19	SF_6, N_2O, CH_4	ATTREX
2012–2022 (98 A)	45 S, 36–40 N, 67 N	10–26	CO_2, CH_4	NOAA GML[c]
08–09/2013 (20 H)	15–52 N	10–21	CO_2, CH_4	SEAC4RS
02/2015 (4 B)	10 S	17–29	CO_2, CH_4, SF_6	Sugawara et al. (2018)
08/2015, 05/2016 (4 A)	49, 54 N	0–32	CO_2, CH_4	Engel et al. (2017)
2016–2018 (15 A)	67 N (11), 52 N (4)	8–30	SF_6	Laube et al. (2020)
07–08/2017 (6 H)	21–30 N	0–20	CO_2, SF_6, C_2F_6, HFC-125	Vogel et al. (2023), Adcock et al. (2021)
2021–2023 (5 A)	39–40 N	10–24	SF_6, CO_2, N_2O, CH_4	NOAA[c]
06–08/2021, 05–07/2022 (30 H)	24–57 N	10–21	SF_6, CO_2, N_2O, CH_4	DCOTTS
02–03/2023 (21 H)	17–81 N	10–20	SF_6, N_2O, CH_4	SABRE

[a]Platforms: H: high altitude aircraft (above 15 km), B: large balloon, A: AirCore balloon. [b]Data and mission information available from https://espoarchive.nasa.gov/archive/browse. [c]Data and project information available from https://gml.noaa.gov/ccgg/arc/?id=144.

- Priority 1: SF_6, CO_2 (CH_4 required for the latter), N_2O
- Priority 2: Other inert tracers (CF_4, C_2F_6, C_3F_8, HFC-23, HFC-125)
- Priority 3: Other chemically active/non-passive species (e.g., CFC-11, CFC-12, HCFC-22, CO, O_3, H_2O)

In some cases, Priority 3 species have been used to derive mean ages indirectly, for example, through a previously established tracer-mean age correlation (e.g., Ehhalt et al., 2007; Ray et al., 2022). We do not consider these here as such approaches inherently incorporate additional uncertainties thus limiting their additional value for long-term trend derivation. The only exception for such chemically active gases is N_2O, justified by the generally

high quality and temporal and spatial density of available observations; as well as its relatively long stratospheric lifetime which allows for compact correlations up to mean ages of well over 4 years. Due to the changing nature of such correlations, continued work is needed to constrain this relation better for future use. In addition, it is worth noting that observations of gravitational separation derived from the ratio of more abundant gases (e.g., Ar/N_2) have recently shown promise as diagnostic tools for air transport processes in the stratosphere (e.g., B. Birner et al., 2020; Sugawara et al., 2018).

Three main platforms have been utilized for obtaining in situ data, with aircraft-based data generally excelling in latitude and longitude coverage (but limited to below ~20 km), and balloon-based data providing access to higher altitudes up to ~35 km. Launches of large balloons (payloads of several hundred kg) have become increasingly rare in recent years, mainly due to the tightening of safety requirements leading to fewer viable launch locations, but also because of the high costs. A more recently established and increasingly popular balloon-based alternative are AirCores—miniature passive air samplers that only weigh a few kg and are therefore both relatively flexibly deployable and cost-effective (Karion et al., 2010). In addition, it is important to make the distinction between in situ measurements carried out aboard the platform, and air sampling with post-flight analysis; the former generally providing more enhanced spatial and temporal sampling whereas the latter allowing for a broader range of trace gases to be analyzed. More details on major field campaigns are given in the platform-based sections below, as well as Table 1. Closely related to the platforms are the actual trace gas detection methods, which are described in Supporting Information S1 (Text S2.1).

4.2.1. Large High-Altitude Balloon

The largest compilation of mean ages derived from large balloon-based instrumentation has been published in Engel et al. (2009). This work combined data from 27 flights carried out between 1975 and 2005 at Northern Hemisphere mid-latitudes (from the U.S., France, and Japan). Various instruments were involved, but the comparability of the derived mixing ratios underlines the aforementioned importance of quality control. Apart from other mid latitude activities (e.g., A. E. Andrews, Daube, et al., 2001), some large balloon flights have been carried out elsewhere, predominantly in the Arctic (A. E. Andrews, Daube, et al., 2001; Engel, 2006; Ray et al., 2017) with a few launches in the tropics (Laube et al., 2010; Leedham Elvidge et al., 2018; Sugawara et al., 2018). All of these are listed in Table 1.

4.2.2. Aircraft

For the aircraft-based data we make a distinction between "normal" (up to about 15 km) and high-altitude aircraft (up to about 20 km), with the latter being able to reach the stratosphere at all latitudes. Much of the available data originates from the former, as high-altitude aircraft are far rarer and considerably more expensive to operate. The comparable wealth of data in the lowermost stratosphere exceeds the scope of this work, but it is worth mentioning some of the more extensive activities, that is, (a) the multi-season field campaigns SPURT (Engel et al., 2006), HIPPO (B. Birner et al., 2020; Wofsy, 2011), and ATOM (Thompson et al., 2022), (b) multiple missions using the American DC8 and the German HALO research aircraft (e.g., Ehhalt et al., 2007; Krause et al., 2018; Wagenhäuser et al., 2023, as well as iii) the long-running CONTRAIL (e.g., Umezawa et al., 2018) and CARIBIC/IAGOS-CARIBIC (Brenninkmeijer et al., 2007) programs. As for high altitude data, these essentially link to three aircrafts, that is, the Russian M55 Geophysica, and the American ER-2 and WB-57, as well as one UAV, that is, the U.S.-based Global Hawk (Glopac and ATTREX missions). All high-altitude aircraft campaigns with publicly available and/or published data of sufficient quality are listed in Table 1, including references to the respective project and/or publication.

4.2.3. AirCores

AirCore-based observations rely on the passive collection of air during the descent part of a weather balloon flight. For relevant trace gases such flights started in 2009 (Karion et al., 2010), and were, for the first years, limited to CO_2 and CH_4 (Engel et al., 2017; Hooghiem et al., 2020; Membrive et al., 2017; Wagenhäuser et al., 2021). More recently, SF_6 and N_2O have also become available (Laube et al., 2020; J. Li et al., 2023). AirCores are sampling from the stratosphere to the ground, and most of the focus so far has been on the validation of remote sensing-based measurements (e.g., for trace gas total column derivation, Agustí-Panareda et al., 2023). While much data exists, most of it has not yet been used for stratospheric transport studies. Nevertheless, it has

been demonstrated that it is possible to derive mean ages from AirCore-based CO_2 and CH_4 (Engel et al., 2017) as well as SF_6 (Laube et al., 2020). It is however worth keeping in mind that AirCores tend to sample much smaller amounts of air (typically less than 300 ml for the entire stratospheric part), and therefore are, on an individual sample basis, the least spatially representative in situ technique; though this is somewhat compensated for by the flexibility and cost-effectiveness of the technique enabling much more frequent flying. All available data sets are again listed in Table 1.

4.3. Remote Sensing Observations

Remote sensing instruments on balloon-borne and space-based platforms have provided vertical profiles of trace gases that can be used with various methods to determine the stratospheric mean age of air. While remote sensing observations from aircraft also exist, they typically cover a limited region of the atmosphere at or below the flight altitude only. We focus here on instruments and missions that provide vertically resolved information on the priority 1 gases (see Section 4.2) over a wider vertical range of the atmosphere, with a particular focus on the period from 2000 to present. A more detailed summary of the balloon-borne and space-based remote sensing measurements, including older missions and those that measure priority 2 and 3 gases, can be found in Supporting Information S1 (see Text S2.2).

The first remote sensing measurements of stratospheric trace gases were made from high-altitude balloons (Murcray et al., 1975). Over the past decades, several balloon-borne instruments have been measuring stratospheric tracers from the three priority groups noted above. These instruments include the MkIV interferometer (Toon, 1991, operating 1989-present), Limb Profile Monitor of the Atmosphere (Camy-Peyret, 1995, operated 1992–2009), Michelson Interferometer for Passive Atmospheric Sounding (MIPAS-B/B2) (von Clarmann et al., 1993, operated 1989–2014), and GLORIA-B (Gimbaled Limb Observer for Radiance Imaging of the Atmosphere-Balloon) (Friedl-Vallon et al., 2014; Riese et al., 2014, operating 2021-present). With respect to the priority 1 tracers, all of these instruments retrieve profiles of N_2O and CH_4 and the MkIV interferometer also provides SF_6 and CO_2 and GLORIA-B provides SF_6. To date, stratospheric age of air has not been determined from balloon-based remote sensing profiles.

Several space missions have provided data on long-lived tracers that can be used to derive information on age of stratospheric air. For priority 1 gases, these satellite missions are compiled in Table 2, along with information on the year(s) of the mission, the latitudinal coverage, and the species measured. For priority 2 and 3 tracers, this information is given in Supporting Information S1 (see Table S1). Of these missions, the Halogen Occultation Experiment on the Upper Atmosphere Research Satellite (Gunson et al., 1996), the Sub-Millimeter Radiometer (SMR) on Odin (Urban et al., 2005), MIPAS on Envisat (Fischer et al., 2008), the Atmospheric Chemistry Experiment Fourier Transform Spectrometer (ACE-FTS) on SCISAT (Bernath et al., 2005) and the Microwave Limb Sounder on the Aura satellite (Aura-MLS) (Waters et al., 2006) have provided time series of stratospheric tracer measurements extending longer than a decade (some more than 20 years) and SMR, Aura-MLS, and ACE-FTS are still operating at present. The High Resolution Dynamics Limb Sounder on Aura (Gille et al., 1980) and the Improved Limb Atmospheric Spectrometer (ILAS-II) (Nakajima et al., 2006) provide more limited temporal coverage. The space-based instruments that provide priority 1 tracer measurements prior to 2000 are also listed in Table 2 and details about these observations are provided in Supporting Information S1.

From here, we highlight those missions and measurements that have been used to derive stratospheric age of air from remote sensing. Following the first space measurements of SF_6 by the Atmospheric Trace Molecule Spectroscopy Experiment (ATMOS) on the Space Shuttle (e.g., Rinsland et al., 1990, 1996), there are two satellite missions only that provide SF_6 among various tracers, namely ACE-FTS on the SCISAT satellite, and MIPAS on Envisat. Those will be described in more detail in the following. Other than that, UARS-HALOE CH_4 and H_2O from 1986 to 1998 were used by Johnson et al. (1999) to derive stratospheric age spectra, and Schoeberl et al. (2005) used the first year of ACE-FTS measurements of CFC-11, CFC-12, CH_4 and N_2O to determine age spectra. Furthermore, the dense global measurements of N_2O by Aura-MLS were used to determine age of air by Linz et al. (2017).

ACE-FTS is a high-resolution infrared spectrometer that operates from a 650 km circular orbit with a high inclination of 74° and records up to 30 profiles (15 sunrise, 15 sunset) per day. It has been taking solar occultation measurements since February 2004, which are processed at the ACE Science Operations Center at the University of Waterloo (e.g., Boone et al., 2020, 2023). The high signal-to-noise ratio of the spectra allows ACE-FTS to

Table 2
Space Missions Measuring Priority 1 Stratospheric Age Tracers

Instrument	Period	Latitude	SF_6	N_2O	CH_4
ACE-FTS	2004-present	−85 to 85	x	x	x
ATMOS-SL3	1985	−47 to −51 and 26–35	x	x	x
ATMOS-ATLAS-1	1992	−55 to 0 and 0–31	x	x	x
ATMOS-ATLAS-2	1993	−50 to −10 and 63–68	x	x	x
ATMOS-ATLAS-3	1994	−65 to −73 and 3–49	x	x	x
Aura-MLS	2004-present	Global		x	
Aura-HIRDLS	2004–2008	Global		x	x
CRISTA	1994	−59 to 64		x	x
CRISTA-2	1997	−74 to 74		x	x
Grille-SL1	1983	−68 to 43		x	x
ILAS	1996–1997	57–73 and −63 to −88		x	x
ILAS-II	2003	56–70 and −63 to −88		x	x
MIPAS	2002–2012	−87 to 87	x	x	x
Nimbus-7 SAMS	1979–1981	−50 to 68		x	x
Odin-SMR	2001-present	Global		x	
UARS-CLAES	1991–1993	−80 to 34 and −34 to 80		x	
UARS-HALOE	1991–2005	−80 to 34 and −34 to 80			x
UARS-ISAMS	1991–1992	−80 to 34 and −34 to 80		x	

Note. Note, for solar occultation measurements, sunrises, and sunsets sample different latitudes.

measure many tracers that can be used to infer age of air. Vertically resolved measurements of more than 40 trace gases are retrieved routinely, including SF_6, N_2O, CH_4, CFC-11, CFC-12, HCFC-22, CCl_4, CFC-113, CH_3Cl, and H_2O. However, due to SCISAT's high inclination orbit, 3 months of measurements are required to sample all latitudes. In addition to the study by Schoeberl et al. (2005), SF_6 measured by ACE-FTS has recently been used to infer age of air using the convolution method described in Section 4.1 over the observation period from 2004 to 2021 (see Section 4.4 and Saunders et al., 2024). ACE-FTS measurements have been validated through comparisons with other satellites. ACE-FTS and MIPAS climatologies generally agree well (see Section 4.4), and more detailed comparisons found that ACE-FTS and MIPAS SF_6 profiles agree to within 10% globally and agree within one standard deviation with in situ balloon profiles (Saunders et al., 2024). An earlier ACE-FTS SF_6 product compared well with the SLIMCAT 3D chemical transport model over all altitudes (Brown et al., 2022). ACE-FTS and MIPAS CH_4 measurements have been compared by Plieninger et al. (2016). Comparisons of ACE-FTS N_2O with MIPAS and Aura-MLS were presented by Sheese et al. (2017).

MIPAS was an infrared limb-emission sounder on Envisat (Fischer et al., 2008). It operated between 2002 and 2012 from a sun-synchronous polar orbit and provided about 1,300 trace gas profiles per day (about 1,000 profiles per day before 2005). Global vertically resolved distributions of SF_6, N_2O, CH_4, CFC-11, CFC-12, HCFC-22, CCl_4, CFC-113, CH_3Cl, and H_2O were derived, among others, from the spectral data over the full mission lifetime. Most data products have been retrieved by four different processors run by four scientific teams. We focus here on the official data record released by ESA (https://earth.esa.int/eogateway/instruments/mipas/products-information, last access 18 September 2023), and the one produced by a research data processor run within a collaboration of Institute of Meteorology and Climate Research, Karlsruhe Institute of Technology (IMK-KIT) and Instituto de Astrofisica de Andalucia (IAA), CSIC (https://www.imk-asf.kit.edu/english/308.php). These data are referred to as IMK/IAA data in the following. The other two data records have been retrieved by the University of Oxford (see http://eodg.atm.ox.ac.uk/MIPAS/, last accessed on 9 June 2023), and by CNR-ISAC—Istituto di Scienze dell'Atmosfera e del Clima del Consiglio Nazionale delle Ricerche (CNR-ISAC), Bologna, Italy (https://www.isac.cnr.it/~rss/mipas2d.htm, last accessed 9 June 2023).

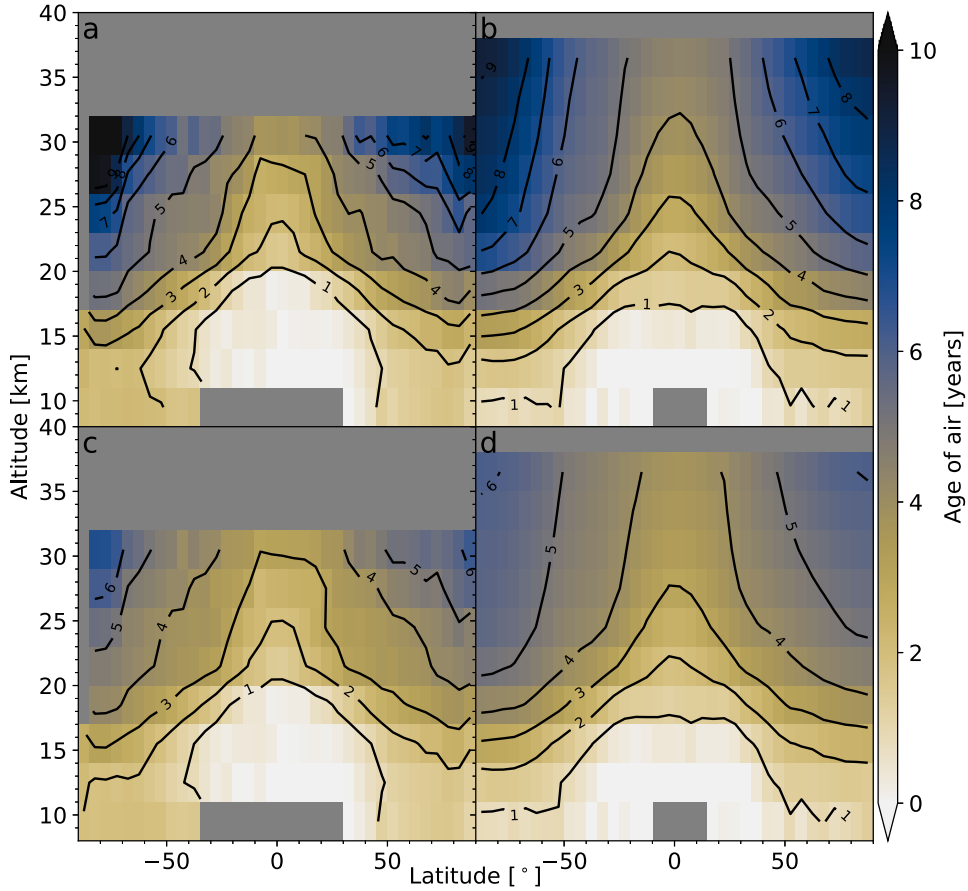

Figure 5. Global mean age climatologies from satellite data, based on (a) Atmospheric Chemistry Experiment Fourier Transform Spectrometer (ACE-FTS) v3.5/3.6 (2004–2020), (b) MIPAS V5R_224/225 (2005–2012), (c) ACE-FTS sink-corrected, and (d) MIPAS sink-corrected. Data are zonally averaged, and averaged over all available years.

The demonstration that MIPAS spectra contain information on SF_6 distributions was provided by Burgess et al. (2004) who presented mean profiles for various latitudes derived from MIPAS spectral measurements in September 2002. Currently SF_6 is only retrieved with the IMK/IAA processor. The first global data record for the early mission years from 2002 to 2004 were provided by Stiller et al. (2008). Stiller et al. (2012), and Haenel et al. (2015) used improved MIPAS data versions and extended the data record to the full mission lifetime. Stiller et al. (2008, 2012), and Haenel et al. (2015) derived an age of air monthly zonal mean data set that covered, for the first time, the full globe up to about 40 km altitude and, in its last version, also the full 10 years of MIPAS' operation time (see Figure 5). Linear trends over the 10 year record of age depending on latitude and altitude were also derived. They showed an unexpected change of the Brewer-Dobson circulation with air becoming younger in the Southern hemisphere and the tropics, while becoming older in the Northern hemisphere. Stiller et al. (2017) traced this behavior back to a shift of the tropical pipe as part of natural variability over the observation period. MIPAS age has been widely used for model evaluation (e.g., Abalos et al., 2021; Eichinger et al., 2019, see also Section 5), and many other applications, for example, to determine the atmospheric lifetime of SF_6 (Kovács et al., 2017).

Methane and nitrous oxide belong to the standard products of MIPAS and are also made available by ESA. Their latest data version, version 8.22, is derived from the spectral version 8.03 and available via https://doi.org/10.5270/EN1-c8hgqx4 (Dinelli et al., 2021; Raspollini et al., 2022). The latest data version of CH_4 and N_2O from MIPAS IMK/IAA so far was provided by Glatthor et al. (2023). The previous data version, published by Plieninger et al. (2015) and validated by Plieninger et al. (2016) was found to have a high bias of CH_4 in the order of 0.1 ppmv below about 25 km altitude, while for N_2O, comparisons to other instruments were inconclusive with

respect to a bias. Further tracers available from the ESA processing are CFC-11, CFC-12, HCFC-22, CCl_4, CH_3Cl, and H_2O. All these data products, and additionally, CFC-113 and CO, are also available from the IMK/IAA processor.

Next to SF_6-based mean age, vertically and latitudinally resolved stratospheric circulation distributions (von Clarmann et al., 2021, see also Section 4.5) were derived from the IMK/IAA MIPAS data of SF_6 (Haenel et al., 2015), CFC-11, CFC-12, and HCFC-22 (Stiller et al., 2023), H_2O (Milz et al., 2009; von Clarmann et al., 2009), CCl_4 (Eckert et al., 2017), and CO (Funke et al., 2009). Zonal means of tracers from the IMK/IAA MIPAS and ACE-FTS data processors were calculated and compared to the products of other satellite instruments (UARS-HALOE, Odin-SMR, ACE-FTS, Aura-MLS, Aura-HIRDLS) within the SPARC Data Initiative (Hegglin & Tegtmeier, 2017; Hegglin et al., 2021; Tegtmeier et al., 2016). The zonal mean data are available from zenodo (https://zenodo.org/record/4265393, Hegglin et al. (2020, 2021)).

4.4. Summary of Currently Available Observational Age Products

As discussed in the last sections, both additional in situ as well as satellite-based remote sensing age data have become available for the last decades. Based on the consolidated method presented in Section 4.1.5, mean ages based on SF_6 observations were re-calculated for data from two satellite missions (ACE-FTS v3.5/3.6 and MIPAS V5R_224/225) as well as a large number of balloon and aircraft-based in situ observations (see Table 1; spanning from years 1975–2017 for balloon data and 1991 to 2023 for aircraft data). Mean age based on CO_2 was not re-calculated, as this will require additional refinement of the method to account for the seasonal cycle in CO_2. Therefore, mean ages based on CO_2 is provided for calculations as originally published. In addition to the new calculation method of SF_6-based mean ages, those ages are also provided with the sink correction scheme applied that was recently developed by Garny, Eichinger, et al. (2024).

Satellite-based instruments provide information on the global climatological distribution of mean age (see Figure 5). Both products suggest very old air in the high-latitude stratosphere with mean ages above 8 years. When applying the sink correction, mean ages are reduced to below 6 years. MIPAS and ACE-FTS based mean ages agree generally very well (see also Figures 6 and 10 for profiles). Discrepancies in the tropics likely arise from sparse sampling by ACE-FTS is this region. In Figure 6, the satellite-based mean ages are compared to profiles based on averaged balloon and aircraft data for five latitude bands. Note that the number of available measurements drastically varies between the latitude bands, with the highest data density in northern hemisphere mid-latitudes (see Figure S4 in Supporting Information S1). In particular the balloon profiles are only based on 2 and 3 flights in the tropics and northern high-latitudes, respectively, limiting their representativeness. At northern high-latitudes, one of the three profiles is taken in March within the polar vortex (Ray et al., 2017), with extremely old air (see also Figure S5 in Supporting Information S1 for seasonally resolved profiles), and the older ages in the balloon data compared to the satellite data likely result from this over-representation of polar vortex air in the average balloon profile. Overall, but in particular at northern mid-latitudes, where most data is available, mean ages from different data sources agree remarkably well. The mean ages from SF_6 without the sink correction show a clear bias toward older age compared to the CO_2 mean ages, but upon application of the sink correction this bias is clearly reduced. This can be seen more clearly when comparing concurrent observations of CO_2 and SF_6 mean ages in a scatter diagram (see Figure 7), demonstrating the improved agreement in particular for older air. For very young air, mean ages from CO_2 are problematic due to the seasonal cycle, thus only ages above 1 year are compared here. Figure 7 further demonstrates that the effect of the new consolidated calculation method applied for SF_6-based data overall has a relatively small effect, but is still desirable to exclude methodological reasons for disagreement between data sets.

Overall, the available in situ and remote sensing mean age data has substantially improved in quality and also became much more consistent. In northern mid-latitudes, the available in situ data appears to be rich enough to have converged to climatological values, while the limits in terms of spatial and temporal representativity remains valid at other latitudes. Given the good agreement between in situ and remote sensing data at northern mid-latitudes, the remote sensing mean age climatologies can confidently be used for scientific studies and model evaluation (see Section 5). At the same time, filling gaps in in situ observation will remain of high importance to evaluate remote sensing data, specifically in the tropical and southern hemispheric stratosphere.

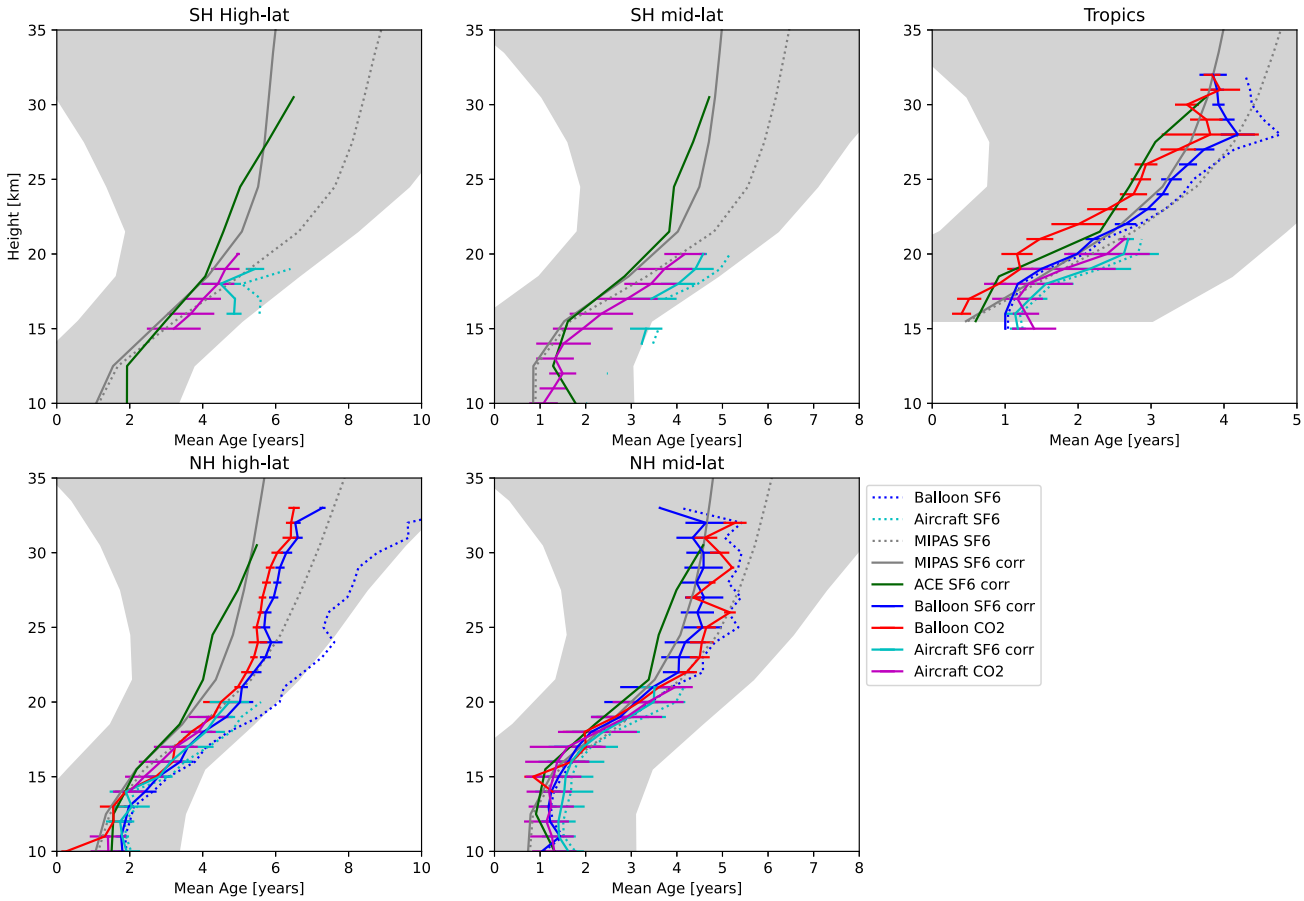

Figure 6. Mean age profiles averaged over high-latitudes (90°–60°), mid-latitudes (60°–30°) of each hemisphere, and tropics (−30° to 30°) from SF_6 satellite data (MIPAS, gray dashed line uncorrected mean, solid line sink-corrected mean, and gray shading displays range of ±1 standard deviation of the sink-corrected data) and from ACE (darkgreen, shown is only the sink-corrected mean) and averaged over available balloon flights (blue dotted: SF_6 mean ages; blue solid: SF_6 mean ages with the sink correction applied; red: CO_2 mean ages) and averaged over available aircraft flights (light-blue dotted: SF_6 mean ages; light-blue solid: SF_6 mean ages with the sink correction applied; magenta: CO_2 mean ages).

4.5. Age-Related Transport Diagnostics From Observed Tracers

4.5.1. Empirical Age Spectra From Measured Tracers

The calculation of age spectra from trace gas measurements is a challenging problem primarily due to the limited ability of any single trace gas to constrain the full shape of the age spectra. Initial efforts focused on trace gases such as CO_2, H_2O or CH_4 (A. E. Andrews et al., 1999; A. E. Andrews, Boering, et al., 2001; Johnson et al., 1999), which have unique growth rates and/or seasonal variability, or trace gases such as N_2O and other photolytic tracers (Ehhalt et al., 2007; Schoeberl et al., 2000, 2005), which are shorter lived and thus sensitive to different parts of the age spectra. The sensitivity of stratospheric age spectra to a wide range of trace gases with different lifetimes and variability was described in Podglajen and Ploeger (2019).

Recent estimates of age spectra have focused on the troposphere and lower stratosphere where transport times from the surface can be very short (hours to days) and thus require the addition of trace gases with shorter lifetimes than those considered in the stratosphere. Age spectra for transport from the NH to SH surface (Holzer & Waugh, 2015), in the tropical Pacific (Luo et al., 2018) and the North American monsoon UT/LS (Ray et al., 2022) made use of a wide range of trace gases to define basic features of the age spectra in these regions.

Issues still remain in estimating the full age spectra from trace gas measurements in either the troposphere or stratosphere. In particular, while the above studies were able to constrain the mean, mode and width of the age

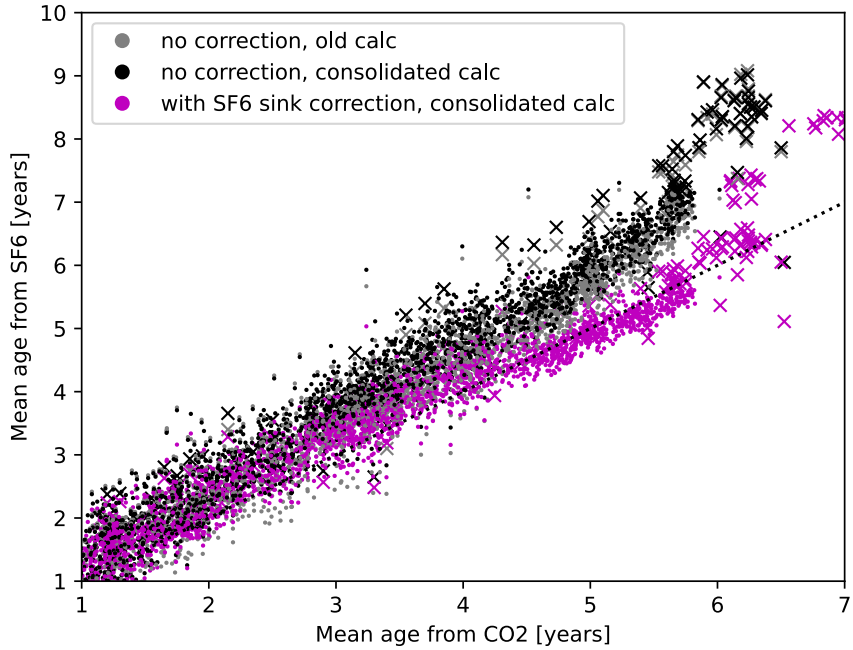

Figure 7. Mean age from aircraft data (dots) and balloon profiles (crosses) from concurrent observations of SF_6 and CO_2 for mean ages with the originally published calculation (gray), with the consolidated method for SF_6 (black), and in addition with the SF_6 sink correction applied (magenta).

spectra they were generally unable to constrain more detailed features such as those due to seasonal and interannual variability or the shape of the long tail out to many decades.

4.5.2. Transport Diagnostics Beyond Age

Deriving stratospheric transport characteristics from observed trace gases can be challenging (see Section 4.1), and often only a limited set of species is available from specific observational platforms. Therefore, transport diagnostics from other trace gas species than the usual age tracers have often been utilized as alternative or complementing approach to characterize stratospheric transport. This section briefly summarizes such past approaches based on water vapor, the CO_2 seasonal cycle, and the general inversion of the trace gas continuity equation. Another diagnostic framework that has been applied often to understand transport are tracer-tracer relationships. Given two independent tracers with different sources or sinks are transported by the same circulation, shifts in tracer-tracer correlations can indicate circulation changes (e.g., Bönisch et al., 2009). Tracer-tracer correlations were extensively reviewed by Plumb (2007), and we refer the reader to this review for further information.

Most water vapor enters the stratosphere through the tropical tropopause layer, where extremely low temperatures cause dehydration through freeze-drying (Fueglistaler et al., 2009). The annual cycle in tropical tropopause temperatures is imprinted on the water vapor concentrations, which are then propagated upward by the BDC, creating the water vapor tape recorder signal first identified by Mote et al. (1996). This tape recorder signal has been used as a diagnostic of the upwelling circulation (Flury et al., 2013; Niwano et al., 2003; Schoeberl et al., 2008), but significant vertical mixing in the lowermost stratosphere (Glanville & Birner, 2017) and the contribution of methane oxidation in the middle and upper stratosphere mean that it has only a weak correlation with either the diabatic or residual circulation (Linz et al., 2019). The attenuation of the water vapor anomalies as they move upward through the stratosphere has been used to provide constraints on vertical diffusion and mixing of extratropical air into the tropics (Mote et al., 1996). Such analysis can only provide upper limits on the two effects since their impacts on the signal are similar.

Similarly, the conservation property of stratospheric total water $H_2O_e + 2\alpha CH_4$ has been used to deduce changes in stratospheric age of air by Hegglin et al. (2014), and the method has been further evaluated by Poshyvailo-

Strube et al. (2022). In this approach, the change in stratospheric water vapor is divided into changes in stratospheric entry water vapor and methane and changes in the methane fractional release factor

$$\Delta H_2O = \Delta H_2O_{[e]} + 2\,\alpha\Delta CH_{4[e]} + 2CH_{4[e]}\Delta\alpha. \quad (19)$$

Here, the stratospheric entry values, denoted by a subscript $[e]$ have been diagnosed at the tropical tropopause and propagated to the stratospheric location under consideration, and the change in the fractional release factor $\alpha = 1 - \frac{CH_4}{CH_{4[e]}}$ are mainly caused by changes in the stratospheric circulation and can be translated into changes in mean age of air based on the compact correlation between fractional release and age (Hegglin et al., 2014). The advantage of the total water method is the better availability of high quality stratospheric water vapor observations compared to observations of long-lived age tracers. However, the method is based on a number of approximations, like uniformity of the α-age correlation and assumptions on propagation of entry mixing ratios, which could have significant effects on the estimated age change (Poshyvailo-Strube et al., 2022).

Another trace gas with a seasonal cycle at the tropical tropopause is CO_2. The propagation of the seasonal cycle upward and poleward has been used to estimate tropical upwelling rates and outward mixing from the tropics to the extratropics, respectively, using N_2O as the vertical coordinate (Boering et al., 1996). The N_2O vertical coordinate allows the combination of tropical and extratropical data, since both are influenced similarly by seasonal and Quasi-Biennial Oscillation (QBO) variations in lower stratospheric transport resulting in a compact N_2O-mean age correlations across latitudes and seasons (Plumb & Ko, 1992). The seasonal cycle and long-term trend together have been used to derive an empirical age spectrum for the tropical lower stratosphere (A. E. Andrews et al., 1999) and for the midlatitude lower stratosphere (A. E. Andrews, Boering, et al., 2001). Similar to water vapor, CH_4 oxidation must be accounted for in the analysis, and the use of N_2O as a vertical coordinate limits the usefulness of the derived upwelling velocities because the location of N_2O isopleths vary seasonally.

A particularly elegant method to infer transport properties from trace gas measurements is the direct inversion of the tracer continuity equation. This approach, as developed in the Analysis of the Circulation of the Stratosphere (ANCISTRUS) model (von Clarmann & Grabowski, 2016, 2021), provides meridional circulation velocities and eddy mixing coefficients from mixing ratios of a suite of trace species. Advantages of this approach are the direct deduction of circulation vectors without the detour via age of air, the insensitivity to chemistry outside the region of interest such as the mesospheric SF_6 when evaluating stratospheric transport, and the potential to use a variety of non-ideal chemical tracers by integrating stratospheric chemistry effects in a straightforward manner. On the other hand, in all past applications the mixing coefficients have been further constrained due to the mathematical complexity of the inversion, such that resulting velocities have to be interpreted as effective velocities including both advection velocities and eddy transport contributions. Figure 8 presents an example of the effective velocity fields derived with ANCISTRUS. In this specific case, the mixing coefficients were forced to zero by regularization. These effective velocities thus include also the contributions of mixing. For more details, see von Clarmann et al. (2021).

5. Age of Air in Models

Age of air is a useful diagnostic for evaluating stratospheric transport in atmospheric models. This diagnostic can be applied to a variety of different models, including Chemistry Transport Models (CTM), comprehensive Chemical Climate Models, and also idealized models like 2D zonal mean models, box models, or TLP models (see Section 3). These models generally apply very different resolutions, numerical schemes for advection and vertical diffusion, and age of air diagnostics are frequently used for model transport assessments (e.g., Abalos et al., 2021).

5.1. Implementation of Age Tracers in Models

The most common age of air diagnostic used is the mean age. Alternatively to the calculation of mean age as first moment of the age spectrum, stratospheric mean age can be more easily calculated in models following one of two common approaches. First, mean age can be calculated by advecting an inert "clock-tracer" with a linearly increasing source at a boundary surface in the troposphere. By comparison of the observed stratospheric mixing ratio and the tropospheric reference time series the mean age can be estimated simply by the lag time between the time series (see Section 2). The second approach solves the ideal age equation (Equation 6) using a tracer with

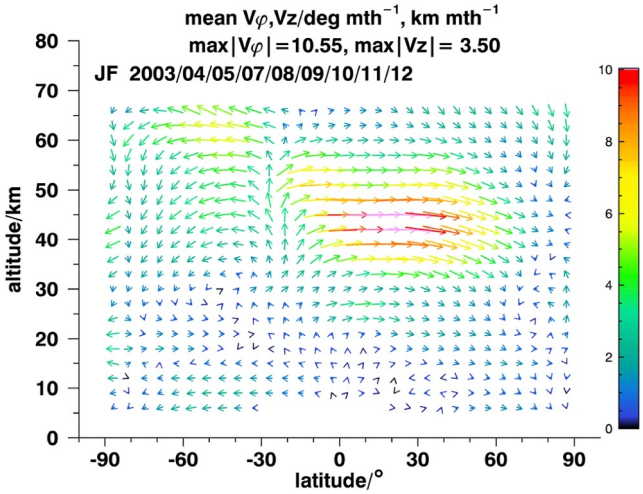

Figure 8. Mean monthly circulation pattern for January–February, derived from zonal mean distributions of the trace gases SF_6, CFC-11, CFC-12, HCFC-22, CCl_4, N_2O, CH_4, H_2O, and CO, and the years given by the header, from MIPAS observations. Maximum velocities in meridional and vertical direction are also provided by the header. The color coding and length of the arrows is given by $\sqrt{(\nu_\phi degree^{-1} month)^2 + (\nu_z km^{-1} month)^2}$ for ν_ϕ and ν_z in units of degree per month and kilometer per month. Pink arrows refer to velocities higher than representable by the color scale chosen. For more details, see von Clarmann et al. (2021).

constant boundary value and a global "chemical" unit source (Hall & Plumb, 1994). Commonly used source boundaries are the tropopause or the surface, with respective mean ages differing by the tropospheric transport time scale. The exact definition of source boundary surfaces needs to be considered when intercomparing mean age from different models.

Calculation of the full age of air spectrum has only been realized in a few models, so far (Fritsch et al., 2020; F. Li et al., 2012; Ploeger & Birner, 2016). Such calculations are based on a suite of multiple "pulse tracers," inert tracers with a delta distribution-like pulse emission at the boundary surface. Specifically, given N inter pulse tracers with pulses at source times t_i, and hence source time history $\chi_{0i}(t) = \delta(t - t_i)$ (here i labels the N different tracers), Equation 2 reduces to

$$G(r,t,t_i) = \chi_i(r,t). \tag{20}$$

Therefore, the age spectrum can be directly inferred from the pulse tracer mixing ratios. Mathematically, this approach is known as deriving the Green's function as fundamental solution of the tracer transport equation (e.g., Holzer & Hall, 2000, see also Section 2). Equation 20 shows that the age spectrum resolution along transit time depends on the frequency of tracer pulse emissions. Details in implementing the pulse tracers in models, such as emission frequency and pulse duration, need to be considered when inter-comparing different models (for more details on the method see e.g., Ploeger & Birner, 2016). Comparison of mean age calculated as first moment of the age spectrum and from a linearly increasing clock-tracer shows that the results from both methods are generally consistent, but that the first moment of the spectrum critically depends on the length of the spectrum tail resolved by the simulation (Ploeger & Birner, 2016, Figures 4 and A1).

Next to age of air, model studies have also employed other realistic and artificial tracers to study transport. Realistic tracers can be used for direct comparisons of transport-related diagnostics to observational data, for example, the water vapor tape recorder (see Section 4.5). Commonly employed artificial tracers include tracers with specific source regions and a fixed exponential decay, targeted toward a special region or transport barrier. To name one of many examples, the so-called e90 tracer with constant surface emissions and an e-folding lifetime of 90 days was designed and employed to study troposphere-stratosphere transport (Abalos et al., 2017, 2020; Orbe et al., 2020).

5.2. Mean Age in Global Model Simulations

The climatological mean age distribution from the newest generation chemistry-climate models (CCMI2 multi-model mean [MMM]) and reanalyses-driven transport model simulations (multi-reanalysis mean) is compared in Figure 9, and for comparison the satellite climatologies are repeated from Figure 5. The general characteristics in stratospheric mean age in the different data sets are qualitatively similar. Low mean age values are present in the tropical stratosphere, the region of upwelling of young tropospheric air into the stratosphere, and age increases with altitude and latitude. However, quantitatively the data sets show significant differences. Highest mean age are found for the satellite observations. Applying the SF_6 sink correction decreases these high age values and reduces the difference to models. The climate model mean age shows generally lowest values, while reanalysis-based mean age are similar to the satellite observations. The inter-model spread (Figure 9, black contours) shows larger differences between reanalyses (up to 1.2 years) than climate models, which is related to significant differences in the climatological strength of the stratospheric circulation in current reanalyses (Ploeger et al., 2019, 2021). While the uncertainty across models is largest at higher levels and latitudes (up to 0.8 years spread in mid- and high latitudes above 30 hPa), the largest spread between reanalyses occurs in the lower stratosphere.

Mean age of air from climate models is compared to different observations at 20 km altitude and in terms of vertical profiles in the tropics and northern mid and high latitudes in Figure 10. In agreement with Section 4.4, observational climatologies are generally in good agreement with each other and are thus a good basis to evaluate

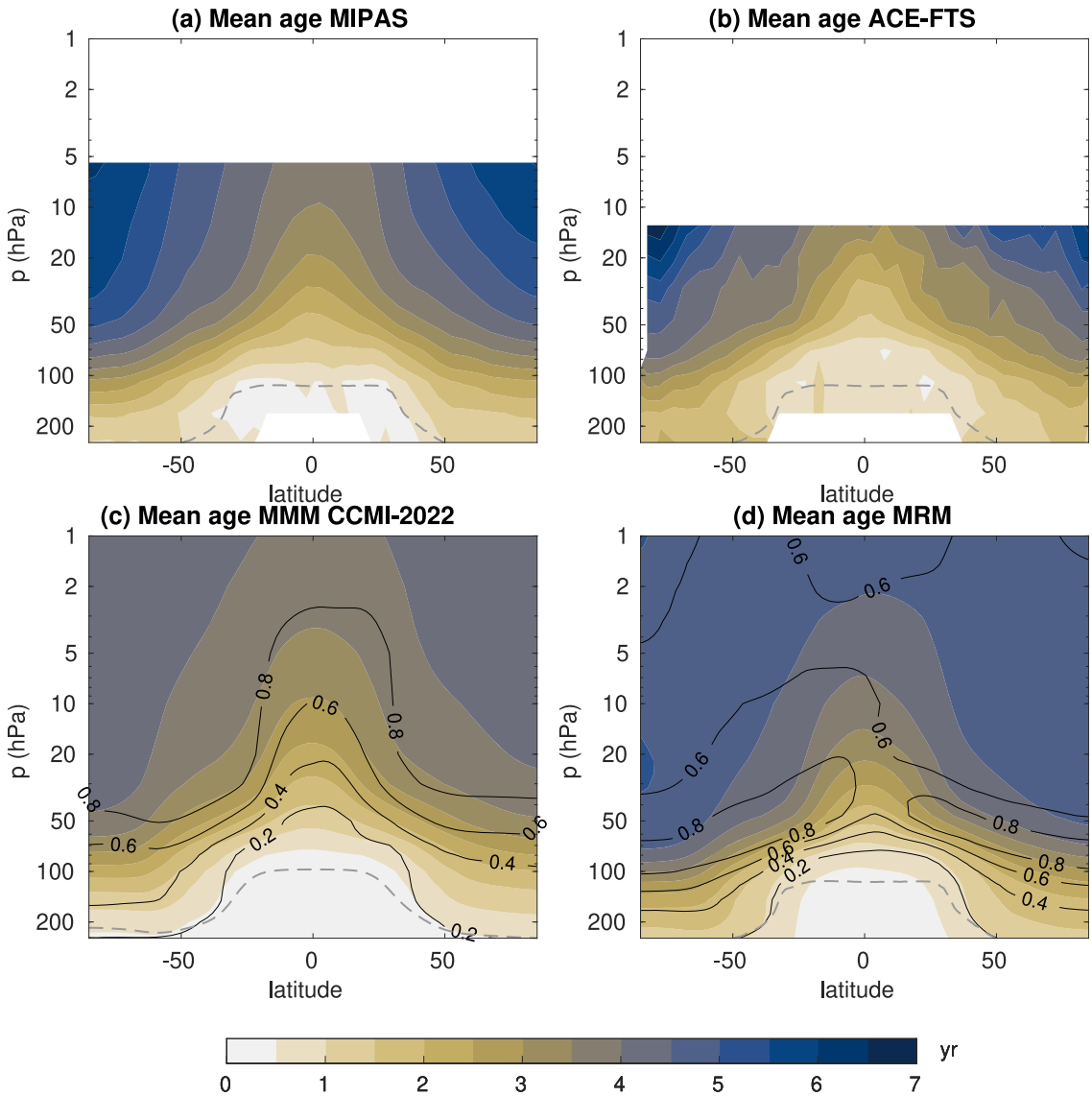

Figure 9. Zonal mean distribution of mean age of air from observations, chemistry-climate models and reanalyses. (a) MIPAS, (b) Atmospheric Chemistry Experiment Fourier Transform Spectrometer (ACE-FTS). Both satellite-based mean ages are sink corrected, same data products as in Figures 5c and 5d. Panel (c) same, but for multi-model mean (MMM) of 7 CCMI2 models (refD1 simulations). (b) Same, but for multi-reanalysis mean (MRM) from CLaMS offline-model simulations driven with ERA5, ERA-Interim and JRA55 reanalysis data. Black contours show the standard deviation, in years, across the models/reanalyses in panels (c) and (d). The dashed gray lines depict the thermal tropopause for the MMM (c) and MRM (a), (b), and (d). Time average is from 2002 to 2012, except for ACE-FTS (2005–2012).

models, which remained difficult even in recent work (e.g., Abalos et al., 2021). An exceptions from the good agreement is the high-latitude in situ profile, likely because of poor representativeness given it is based on only few balloon flights. In general, climate models still underestimate stratospheric mean age across latitudes and altitudes. We can report clear improvement compared to the climate models from two decades ago as presented by Waugh and Hall (2002), with an increase in the MMM of roughly 1 year at all latitudes at 20 km altitude. Over the different generations of model intercomparison projects, progress could be reported between CCMVal-2 and CCMI-1 (Dietmüller et al., 2018), but since then the still overall large spread across models appears to stagnate (for CMIP6 and CCMI-2022 see Abalos et al., 2021, and Figure 10, respectively).

The inter-model differences in age of air are related to differences in the representation of circulation and of transport processes in different models. In general, differences in residual circulation and mixing processes are both responsible for the spread in age of air between models, although eddy mixing effects appear to be the dominant factor to explain inter-model differences (Dietmüller et al., 2018; Gupta et al., 2021). Furthermore, age

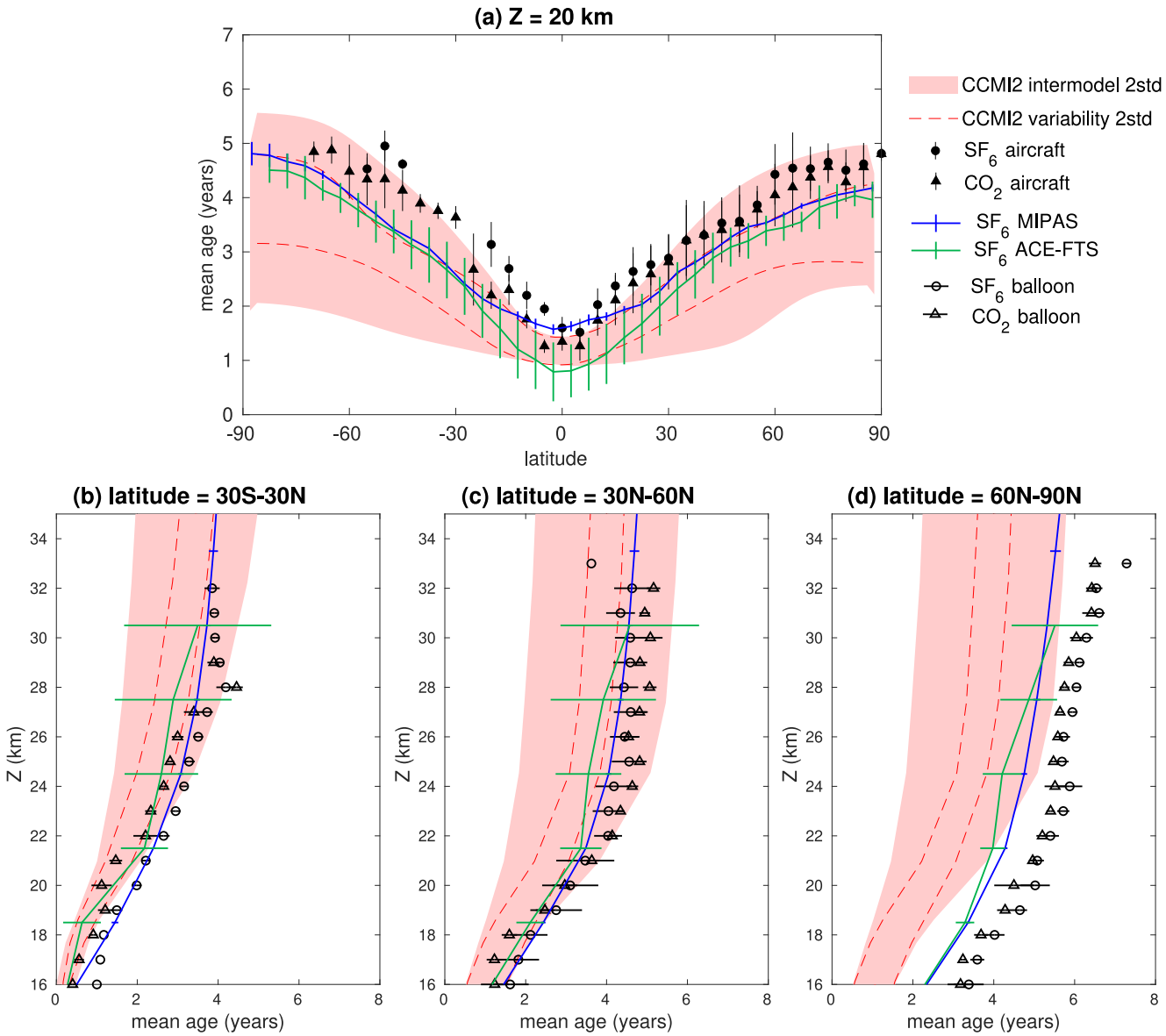

Figure 10. (a) Latitudinal structure of mean age of air at 20 km from observations and models as a function of latitude. (b–d) Mean age vertical profiles in the tropics (30°S–30°N), mid-latitudes (30°N–60°N) and high latitudes (60°N–90°N). In situ aircraft and balloon observations as described in Section 4.4, (black symbols), satellite estimates include MIPAS (blue) and Atmospheric Chemistry Experiment Fourier Transform Spectrometer (green). All SF_6-based ages have been corrected for the chemical sink. Model data is from CCMI2 refD1 simulations from 6 models, averaged over 1975 to 2018, with the intermodel spread shown as the two standard deviation range across models (shading), and the interannual and intraseasonal variability is shown as the two standard deviation averaged for all models (dashed lines).

of air model differences can be caused by differences in model numerics and related differences in numerical diffusion. In this regard, differences in model resolution as well as in the dynamical core may cause substantial differences in stratospheric age of air due to differences in resolved circulation and in the numerical representation of transport processes (Gupta et al., 2020, 2021). Similarly, differences in the representation of trace gas transport have been shown to affect stratospheric age of air, with a more diffusive transport scheme resulting in younger air in most regions of the stratosphere (Charlesworth et al., 2020).

5.3. Age Spectra in Models

The age spectrum by definition resolves the transit time scales of the different transport pathways and processes and can be used as a diagnostic for residual circulation, mixing, and diffusion. In particular, the modal age of the spectrum, the transit time of the highest spectrum peak which is characterizing the most probable transit time, is

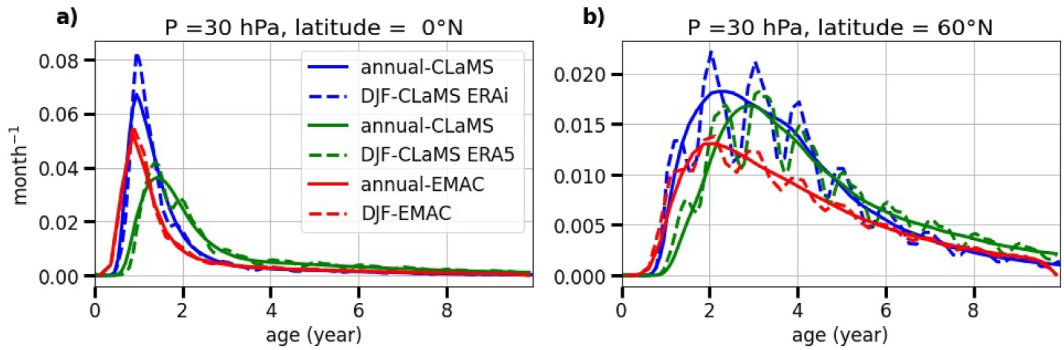

Figure 11. Tropical and extratropical age spectra from comprehensive models: Chemistry Transport Models simulations with CLaMS driven by the reanalysis ERA-Interim (blue) and ERA5 (green) taken from Ploeger et al. (2021) and GCM simulations with EMAC (red) taken from Fritsch et al. (2020). Note that the resolution along the transit time axis differs between CLaMS (1 month) and EMAC (3 months), which contributes to smooth the peaks in EMAC relative to CLaMS.

mainly affected by the bulk transport as related to the residual circulation (Waugh & Hall, 2002). Strahan et al. (2009) found good agreement between modal ages and the time scale of residual circulation upwelling in the tropical pipe. A global analysis of model age spectra further showed that in the tropical lower stratosphere and in the wintertime middle to high-latitude stratosphere (above about 500 K) the age spectrum modal age is a good proxy for residual circulation timescales (Ploeger & Birner, 2016), in agreement with results from the conceptual TLP model (see Section 3.1). The age spectrum tail, on the other hand, is strongly affected by mixing processes and recirculation of aged air into the tropics, such that recirculation changes can be diagnosed from changes in the age spectrum tail (F. Li et al., 2012).

Age spectra therefore could serve to reveal the influence of different processes on transport times in comprehensive models. However, the high number of pulse tracers necessary to derive age spectra so far limits the available model simulations of age spectra. Here, we discuss exemplarily the comparison of age spectra from two CTM simulations (with CLaMS) and one free-running global model simulation (EMAC). The spectra from the comprehensive models show more detailed structure in the age spectra compared to the idealized TLP model-based spectra discussed in Section 3.1, as more detailed transport processes are included (Figure 11). Consequently, the structures in age spectra in the real atmosphere and in models with increased resolution (which resolve more details on transport processes) can be expected to be even more plentiful. The annual peaks in the age spectra are clear imprints of the seasonality in stratospheric transport (Ploeger & Birner, 2016; Reithmeier et al., 2008), and are absent in annual mean spectra. The prominence of these multiple spectrum peaks depends on the model transport and likely degrades for more diffusive transport schemes (as here for EMAC compared to CLaMS).

The comparison between the spectra for the different models in Figure 11 shows that stratospheric age spectra are very sensitive to inter-model differences in transport. Significant differences exist both between different models (EMAC, CLaMS) and between different reanalysis used to drive the same model (CLaMS driven with ERA5 and ERA-Interim). The difference in the modal ages in the tropical age spectra, for instance, must be caused by differences in tropical residual circulation upwelling and/or vertical diffusion in the models (compare the TLP-model discussion in Section 3.1). The fact that the decrease in modal age coincides with a decrease in the spectrum tail points to differences in residual circulation upwelling as a cause for the spectra differences. As the EMAC model spectrum shows the youngest modal age, this indicates that the model has the fastest tropical upwelling, whereas ERA5 upwelling being slowest and ERA-Interim upwelling being in between (Figure 11), in agreement with previous reanalysis inter-comparisons (Ploeger et al., 2021). The lower height of the maxima together with a shift to younger peak transit times could indicate stronger vertical diffusion in EMAC compared to both CLaMS simulations, consistent with work by Charlesworth et al. (2020) and with the TLP model results presented in Section 3 (note that increased horizontal diffusion could enhance aging by mixing). Overall, age spectra appear to be very valuable diagnostics to quantify such model transport differences and to identify model deficits.

6. Age-Of-Air Variability and Trends

The stratospheric Brewer-Dobson circulation is affected by various modes of variability which also imprint on stratospheric age of air. Next to irregular internal variability of the atmosphere, the most relevant quasi-periodic variability factors include the QBO and the El Niño Southern Oscillation (ENSO). Moreover, variations in stratospheric aerosol optical depth due to volcanic eruptions can cause variations in age, and anthropogenic factors like changes in ODS and GHG can lead to forced long-term trends.

6.1. Interannual Variability in Age

The QBO is known to modulate tropical upwelling by inducing anomalously strong upwelling during easterly shear phase and anomalously weak upwelling during the westerly shear phase. The QBO also affects mixing between tropics and extratropics, which weakens during the easterly shear phase and strengthens during the westerly shear phase (Baldwin et al., 2001). Hence, anomalously low (high) mean age is found in the tropical lower stratosphere during easterly (westerly) shear phase, and this signal further propagates through the stratosphere (e.g., Diallo et al., 2012).

ENSO is characterized by increased upwelling during positive (El Niño) phase which decreases age of air, and by decreased upwelling and increased age of air during negative La Niña phase (Calvo et al., 2010; Konopka et al., 2016). Moreover, ENSO causes structural changes in the stratospheric circulation pattern, with the shallow Brewer-Dobson circulation branch shifting upwards during El Niño phase (Diallo et al., 2019).

Volcanic aerosol following strong eruptions reaching the stratosphere affects atmospheric temperatures with implications for wave propagation and circulation. However, the aerosol effects on the Brewer-Dobson circulation and age of air are controversially debated based on climate models (Muthers et al., 2016) and reanalyses (Diallo et al., 2017).

Another potential factor influencing variability in transport and mixing in the lower stratosphere is the Asian monsoon in boreal summer (e.g., Konopka et al., 2010; Shuckburgh et al., 2009). The Asian monsoon circulation, characterized by strong convection in the troposphere and a confining anticyclonic circulation at upper levels, provides a particularly rapid pathway for air masses into the stratosphere such that variability in the related processes affects variability in lower stratospheric composition and age (e.g., Garny & Randel, 2013). Furthermore, the comparatively high mixing ratios of SF_6 in monsoon air masses complicate the use of this species as an age tracer.

Inter-annual variability in mean age from satellite observations, climate models, and reanalyses is shown in Figure 12 for the tropical and middle latitude stratosphere at 70 and 30 hPa. The power spectra from an FFT analysis of these deseasonalized time series show distinct peaks. The clearest spectral peak occurs at about 28 months and is attributed to the QBO. QBO-related mean age variability is strongest in the tropical stratosphere at 30 hPa, but also emerges clearly from the spectra at other locations, and is stronger in reanalyses than climate models (see also Figure 13).

Further peaks in the spectra between 3 and 7 years are most likely associated with ENSO, and they are relatively stronger in the lower stratosphere (70 hPa) compared to 30 hPa. Amplitudes of age variability are stronger in reanalyses than in climate models (Figure 13). This difference between reanalyses and climate models is most pronounced at even longer periods around 10 years and beyond (not shown). At these longer, decadal timescales, reanalyses show significantly stronger variability compared to climate models. Variations on these time scales are likely related to volcanic aerosol (e.g., after the 1991 Mount Pinatubo eruption), or a combination of different variability modes.

The variability in age deduced from MIPAS observations (black symbols in Figure 12) is similar to the reanalysis-based estimates, demonstrating that global satellite mean age data are well suited for studies of stratospheric variability (see e.g. Haenel et al., 2015; Stiller et al., 2012). However, the available record of about 10 years is rather short for analysis of inter-annual variability. For ACE-FTS mean age data (gray symbols), the available record is longer, but the data is prone to large scatter, likely due to the sparse sampling. Therefore, for an observation-based analysis of inter-annual transport variability improved observations of high sampling and high precision would be beneficial.

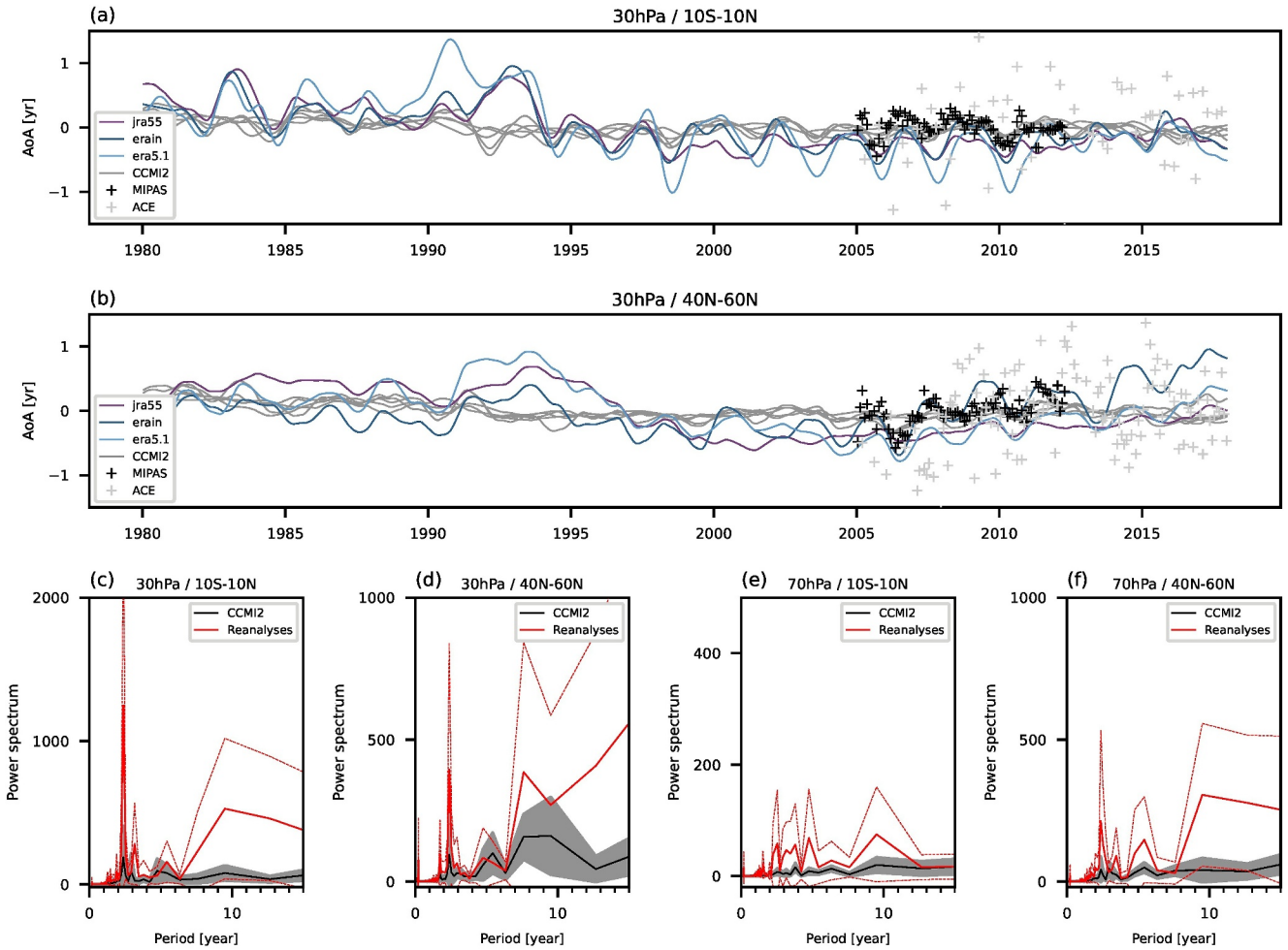

Figure 12. Mean age of air variability in reanalyses and climate models. (a) Deseasonalized anomaly of mean age in the tropics (10°S–10°N) at 30 hPa from CCMI2 climate models (gray), reanalyses (colored), MIPAS (black crosses), and Atmospheric Chemistry Experiment Fourier Transform Spectrometer (gray crosses) satellite data. Panel (b) same, but in middle latitudes (40°N–60°N). (c–f) Power spectrum of mean age variability at 30 and 70 hPa, in the tropics (10°S–10°N) and in middle latitudes (40°N–60°N) for CCMI2 (multi-model mean in black, 1 – σ range as gray shading) and reanalyses (multi-reanalysis mean as thick red, 1 – σ range as thin dashed red lines). Data has been smoothed using 3 and 6 months running means.

An attribution of mean age variability to different drivers based on a multi-linear regression analysis (MLR) is presented in Figure 13 (see Diallo et al., 2017, for details on the method). The variations in age in response to QBO and ENSO are of similar magnitude, and both drivers contribute significantly to age of air variability.

The mean age variations related to QBO and ENSO show distinct patterns throughout the stratosphere. For QBO variability, strongest variations occur in the tropical lower stratosphere, but significant variations extend to middle and high latitudes. The global pattern of QBO variations is qualitatively similar between climate models and reanalyses, though the QBO variability in reanalyses is stronger.

For ENSO-induced mean age variations the differences between climate models and reanalyses are larger than for the QBO. At lower levels, below about 20 km, there is qualitative agreement with El Niño decreasing mean age, and this effect is stronger in reanalyses than climate models. Above, however, the ENSO-induced effects substantially differ between the two data sets. In this region, which is mainly affected by the deep Brewer-Dobson circulation branch, climate models show mean age decreases during El Niño while reanalyses show mean age increases.

Particularly challenging is the interpretation of multi-year and decadal variability in mean age, which may result from low-frequency variability modes in the climate system or from the interplay between different of the above mentioned drivers. In this respect, a link between the Pacific Decadal Oscillation and the stratospheric circulation

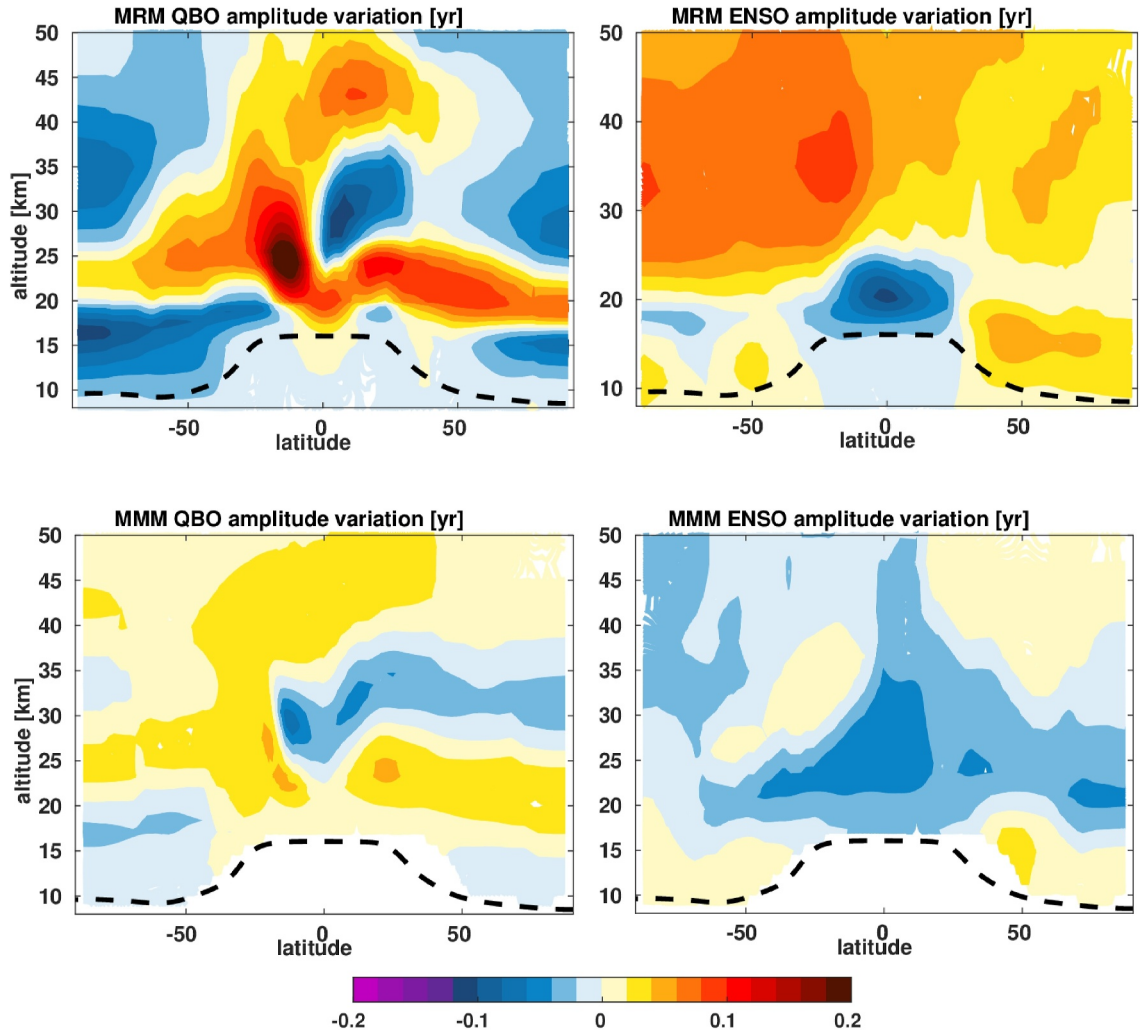

Figure 13. Variability amplitude in mean age of air for the Quasi-Biennial Oscillation and El Niño Southern Oscillation, estimated with a multiple regression over the 1989–2015 time period for (top) reanalyses, and (bottom) for climate models (CCMI2 RefD1 simulations). Shown are multi-reanalysis mean and multi-model means.

has been identified in chemistry climate model simulations with related effects on stratospheric composition (Iglesias-Suarez et al., 2021). Furthermore, the interplay between the QBO and the seasonal cycle has been proposed to cause a robust mean age increase in the Northern hemisphere relative to the Southern hemisphere after the turn of the millennium (Strahan et al., 2020), which causes a structural change in the pattern of the Brewer-Dobson circulation (Han et al., 2019; Ploeger & Garny, 2022). Similarly, Neu et al. (2018) have shown that changes in the relative duration of easterly and westerly shear phases of the QBO can drive decadal-scale circulation variations which make detection of long-term changes in age challenging. In general, multi-year and decadal variability in mean age and relation to drivers of variability appears not well understood, hitherto.

6.2. Long-Term Age Trends

Over the last two decades a large number of studies have investigated the impact of external forcings on stratospheric age. Climate models project an acceleration of the Brewer-Dobson circulation in response to increasing GHG, resulting in an overall decrease in mean age (Butchart, 2014). However, observational estimates of age trends over the last decades have put into question this model result, and a growing body of literature is devoted to understanding this discrepancy. In this section we summarize and describe the current state of knowledge on forced trends in age, guided by the following overarching questions: (a) Do observational and modeled age trends disagree when taking all the uncertainty into account? (b) What degree of confidence do we place in current trend estimates? (c) When will trends become detectable? It is important to note that the term

"trend" here refers to an externally-forced long-term change. Therefore, a linear fit over a short timeseries (less than about 30 years) is not necessarily a trend, as it can be largely affected by internal climate variability.

6.2.1. Drivers and Mechanisms of Age Trends

Studies on the mechanisms driving age trends are largely based on climate models, which project an acceleration of the residual circulation due to the increase in GHG. This residual circulation acceleration was first noted in early climate model experiments (Rind et al., 1990) and has been remarkably robust over many generations of climate models. The residual circulation acceleration speeds up transport and results in a global reduction of mean age throughout the stratosphere (Butchart, 2014). The dynamical mechanism involves an enhancement of wave dissipation in the subtropical lower stratosphere due to the upward shift of the critical lines associated with the strengthening of the upper flanks of the subtropical jets in response to tropical upper tropospheric warming (Garcia & Randel, 2008; Shepherd & McLandress, 2011). While all models consistently show an acceleration of the residual circulation, the contribution of different waves in the forcing is more uncertain, especially for the upper branch of the BDC where the contribution from parameterized gravity waves is largest (Abalos et al., 2021; Butchart et al., 2010). The acceleration of the deep branch is closely connected with trends in the polar vortices, as both are linked to wave dissipation, and both resolved Rossby and parameterized gravity waves are filtered by the zonal wind (Palmeiro et al., 2014). Polar vortex trends are highly uncertain and inconsistent across models in the northern hemisphere. This uncertainty is related to the large inter-annual variability in the polar stratosphere, the counteracting effects of cooling by increased GHG and polar warming due to adiabatic heating by the BDC acceleration, and also to uncertainties in wave generation in the troposphere (Karpechko et al., 2022).

In addition to the effects of GHG, several studies over the last two decades have shown that ozone depletion due to increasing ODS has contributed substantially to the BDC residual circulation acceleration (F. Li et al., 2018; Oman et al., 2009; Lin & Fu, 2013; Polvani et al., 2018). The mechanism involves cooling of the austral polar lower stratosphere in late spring linked to the ozone hole, and associated strengthening of the zonal winds in early summer, which delays the breakdown of the polar vortex and thus allows for enhanced wave propagation in this season and causes a strengthening in the stratospheric circulation (Abalos et al., 2019; F. Li et al., 2018; McLandress et al., 2011; Oberländer et al., 2013). These studies showed that the decline of ODS concentrations thanks to the Montreal Protocol results in a 50% reduction of the global mean stratospheric mean age trend between the periods before and after the year 2000, which corresponds to the peak of ODS concentrations (Figure 14).

While the trends in the residual circulation have received more attention historically, the importance of changes in mixing for the net transport trends has been recognized over the last years. Indeed, Eichinger et al. (2019) found that the residual mean transport alone dominates age trends only in the polar lower stratosphere, whereas in general reduced aging by mixing and recirculation is the dominant contributor to the mean age trends in the CCMI models, although partly related to the residual circulation trends. They also showed that the spread in mean age trends across models can be partly explained by the change in mixing efficiency in the models. In the lower stratosphere, enhanced wave breaking leads to enhanced eddy mixing, while in winter the stronger jets act as stronger transport barriers and reduce eddy mixing (Abalos & de la Cámara, 2020). The connections between changes in mixing estimates and mean age remain an open issue that needs further research. In addition to the changes in mixing, other uncertainties in modeling mean age, discussed in Section 5 can affect the trends, including the diffusion in models, which can be affected by model numerics, transport scheme and resolution, among others (e.g., Charlesworth et al., 2020).

6.2.2. Observational Age Trends Estimates

As described in Section 4, a large number of observational data of mean age have become available over the last decades. In particular, the estimation of long-term trends requires high-quality measurements over multiple decades. To date, the only long-term record of high-quality mean age observational data is available from balloon measurements over NH mid-latitudes. This data set was first published in 2009 (Engel et al., 2009), spanning observations from the time period 1975 to 2005, and was updated later with additional observations from 2015 to 2016 (Engel et al., 2017). The reported trends indicated unchanged age over the considered periods, with trends of $+0.24 \pm 0.22$ years/decade (Engel et al., 2009) and 0.15 ± 0.18 years/decade (Engel et al., 2017), respectively. The observational mean age trends come along with large error bars which result from a combination of

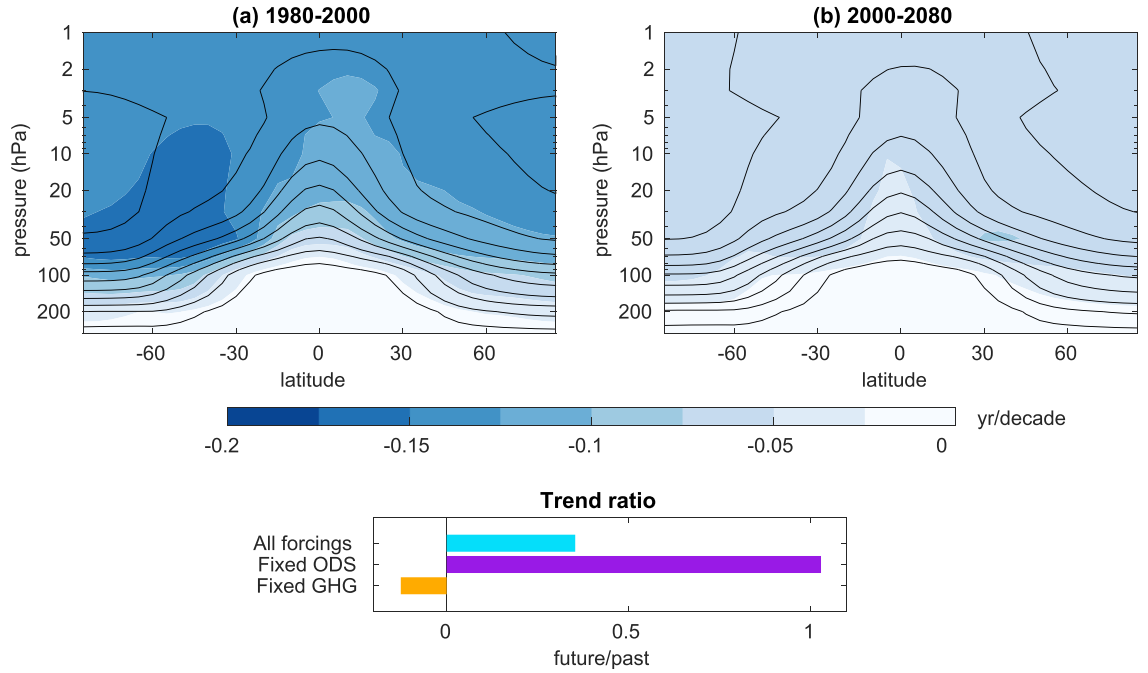

Figure 14. Effects of ozone depleting substances (ODS) and greenhouse gases (GHG) on trends of mean age in models. Trends are larger before 2000 due to the combined effects of both forcings. (a) trends during the ozone depletion period, (b) trends during the ozone recovery period, (c) ratio between future and past trends in control simulations and sensitivity experiments with ODS or GHG fixed to 1960 levels. Adapted from Polvani et al. (2019).

measurement uncertainty, methodological uncertainty (related to mean age calculation from observed trace gases), and sampling uncertainties (the representativeness error due to the sparse sampling), and will be further discussed below. Even given the large uncertainty in the observational trend estimates, the modeled trends lied outside this range (Garny et al., 2022; Waugh, 2009, see also Figure 16).

Several attempts have been made to understand and reduce the uncertainty in observational mean age. Following up from Engel et al. (2009), Ray et al. (2014) included corrections of the data for sampling uncertainty and reported the trend over a range of altitudes. This profile of observational mean age trends is presented in Figure 15. The correction method vastly reduced the error bar, while the mean trend estimates still remained consistent with the Engel et al. (2009) value. The trend profiles further revealed that in the lower stratosphere around 80 hPa, the observational trend estimate is negative and statistically significant. Using a chemistry-climate model to optimize the parameter selection for the derivation of mean age from SF_6 (in particular the ratio of moments), Fritsch et al. (2020) recalculated the trends from Engel et al. (2017) to be 0.07 years/decade. This value is included in Figure 15 for comparison, and the error bars overlap with the Ray et al. (2014) observational estimates.

Figure 15 further summarizes published comparisons between mean age trends from observations, from reanalysis data and from the latest global chemistry-climate model simulations. As reported, mean age trends based on different reanalysis data show strong deviations (Chabrillat et al., 2018; Ploeger et al., 2019, 2021), including negative (JRA-55, ERA5) and positive (ERA-Interim) age trends in northern mid-latitudes between about 30 and 5 hPa (Figure 15). Remarkably, the trend profile based on ERA-Interim is in good agreement with the trend profile derived from observations and it is also ERA-Interim for which the climatological mean age is closest to observation-based estimates (e.g., Ploeger et al., 2021). However, it is not clear whether this agreement occurs for the right reasons and generally the inter-reanalysis differences resemble the fact that the stratospheric circulation is not well constrained in current reanalyses (for a more detailed age of air reanalysis inter-comparison see Fujiwara et al., 2021).

The climate model trend estimates show consistently negative trends over all altitudes in mid-latitudes. In the lower stratosphere, negative age trends from observations, reanalyses and climate models are in good agreement. However, in the middle to upper stratosphere, an apparent discrepancy between age trends from climate models and observations exists, and this discrepancy has been noted for different generations of climate model inter-

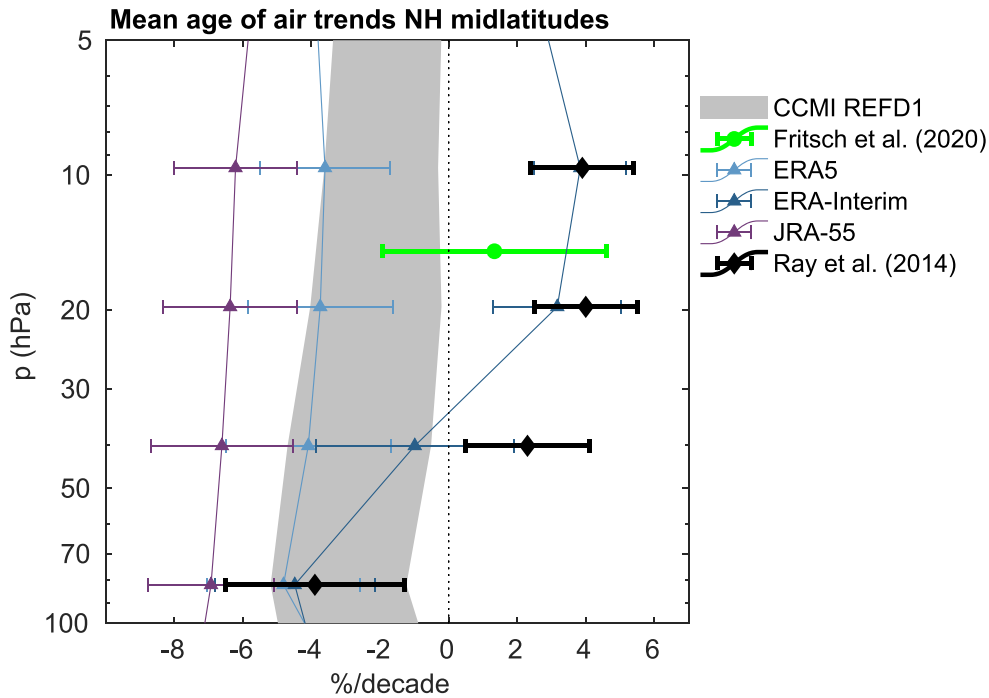

Figure 15. Previously published trend estimates over 1975–2015 at northern mid-latitudes (30–50°N) as a function of altitude derived from balloon observations (black diamonds with error bars and green symbol with error bar), climate models (gray shading) and reanalyses (colored error bars). Model simulations include CCMI-2022 REFD1 simulations (7 models, each with different number of members chosen randomly with a 1,000 Montecarlo sampling). The models and reanalyses results have been averaged over 5 km-thick layers to match the observations. All error bars correspond to one standard deviation uncertainty (95% confidence level). Error bars are associated with inter-annual variability for the reanalyses, with inter-model and inter-member spread for the models, and with observational uncertainties in the observational estimates. Black diamonds with error bars show observations from Ray et al. (2014), plotted at the center of the altitude range that they represent; green rectangles show observations from Engel et al. (2009) updated by Fritsch et al. (2020), and they represent an altitude range of 24–35 km.

comparison projects (e.g., CCMI-1, CCMI-2022, CMIP6 Abalos et al., 2021; Garny et al., 2022). While the sign of the modeled and observed trends is opposite, both may overlap within uncertainty ranges if additional uncertainty due to the mean age calculation method is taken into account (Fritsch et al., 2020, green symbol in Figure 15).

Differences between mean age trends from climate models and observations can also arise from the fact that model ages are typically calculated from ideal age tracers while observational ages are estimated from real tracers with substantial uncertainties. Such uncertainties are related to measurement uncertainty, methodological uncertainty (e.g., non-linear tropospheric increase and assumptions on ratio of moments), and sampling uncertainties due to sparseness of observations (i.e., representativeness error). Methodological and sampling uncertainties have been assessed in a few studies (e.g., Fritsch et al., 2020; Garcia et al., 2011) and are further illustrated and investigated in Supporting Information S1. In summary, the representativeness error is mostly below 10% of the true age value (in agreement with Engel et al., 2009) and causes an increase in standard error of the trend by about 0.1 years/decade (compare Garcia et al., 2011). The methodological uncertainty in the trend estimate arising from the use of realistic tracers CO_2 and SF_6 amounts to another 0.1 years/decade, largely related to uncertainty in the ratio of moments (e.g., Fritsch et al., 2020).

These uncertainties need to be taken into account when assessing stratospheric age of air trends and in particular when comparing trend estimates from observations and models. A synthesis plot of the current state of knowledge on stratospheric mean age trends, including most recent model simulations and a re-assessment of observational age trends, is presented in Figure 16. The figure shows the mean age timeseries in the NH mid-latitude middle stratosphere, the region considered by Engel et al. (2009), and the trend values calculated for the different data sets and different periods. For the model simulations, trends from the full model data are contrasted with trends sub-

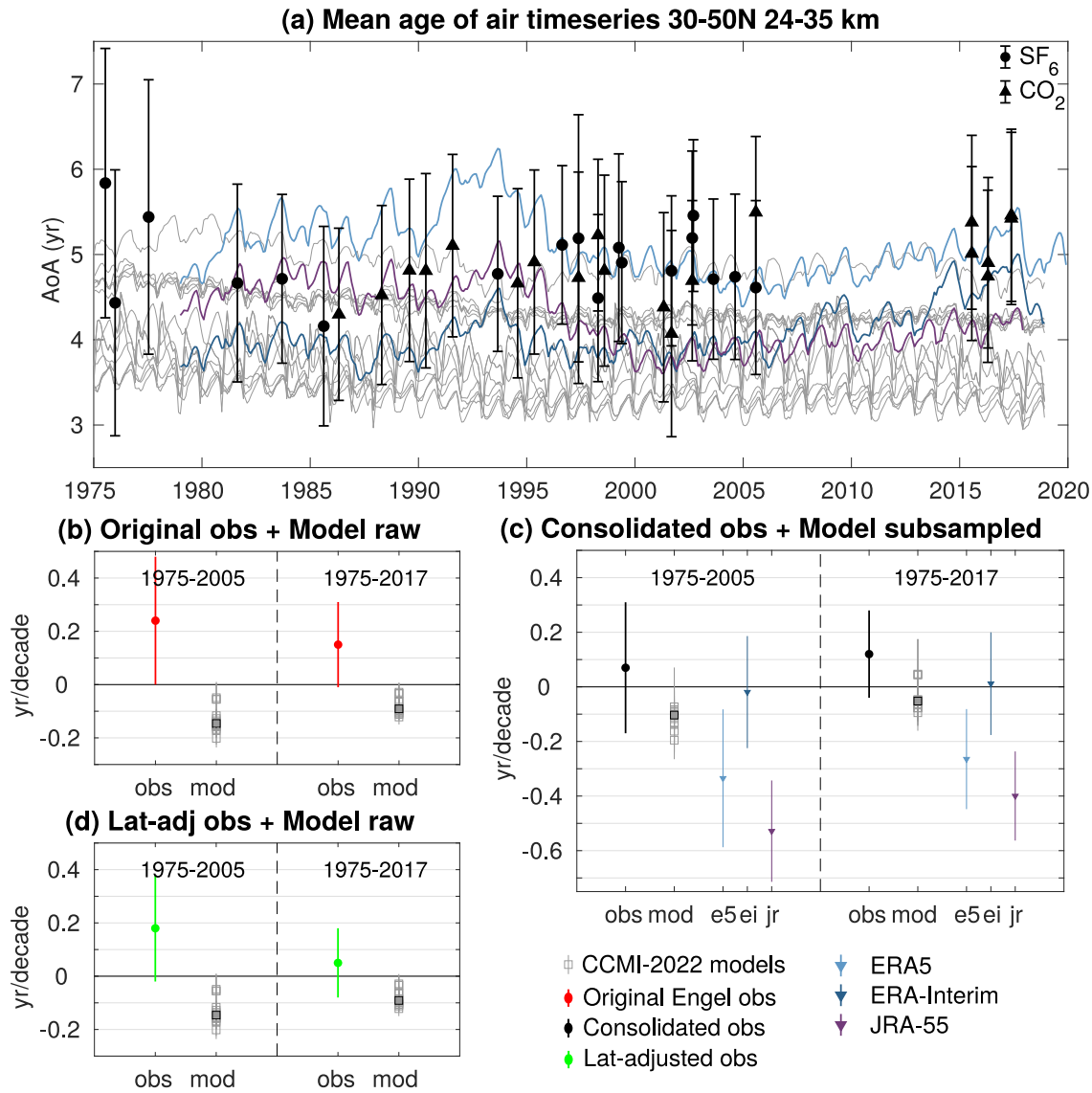

Figure 16. Re-assessment of mean age trends in the middle stratosphere from observations and models. (a) Timeseries of mean age anomalies averaged over 24–35 km height and northern mid-latitudes (30–50°N) from observations (black symbols), CCMI-2022 models (gray lines) and reanalyses (colored lines). Observational mean age from Engel et al. (2017) has been recalculated using the consolidated method (see Section 4.1.5); triangles correspond to SF_6-based and circles to CO_2-based estimates. Panels (b)–(d) shows trends calculated over the periods 1975–2005 and 1975–2017 (from 1981 onwards for reanalyses due to limited data availability) for a variety of data products: (b) observational estimates originally published by Engel et al. (2009, 2017) and trends from CCMI-2022 models based on the full time series. (c) Trends from same observational data, but with mean ages calculated by the consolidated method (Section 4.1.5), compared to CCMI-2022 model data sub-sampled on the measurement latitudes and months (sub-sampling is based on monthly mean, zonal mean data due to limited output availability, see Abalos et al., 2021), and to mean ages calculated in the CLamS transport model from various reanalysis data sets with sub-sampling to days and locations of observations. (d) trends from observational mean ages with consolidated method as in (c), but in addition adjustment of the data to account for latitudinal differences (following the method in Ray et al., 2014), which should be compared to the trends from the full model data. The trend error bars for the observations represent the observational uncertainties associated with the measurements and with the calculation of mean age from them. For the models and reanalyses the error bars correspond to the 95% confidence level, associated with inter-annual variability (reanalyses) and with inter-model and inter-member spread (models).

sampled to the observation locations. Only the latest model output is used (CCMI-2022), but the results are consistent for other model inter-comparison projects (Garny et al., 2022).

The original trend estimate by Engel et al. (2009) over the time period 1975–2005 of 0.24 ± 0.22 years/decade was found to disagree within error margins with model simulated mean age trends (MMM of −0.15 years/decade with a range of −0.23 to +0.01 years/decade, see Figure 16b; see also Waugh, 2009). For the extended period 1975–2016, the observational trend estimate decreases to 0.15±0.16 years/decade, and the models simulate less

negative trends (MMM of −0.10 years/decade with a range of −0.15 to +0.01 years/decade). The latter is explained by the decline of ODSs since about 2000, flattening the age decrease (see Section 6.2.1). Hence, for the extended period, the difference between simulated and observed age trends is decreasing, but the original trend estimate from Engel et al. (2017) and trends based on full model data still disagree. However, since then, both the methodological error and the sampling error were reassessed.

Following research on the methodological uncertainty, the observational age trend based on the data from Engel et al. (2009, 2017) has been re-calculated using the consolidated method proposed in Section 4, resulting in smaller positive trend estimates of 0.07 ± 0.24 years/decade and 0.12 ± 0.16 years/decade for the period 1975–2005 and 1975–2016, respectively (see Figure 16c). When comparing those trends to model data, the sampling uncertainty should be taken into account, and we contrast two methods that have been used to do so. The first method involves sub-sampling of model data to the locations of the observations (following Abalos et al., 2021). This sub-sampling results in model trends of −0.10 years/decade (range for individual models between −0.26 and +0.07 years/decade) and −0.05 years/decade (range −0.16 to +0.18 years/decade) for the period 1975–2005 and 1975–2016, respectively. Hence, the sub-sampled climate model mean age trend lies within the uncertainty range of the observational trend estimate for both periods. The second method to account for the sampling error includes an adjustment of the mean age observations to account for the latitudinal variations, as has been proposed by Ray et al. (2014). Applying a similar adjustment to the observational data (see Supporting Information S1 for details) decreases the observed mean age trend to 0.18 ± 0.20 years/decade and 0.05 ± 0.13 years/decade, for the two periods respectively (see Figure 16d). This adjusted observational trend should be compared to the model trend value without sub-sampling (to avoid double accounting of the sampling error), and also with this method can we conclude that the observational and model trend estimates do not disagree given the uncertainty ranges, in particular for the longer time period. However, it should be noted that the adjusted trend values are somewhat sensitive to the adjustment method (see Supporting Information S1). In summary, we conclude that when taking methodological and sampling uncertainty into account, best estimate climate model and observational mean age trend are still of opposite sign, but given the large uncertainty it cannot be concluded that model trends lie outside the observational range.

The reanalysis-based mean age trends in Figure 16 show a very large spread, suggesting that the stratospheric circulation is not well constrained in current reanalyses. Interestingly, the age trend for ERA-Interim is consistent with the observations also when taking the observational sub-sampling into account. But as discussed above, it is unclear whether this agreement in trends is for the right reason.

6.2.3. Lead Time Required to Detect Trends

Mean age trends over past decades exhibit large uncertainties that prevent knowing their magnitude (and sometimes sign) with confidence. In this section we address the question when trends will become detectable and what length of record (or "lead time") is needed to discern forced trends from internal variability, following the method by Rivoire et al. (2024). Figure 17 shows the detection power, that is, the magnitude of the smallest detectable trends for a given data record as a function of time. A reference is shown for model knowledge (i.e., perfect or omniscient knowledge), that is, the detection power afforded by a continuous time series of perfect age measurements. Using the trend values in Figure 16 we estimate that model trends of order 0.05 years/decade became discernible from internal variability around year 2015 (with a record starting in 1981, and omniscient knowledge). In this context, "discernible from internal variability" is an interpretation of the fact that a trend with magnitude equal to or larger than 0.05 years/decade is only 5% likely to occur purely as a result of internal variability over a ∼35-year-long omniscient record (1981–2015), and the internal variability is deduced from climate model simulations (see caption of Figure 17). It is worth noting that this estimate is less optimistic than the 20 years previously estimated by Abalos et al. (2021) (though the methods used differ).

The detection power granted by the observational record is also shown in Figure 17. The same method is applied, but the model knowledge is degraded to emulate that offered by the high altitude balloon record. The later emergence of trends inferred from this synthetic record reflects the effects of (a) the timing of the historical sampling (1981–2017) including gaps in the record, (b) the typical vertical resolution of high-altitude balloons, (c) changes in latitude of balloon launches, (d) conversion from tracer species to age of air (in this case, using an empirical relationship for N_2O), and (e) a range of possible future sampling frequencies (indicated in the legend). The effects of instrumental uncertainties are not taken into account, and the smallest detectable trends are

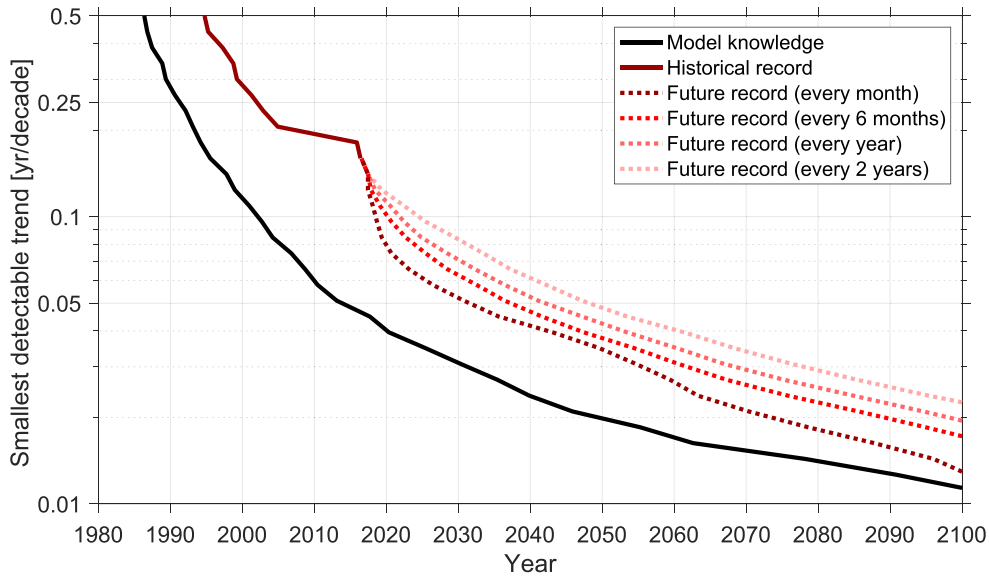

Figure 17. Smallest detectable trends in mean age (30–50 N average at 60 hPa) derived from models (black) and synthetic observations (colors). Data are from CMIP6's UKESM1-0-LL and CNRM-ESM2-1 pre-industrial control runs. Trends are given at the 95% confidence level for a record starting in 1981.

calculated assuming that dynamical variability can be removed (as in Ray et al., 2014). As a result, the smallest detectable trend estimates should be used as lower bounds. The same 0.05 years/decade trend magnitude discussed previously does not emerge until year 2030–2050, depending on future sampling frequency.

Before the 2005–2015 gap in the historical record, limitations of the observational record were responsible for a ∼10-year delay in the emergence of trends. For example, a trend of 0.25 years/decade would have been detectable in 1990 with omniscient knowledge, but only in year 2000 based on the (synthetic) observational record. After the gap in observational data, the delay grew to ∼20 years, highlighting the importance of accounting for observational sampling when analyzing trends. In addition, the delay will continue to worsen over time unless future sampling frequency is twice per year or better.

7. Conclusions

7.1. Achievements Over the Last 20 Years

Our conceptual picture of stratospheric transport had been established two decades ago (Plumb, 2002), along with a solid theoretical understanding of the transport time and age of air concept (Waugh & Hall, 2002, compare their schematic Figure 1 to our Figure 1). As outlined in the introduction, progress has mainly been made on the following three themes: (a) process understanding and diagnostics, (b) quality and quantity of observational data, and (c) diagnosis and understanding of long-term trends. The achievements in these areas are summarized in the following:

1. *Enhanced process understanding and development of process diagnostics enabled the quantification of individual processes from observational data and to understand model deficits*. Based on an overall good theoretical and conceptual framework for age of air, over the last decades substantial progress has been made in quantifying and better understanding the underlying physical relationship of individual transport processes to age of air. The development of dedicated diagnostic frameworks that relate age to the advective circulation strength and eddy mixing enabled (a) better understanding of model differences and deficits and (b) to quantify individual transport processes from observational data, in particular the diabatic circulation based on the age difference diagnostic. Mean age provides a powerful diagnostic to test the integrated tracer transport in a model. However, differences between models or discrepancies to observed age are not easily attributable to a specific process, and even good agreement can occur due to compensating errors. Thus, the development of diagnostics that can constrain individual processes both from observations and from models is a prerequisite for model improvement.

- *Simulation of stratospheric transport by global models has clearly been improved compared to 20 years ago, but there is still substantial spread and biases in the simulation of mean age*. Application of diagnostics to disentangle the effects of residual circulation transport, and mixing/diffusion effects have revealed that the still existing large spread in mean age is largely due to the latter. This can include both effects of resolved eddy mixing, but also effects of unresolved (numerical) diffusion. Indeed, advanced transport schemes with reduced numerical diffusion have been shown to strongly impact age of air. With this knowledge we can also conclude in retrospective that the strong low bias of mean age found by Waugh and Hall (2002) (with age approaching zero at 20 km at the equator for some models) was likely caused by overly strong vertical diffusion caused by low vertical resolution and/or diffusive transport schemes.
- *Quantifying processes from observations*. In order to gain better knowledge of the individual transport processes from observations (e.g., to constrain models), process diagnostics are needed that are based on observations. The diagnostics applied to models outlined above require information of the residual circulation, which is not an observable quantity. Over recent years, a diagnostic has been suggested that can deduce the diabatic circulation based on the latitudinal difference of mean age, that is, is directly accessible from global mean age data, as provided by satellites. Furthermore, efforts to deduce the age spectrum from a range of tracers have been undertaken over recent years. These still involve a number of challenges, but would provide more detailed information on effects of individual processes compared to mean age. However, the calculation of observation-based diagnostics hinges on high-quality observational tracer and age data.

2. *The quality and quantity of observational mean age data has improved over the last decades*. Since the last review paper by Waugh and Hall (2002), our knowledge on age of air from observations has improved drastically. We now have multiple global and temporally coherent data sets of mean age, thanks to remote sensing observations from satellites. Moreover, not only did many additional aircraft observations become available, but also additional age tracers have been explored, and aircores have been established as new observational platforms. Given their cost-efficiency, this technique might provide a wealth of additional data in the future. The compilation of the large number of in situ or direct measurements of tracer concentrations from air samples taken on board of aircrafts or balloons by now can give information on climatologies in the lower stratosphere, in particular at northern mid-latitudes where data density is highest (see Section 4.2). In other regions, sparse sampling is still problematic for this task. Furthermore, so far either the length of the records or the sparseness of data prevent robust conclusion on low frequency variability or long-term forced trends. Remote sensing observations have the advantage to provide global coverage, but available mean age data records have limitations due to uncertainties in the retrieval of tracer concentrations and only cover comparatively short periods. Next to additional data availability, many studies over the past years have led to an enhanced understanding and quantification of the uncertainties in deriving mean age from realistic tracers, both due to their non-linear increase and due to chemical sinks. This highlighted the limitations of observational mean age data in estimating long-term trends, and clearly calls for establishing a consistent and improved method to derive mean age from different data sources. In this review paper, we propose such a consolidated method to calculate mean age from observed, realistic tracers, based on the best current understanding (see Section 4). The use of such a common method, including also a chemical sink correction for SF_6-based mean age, clearly reduced the spread between different mean age data products, including better comparability to model data.
3. *Forced long-term trends in mean age are overall well understood in models, but observational evidence can only confirm model predictions in the lower stratosphere*. The acceleration of the BDC and associated negative mean age trends is one of the most robust model results on climate change related circulation trends and holds over many generations of climate models. The mechanism for an acceleration of the shallow branch forced by increasing GHG concentrations, and in addition by ODS-related ozone depletion, has been well understood for more than a decade. The associated decrease in mean age in the lower stratosphere has been confirmed by observational estimates of mean age trends. Given the high level of mechanistic understanding and agreement of models and observations, we overall have high confidence in an acceleration of the BDC in the lower stratosphere.

   In the middle and upper stratosphere, climate models likewise consistently simulate a decrease in mean age in response to GHG forcing. However, compared to the lower stratosphere the spread is larger between models, and the mechanism is less clear, in particular in the NH, where models disagree on the future development of the polar vortex. We have only limited high quality data available to deduce long-term trends from

observations (see above). The only region with a long enough record are the northern mid-latitudes, in particular thanks to a number of high-altitude balloon flights. This record had suggested a positive, but insignificant increase in mean age in the middle stratosphere, and the apparent discrepancy to model trend estimates has sparked many studies since the first publication of the record in 2009. In particular, the uncertainties associated with the observational record have been extensively studied. Overall, we can now conclude that there is very large uncertainty on observational trend estimates caused by uncertainties related to sampling and by methodological uncertainties when deducing mean age from realistic tracers (see above). By bringing together the gained knowledge on those uncertainties from recent studies, we can now assess that uncertainties in middle stratospheric observational records are too large to disprove the modeled mean age trends. However, model predictions of an accelerating circulation remain only confirmed by observations in the lower stratosphere but *not* in the middle stratosphere.

7.2. Open Issues and Opportunities

Although previous research on stratospheric age of air has substantially enhanced our understanding and quantification of its climatology and trends as described above, it has also prompted several open issues and unveiled potential avenues for exploration:

- *Develop better theoretical and empirical constraints on calculating mean age from realistic tracers.* One major hurdle to study the transport circulation from observations is the large uncertainty in deriving mean age from realistic tracers. From a theoretical or conceptual point of view, a more advanced canonical function of the age spectrum could be beneficial, possibly along with accounting for multiple entry points to the stratosphere, which is particularly relevant in the lowermost stratosphere. Furthermore, better observational or combined model-observation constraints on the ratio-of-moment would be necessary to reduce uncertainty in mean age derived from realistic tracers. Another avenue to derive mean age is to utilize empirical relationships between mean age and trace gas mixing ratios, as has been used in the past to derive mean age from N_2O. However, a better understanding of the spatial and temporal variability of those relationships is necessary to exploit their full potential.
- *Close observational gaps and ensure continued monitoring of stratospheric circulation to better constrain variability and trends.* Next to the issues of the method to derive mean age from trace gases, a significant advancement in our knowledge on the stratospheric transport circulation would come through an improved data record. One opportunity would be to use past satellite or aircraft mission data, or archived air samples to complement our past record of mean age, in particular if combined with novel methods to derive mean age from alternative age tracers. Our past data record in the northern hemispheric extratropics is currently the longest and best record we have, but still uncertainties are too large to constrain variability and in particular long-term trends. In other places on the globe, in particular the tropics and southern hemisphere only few observations exist. Long-term, global and high-cadence measurements are needed to better constrain variations in stratospheric transport associated with the QBO, ENSO, volcanic eruptions and their interactions. Currently those variability modes are not robustly represented in climate models and reanalyses, but are also insufficiently constrained from observations. To reach a better quantification and an improved understanding of stratospheric transport and its variability, global observations of multiple long-lived trace species are required. The quantification of variability modes in stratospheric transport would be an important opportunity for evaluating the ability of global models and reanalyses to capture transport processes correctly, which would also increase our confidence in simulated long-term trends by those models. All available satellite missions measuring stratospheric composition have expired or are at the end of their lifetime (cf. Table 2), thus to reach this goal new satellite missions that observe trace gases throughout the stratosphere are strongly desirable. Next to global observations, long-term continuous and regular measurements by cost efficient local measurement techniques such as aircores would be of high value to estimate long-term trends in the future. The presented time of emergence analysis (Section 6.2) shows that compensating for the loss of detection power imparted by past observational gaps will necessitate future sampling at least twice a year. With this frequency, trends of the magnitude estimated by the models should become detectable by 2035.
- *Deduce improved observational constraints on individual transport processes to advance model improvement.* Observational constraints on stratospheric transport processes are in general insufficient in models and reanalyses. For example, quantitative estimates of mixing effects are needed to constrain mixing in models.

The estimation of age spectra (or related diagnostics like the fraction of young air or higher moments) from observations could also help to constrain processes from observations; however a better quantitative understanding of linking those properties to individual transport processes would be necessary. To make progress, improved observational estimates of mean age and derived quantities will be an important step (see above). For model improvement of stratospheric transport, past work has revealed that advanced, less diffusive transport schemes that preserve tracer gradients are a promising way forward. Also, even most recent reanalyses data sets show large uncertainties in representing the stratospheric circulation and age of air and improvements of underlying forecast models and assimilation schemes seem a very promising way forward.

The lines of work outlined above provide an avenue toward a better understanding, observational quantification and modeling of stratospheric transport and its variability and trends. Those improvements have relevance for:

(a) improved understanding of stratospheric composition changes, for example, the observed ozone decrease in the lower stratosphere over the past two decades that is likely linked to transport variability, but so far neither completely understood nor reproduced by model simulations (e.g., Ball et al., 2018; Hassler et al., 2022).
(b) potentially removing long-standing biases in climate models and reanalyses via improved transport and representation of lower stratospheric water vapor. This bias was recently shown to be strongly mitigated by introducing an advanced, less diffusive transport scheme, and next to healing lower stratospheric temperature biases, also effects on the tropospheric circulation were found (Charlesworth et al., 2023).
(c) studying the (side-)effects of stratospheric aerosol injection (SAI) as one proposed method for climate geoengineering. The distribution of injected material and thus its effects on climate will strongly depend on the stratospheric transport circulation. Thus, a prerequisite for credible projections of the possible effects and side-effects of SAI on climate are models with reliable stratospheric transport (Bednarz et al., 2023; Haywood et al., 2022). To evaluate models with respect to their representation of stratospheric transport, age of air provides a very powerful concept.

Data Availability Statement

The data base of newly complied mean age data from in situ and remote sensing instruments is published by Garny, Saunders, et al. (2024). Python code for the consolidated method to calculate mean age is published by Wagenhäuser et al. (2024). Updated versions of this code will be made available at https://zenodo.org/doi/10.5281/zenodo.11127612.

Acknowledgments
We want to express our gratitude to our team member Thomas von Clarmann, who passed away shortly before completion of this work. Many thoughtful and valuable discussions with Thomas helped to shape this review article. He very much enriched our group, and the wider community, both scientifically and personally. This paper is the outcome from the International Space Science Institute (ISSI) team project on "Stratospheric Age-of-Air: Reconciling Observations and Models." We thank ISSI and the ISSI staff for support of two team meetings held in Bern. MA acknowledges funding from the national Spanish project Recovery (PID2021-124772OB-I00). AE and FP acknowledge funding from the Deutsche Forschungsgemeinschaft (DFG, German Research Foundation)—TRR 301—Project-ID 428312742. FV and FP acknowledge funding from the Deutsche Forschungsgemeinschaft (DFG, German Research Foundation)—Project ID 462476233. Support for this work at U. Toronto was provided by the Canadian Space Agency (Grant 16SUASCMEV) and the Natural Sciences and Engineering Research Council of Canada (Grant RGPIN-2017-06664). Work at the Jet Propulsion Laboratory, California Institute of Technology, was done under contract with NASA (80NM0018D0004). AP acknowledges support from the Agence Nationale de la Recherche (ANR, Grant 21-CE01-0016-01). We thank Aman Gupta and an anonymous reviewer for their detailed comments that led to a much improved paper. Open Access funding enabled and organized by Projekt DEAL.

References

Abalos, M., Calvo, N., Benito-Barca, S., Garny, H., Hardiman, S. C., Lin, P., et al. (2021). The Brewer–Dobson circulation in CMIP6. *Atmospheric Chemistry and Physics*, *21*(17), 13571–13591. https://doi.org/10.5194/acp-21-13571-2021

Abalos, M., & de la Cámara, A. (2020). Twenty-first century trends in mixing barriers and eddy transport in the lower stratosphere. *Geophysical Research Letters*, *47*(21), e2020GL089548. https://doi.org/10.1029/2020GL089548

Abalos, M., Orbe, C., Kinnison, D. E., Plummer, D., Oman, L. D., Jöckel, P., et al. (2020). Future trends in stratosphere-to-troposphere transport in CCMI models. *Atmospheric Chemistry and Physics*, *20*(11), 6883–6901. https://doi.org/10.5194/acp-20-6883-2020

Abalos, M., Polvani, L., Calvo, N., Kinnison, D., Ploeger, F., Randel, W., & Solomon, S. (2019). New insights on the impact of ozone-depleting substances on the Brewer-Dobson circulation. *Journal of Geophysical Research*, *124*(5), 2435–2451. https://doi.org/10.1029/2018JD029301

Abalos, M., Randel, W. J., Kinnison, D. E., & Garcia, R. R. (2017). Using the artificial tracer e90 to examine present and future UTLS tracer transport in WACCM. *Journal of the Atmospheric Sciences*, *74*(10), 3383–3403. https://doi.org/10.1175/JAS-D-17-0135.1

Adcock, K. E., Fraser, P. J., Hall, B. D., Langenfelds, R. L., Lee, G., Montzka, S. A., et al. (2021). Aircraft-based observations of ozone-depleting substances in the upper troposphere and lower stratosphere in and above the Asian summer monsoon. *Journal of Geophysical Research: Atmospheres*, *126*(1), e2020JD033137. https://doi.org/10.1029/2020jd033137

Agustí-Panareda, A., Barré, J., Massart, S., Inness, A., Aben, I., Ades, M., et al. (2023). Technical note: The cams greenhouse gas reanalysis from 2003 to 2020. *Atmospheric Chemistry and Physics*, *23*(6), 3829–3859. https://doi.org/10.5194/acp-23-3829-2023

Andrews, A. E., Boering, K. A., Daube, B. C., Wofsy, S. C., Hintsa, E. J., Weinstock, E. M., & Bui, T. P. (1999). Empirical age spectra for the lower tropical stratosphere from in situ observations of CO_2: Implications for stratospheric transport TM. *Journal of Geophysical Research*, *104*(D21), 26581–26595. https://doi.org/10.1029/1999jd900150

Andrews, A. E., Boering, K. A., Wofsy, S. C., Daube, B. C., Jones, D. B., Alex, S., et al. (2001). Empirical age spectra for the midlatitude lower stratosphere from in situ observations of CO_2' Quantitative evidence for a subtropical "barrier" to horizontal transport. *Journal of Geophysical Research*, *106*(D10), 10257–10274. https://doi.org/10.1029/2000jd900703

Andrews, A. E., Daube, B. C., Wofsy, S. C., Loewenstein, M., Jost, H., Podolske, J. R., et al. (2001). Mean ages of stratospheric air derived from in situ observations of CO, CH_4, and N_2O. *Journal of Geophysical Research*, *106*(D23), 32295–32314. https://doi.org/10.1029/2001jd000465

Andrews, D. G., Holton, J. R., & Leovy, C. B. (1987). *Middle atmosphere dynamics* (2nd ed.). Academic Press.

Baldwin, M. P., Gray, L. J., Dunkerton, T. J., Hamilton, K., Haynes, P. H., Randel, W. J., et al. (2001). The quasi-biennial oscillation. *Reviews of Geophysics*, *39*(2), 179–230. https://doi.org/10.1029/1999RG000073

Ball, W. T., Alsing, J., Mortlock, D. J., Staehelin, J., Haigh, J. D., Peter, T., et al. (2018). Evidence for a continuous decline in lower stratospheric ozone offsetting ozone layer recovery. *Atmospheric Chemistry and Physics*, *18*(2), 1379–1394. https://doi.org/10.5194/acp-18-1379-2018

Banerjee, A., Chiodo, G., Previdi, M., Ponater, M., Conley, A., & Polvani, L. (2019). Stratospheric water vapor: An important climate feedback. *Climate Dynamics*, *53*(3–4), 1697–1710. https://doi.org/10.1007/s00382-019-04721-4

Bednarz, E. M., Visioni, D., Kravitz, B., Jones, A., Haywood, J. M., Richter, J., et al. (2023). Climate response to off-equatorial stratospheric sulfur injections in three Earth system models—Part 2: Stratospheric and free-tropospheric response. *Atmospheric Chemistry and Physics*, *23*(1), 687–709. https://doi.org/10.5194/acp-23-687-2023

Bernath, P. F., McElroy, C. T., Abrams, M. C., Boone, C. D., Butler, M., Camy-Peyret, C., et al. (2005). Atmospheric chemistry experiment (ACE): Mission overview. *Geophysical Research Letters*, *32*(15), L15S01. https://doi.org/10.1029/2005GL022386

Birner, B., Chipperfield, M. P., Morgan, E. J., Stephens, B. B., Linz, M., Feng, W., et al. (2020). Gravitational separation of Ar/N_2 and age of air in the lowermost stratosphere in airborne observations and a chemical transport model. *Atmospheric Chemistry and Physics*, *20*(21), 12391–12408. https://doi.org/10.5194/acp-20-12391-2020

Birner, T., & Bönisch, H. (2011). Residual circulation trajectories and transit times into the extratropical lowermost stratosphere. *Atmospheric Chemistry and Physics*, *11*(2), 817–827. https://doi.org/10.5194/acp-11-817-2011

Bischof, W., Borchers, R., Fabian, P., & Krüger, B. C. (1985). Increased concentration and vertical distribution of carbon dioxide in the stratosphere. *Nature*, *316*(6030), 708–710. https://doi.org/10.1038/316708a0

Boering, K. A., Wofsy, S. C., Daube, B. C., Schneider, H. R., Loewenstein, M., Podolske, J. R., & Conway, T. J. (1996). Stratospheric mean ages and transport rates from observations of carbon dioxide and nitrous oxide. *Science*, *274*(5291), 1340–1343. https://doi.org/10.1126/science.274.5291.1340

Bönisch, H., Engel, A., Curtius, J., Birner, T., & Hoor, P. (2009). Quantifying transport into the lowermost stratosphere using simultaneous in-situ measurements of SF_6 and CO_2. *Atmospheric Chemistry and Physics*, *9*(16), 5905–5919. https://doi.org/10.5194/acp-9-5905-2009

Boone, C., Bernath, P., Cok, D., Jones, S., & Steffen, J. (2020). Version 4 retrievals for the atmospheric chemistry experiment Fourier transform spectrometer (ACE-FTS) and imagers. *Journal of Quantitative Spectroscopy and Radiative Transfer*, *247*, 106939. https://doi.org/10.1016/j.jqsrt.2020.106939

Boone, C., Bernath, P., & Lecours, M. (2023). Version 5 retrievals for ACE-FTS and ACE-imagers. *Journal of Quantitative Spectroscopy and Radiative Transfer*, *310*, 108749. https://doi.org/10.1016/j.jqsrt.2023.108749

Boucher, O., Friedlingstein, P., Collins, B., & Shine, K. P. (2009). The indirect global warming potential and global temperature change potential due to methane oxidation. *Environmental Research Letters*, *4*, 044007. https://doi.org/10.1088/1748-9326/4/4/044007

Brenninkmeijer, C. A. M., Crutzen, P., Boumard, F., Dauer, T., Dix, B., Ebinghaus, R., et al. (2007). Civil aircraft for the regular investigation of the atmosphere based on an instrumented container: The new CARIBIC system. *Atmospheric Chemistry and Physics*, *7*(18), 4953–4976. https://doi.org/10.5194/acp-7-4953-2007

Brewer, A. W. (1949). Evidence for a world circulation provided by measurements of helium and water vapour distribution in the stratosphere. *Quarterly Journal of the Royal Meteorological Society*, *75*(326), 351–363. https://doi.org/10.1002/qj.49707532603

Brown, A. T., Volk, C. M., Schoeberl, M. R., Boone, C. D., & Bernath, P. F. (2022). Stratospheric lifetimes of CFC-12, CFC-12, CCL_4, CH_4, CH_3Cl and N_2O from measurements made by the atmospheric chemistry experiment-fourier transform spectrometer (ACE-FTS). *Atmospheric Chemistry and Physics*, *13*(14), 6921–6950. https://doi.org/10.5194/acp-13-6921-2013

Burgess, A. B., Grainger, R. G., Dudhia, A., Payne, V. H., & Jay, V. L. (2004). Mipas measurement of sulphur hexafluoride (SF_6). *Geophysical Research Letters*, *31*(5). https://doi.org/10.1029/2003GL019143

Butchart, N. (2014). The Brewer-Dobson circulation. *Reviews of Geophysics*, *52*(2), 157–184. https://doi.org/10.1002/2013RG000448

Butchart, N., Cionni, I., Eyring, V., Shepherd, T. G., Waugh, D. W., Akiyoshi, H., et al. (2010). Chemistry-climate model simulations of twenty-first century stratospheric climate and circulation changes. *Journal of Climate*, *23*(20), 5349–5374. https://doi.org/10.1175/2010JCLI3404.1

Calvo, N., Garcia, R. R., Randel, W. J., & Marsh, D. (2010). Dynamical mechanism for the increase in tropical upwelling in the lowermost tropical stratosphere during warm ENSO events. *Journal of the Atmospheric Sciences*, *67*(7), 2331–2340. https://doi.org/10.1175/2010JAS3433.1

Camy-Peyret, C. (1995). Balloon-borne infrared fourier transform spectroscopy for measurements of atmospheric trace species. *Spectrochimica Acta Part A: Molecular and Biomolecular Spectroscopy*, *51*(7), 1143–1152. https://doi.org/10.1016/0584-8539(94)00145-2

Chabrillat, S., Vigouroux, C., Christophe, Y., Engel, A., Errera, Q., Minganti, D., et al. (2018). Comparison of mean age of air in five reanalyses using the BASCOE transport model. *Atmospheric Chemistry and Physics*, *18*(19), 14715–14735. https://doi.org/10.5194/acp-18-14715-2018

Charlesworth, E. J., Dugstad, A.-K., Fritsch, F., Jöckel, P., & Plöger, F. (2020). Impact of Lagrangian transport on lower-stratospheric transport time scales in a climate model. *Atmospheric Chemistry and Physics*, *20*(23), 15227–15245. https://doi.org/10.5194/acp-20-15227-2020

Charlesworth, E. J., Ploeger, F., Birner, T., Baikhadzhaev, R., Abalos, M., Abraham, L., et al. (2023). Stratospheric water vapor affecting atmospheric circulation. *Nature Communications*, *14*(1), 3925. https://doi.org/10.1038/s41467-023-39559-2

Daniel, J. S., Reimann, S., Ashford, P., Fleming, E. L., Hossaini, R., Lickley, M. J., et al. (2022). Stratospheric ozone changes and climate. In WMO (Ed.), *Scientific assessment of ozone depletion: 2022, GAW report no. 278 (chapter 7), Geneva, Switzerland* (p. 509)

Daniel, J. S., Schauffler, S. M., Pollock, W. H., Solomon, S., Weaver, A., Heidt, L. E., et al. (1996). On the age of stratospheric air and inorganic chlorine and bromine release. *Journal of Geophysical Research*, *101*(D11), 16757–16770. https://doi.org/10.1029/96jd01167

Diallo, M., Konopka, P., Santee, M. L., Müller, R., Tao, M., Walker, K. A., et al. (2019). Structural changes in the shallow and transition branch of the Brewer–Dobson circulation induced by El Niño. *Atmospheric Chemistry and Physics*, *19*(1), 425–446. https://doi.org/10.5194/acp-19-425-2019

Diallo, M., Legras, B., & Chédin, a. (2012). Age of stratospheric air in the ERA-Interim. *Atmospheric Chemistry and Physics*, *12*(24), 12133–12154. https://doi.org/10.5194/acp-12-12133-2012

Diallo, M., Ploeger, F., Konopka, P., Birner, T., Müller, R., Riese, M., et al. (2017). Significant contributions of volcanic aerosols to decadal changes in the stratospheric circulation. *Geophysical Research Letters*, *12*(20), 10780–10791. https://doi.org/10.1002/2017gl074662

Dietmüller, S., Eichinger, R., Garny, H., Birner, T., Boenisch, H., Pitari, G., et al. (2018). Quantifying the effect of mixing on the mean age of air in CCMVAL-2 and CCMI-1 models. *Atmospheric Chemistry and Physics*, *18*(9), 6699–6720. https://doi.org/10.5194/acp-18-6699-2018

Dietmüller, S., Garny, H., Plöger, F., Jöckel, P., & Cai, D. (2017). Effects of mixing on resolved and unresolved scales on stratospheric age of air. *Atmospheric Chemistry and Physics*, *17*(12), 7703–7719. https://doi.org/10.5194/acp-17-7703-2017

Dinelli, B. M., Raspollini, P., Gai, M., Sgheri, L., Ridolfi, M., Ceccherini, S., et al. (2021). The ESA MIPAS/Envisat level2-v8 dataset: 10 years of measurements retrieved with ORM v8.22. *Atmospheric Measurement Techniques*, *14*(12), 7975–7998. https://doi.org/10.5194/amt-14-7975-2021

Eckert, E., von Clarmann, T., Laeng, A., Stiller, G. P., Funke, B., Glatthor, N., et al. (2017). MIPAS IMK/IAA carbon tetrachloride (CCl_4) retrieval and first comparison with other instruments. *Atmospheric Measurement Techniques*, *10*(7), 2727–2743. https://doi.org/10.5194/amt-10-2727-2017

Ehhalt, D. H., Rohrer, F., Blake, D. R., Kinnison, D. E., & Konopka, P. (2007). On the use of nonmethane hydrocarbons for the determination of age spectra in the lower stratosphere. *Journal of Geophysical Research*, *112*(D12), D12208. https://doi.org/10.1029/2006JD007686

Eichinger, R., Dietmüller, S., Garny, H., Šácha, P., Birner, T., Bönisch, H., et al. (2019). The influence of mixing on the stratospheric age of air changes in the 21st century. *Atmospheric Chemistry and Physics*, *19*(2), 921–940. https://doi.org/10.5194/acp-19-921-2019

Engel, A. (2006). Physics observation of mesospheric air inside the arctic stratospheric polar vortex in early 2003 (pp. 267–282).

Engel, A., Bönisch, H., Brunner, D., Fischer, H., Franke, H., Günther, G., et al. (2006). Highly resolved observations of trace gases in the lowermost stratosphere and upper troposphere from the spurt project: An overview. *Atmospheric Chemistry and Physics*, *6*(2), 283–301. https://doi.org/10.5194/acp-6-283-2006

Engel, A., Bönisch, H., Ostermöller, J., Chipperfield, M. P., Dhomse, S., & Jöckel, P. (2018). A refined method for calculating equivalent effective stratospheric chlorine. *Atmospheric Chemistry and Physics*, *18*(2), 601–619. https://doi.org/10.5194/acp-18-601-2018

Engel, A., Bönisch, H., Ullrich, M., Sitals, R., Membrive, O., Danis, F., & Crevoisier, C. (2017). Mean age of stratospheric air derived from aircore observations. *Atmospheric Chemistry and Physics*, *17*(11), 6825–6838. https://doi.org/10.5194/acp-17-6825-2017

Engel, A., Mobius, T., Boenisch, H., Schmidt, U., Heinz, R., Levin, I., et al. (2009). Age of stratospheric air unchanged within uncertainties over the past 30 years. *Nature Geoscience*, *2*(1), 28–31. https://doi.org/10.1038/ngeo388

Engel, A., Strunk, M., Müller, M., Haase, H.-P., Poss, C., Levin, I., & Schmidt, U. (2002). The temporal development of total chlorine in the high latitude stratosphere based on reference distributions of mean age derived from CO_2 and SF_6. *Journal of Geophysical Research*, *107*(D12), 4136. https://doi.org/10.1029/2001JD000584

Fischer, H., Birk, M., Blom, C., Carli, B., Carlotti, M., von Clarmann, T., et al. (2008). MIPAS: An instrument for atmospheric and climate research. *Atmospheric Chemistry and Physics*, *8*(8), 2151–2188. https://doi.org/10.5194/acp-8-2151-2008

Flury, T., Wu, D. L., & Read, W. G. (2013). Variability in the speed of the Brewer–Dobson circulation as observed by Aura/MLS. *Atmospheric Chemistry and Physics*, *13*(9), 4563–4575. https://doi.org/10.5194/acp-13-4563-2013

Forster, P., & Shine, K. (1997). Radiative forcing and temperature trends from stratospheric ozone change. *Journal of Geophysical Research*, *102*, 10841–10856. https://doi.org/10.1029/96JD03510

Friedl-Vallon, F., Gulde, T., Hase, F., Kleinert, A., Kulessa, T., Maucher, G., et al. (2014). Instrument concept of the imaging Fourier transform spectrometer gloria. *Atmospheric Measurement Techniques*, *7*(10), 3565–3577. https://doi.org/10.5194/amt-7-3565-2014

Fritsch, F., Garny, H., Engel, A., Bönisch, H., & Eichinger, R. (2020). Sensitivity of age of air trends to the derivation method for non-linear increasing inert SF_6. *Atmospheric Chemistry and Physics*, *20*(14), 8709–8725. https://doi.org/10.5194/acp-20-8709-2020

Fueglistaler, S., Legras, B., Beljaars, A., Morcrette, J.-J., Simmons, A., Tompkins, A. M., & Uppala, S. (2009). The diabatic heat budget of the upper troposphere and lower/mid stratosphere in ECMWF reanalyses. *Quarterly Journal of the Royal Meteorological Society*, *135*(638), 21–37. https://doi.org/10.1002/qj.361

Fujiwara, M., Manney, G. L., Gray, L. J., & Wright, J. S. (2021). SPARC reanalysis intercomparison project (S-RIP) final report. In *WCRP-6/2021, SPARC report*. https://doi.org/10.17874/800dee57d13

Funke, B., López-Puertas, M., García-Comas, M., Stiller, G. P., von Clarmann, T., Höpfner, M., et al. (2009). Carbon monoxide distributions from the upper troposphere to the mesosphere inferred from 4.7 μm non-local thermal equilibrium emissions measured by MIPAS on Envisat. *Atmospheric Chemistry and Physics*, *9*(7), 2387–2411. https://doi.org/10.5194/acp-9-2387-2009

Garcia, R. R., & Randel, W. J. (2008). Acceleration of the Brewer–Dobson circulation due to increases in greenhouse gases. *Journal of the Atmospheric Sciences*, *65*(8), 2731–2739. https://doi.org/10.1175/2008JAS2712.1

Garcia, R. R., Randel, W. J., & Kinnison, D. E. (2011). On the determination of age of air trends from atmospheric trace species. *Journal of the Atmospheric Sciences*, *68*(1), 139–154. https://doi.org/10.1175/2010JAS3527.1

Garny, H., Birner, T., Boenisch, H., & Bunzel, F. (2014). The effects of mixing on age of air. *Journal of Geophysical Research*, *119*, 7015–7034. https://doi.org/10.1002/2013JD021417

Garny, H., Eichinger, R., Laube, J. C., Ray, E. A., Stiller, G. P., Bönisch, H., et al. (2024). Correction of stratospheric age of air (AoA) derived from sulfur hexafluoride (SF_6) for the effect of chemical sinks. *Atmospheric Chemistry and Physics*, *24*, 4193–4215. https://doi.org/10.5194/acp-24-4193-2024

Garny, H., Hendon, H., Abalos, M., Chiodo, G., Purich, A., Randel, W. J., et al. (2022). Stratospheric ozone changes and climate. In WMO (Ed.), *Scientific assessment of ozone depletion: 2022, GAW report no. 278 (chapter 5), Geneva, Switzerland* (p. 509)

Garny, H., & Randel, W. J. (2013). Dynamic variability of the Asian monsoon anticyclone observed in potential vorticity and correlations with tracer distributions. *Journal of Geophysical Research*, *118*(24), 13421–13433. https://doi.org/10.1002/2013JD020908

Garny, H., Saunders, L. N., Voet, F., Ray, E., von Clarmann, T., Bönisch, H., et al. (2024). Age of stratospheric air: Observational data sets [Dataset]. *Zenodo*. https://doi.org/10.5281/zenodo.11267157

Gille, J. C., Bailey, P. L., Russell, J. M., Russell, J. M., Massey, H. S. W., Beynon, W. J. G., et al. (1980). Temperature and composition measurements from the l.r.i.r. and l.i.m.s. experiments on nimbus 6 and 7. *Philosophical Transactions of the Royal Society of London. Series A, Mathematical and Physical Sciences*, *296*(1418), 205–218. https://doi.org/10.1098/rsta.1980.0165

Glanville, A. A., & Birner, T. (2017). Role of vertical and horizontal mixing in the tape recorder signal near the tropical tropopause. *Atmospheric Chemistry and Physics*, *17*(6), 4337–4353. https://doi.org/10.5194/acp-17-4337-2017

Glatthor, N., von Clarmann, T., Funke, B., García-Comas, M., Grabowski, U., Höpfner, M., et al. (2023). IMK/IAA MIPAS retrievals version 8: CH_4 and N_2O. In *Atmospheric measurement techniques discussions* (pp. 1–35). https://doi.org/10.5194/egusphere-2023-919

Gunson, M. R., Abbas, M. M., Abrams, M. C., Allen, M., Brown, L. R., Brown, T. L., et al. (1996). The atmospheric trace molecule spectroscopy (ATMOS) experiment: Deployment on the ATLAS space shuttle missions. *Geophysical Research Letters*, *23*(17), 2333–2336. https://doi.org/10.1029/96GL01569

Gupta, A., Gerber, E. P., & Lauritzen, P. H. (2020). Numerical impacts on tracer transport: A proposed intercomparison test of atmospheric general circulation models. *Quarterly Journal of the Royal Meteorological Society*, *146*(733), 3937–3964. https://doi.org/10.1002/qj.3881

Gupta, A., Gerber, E. P., Plumb, R. A., & Lauritzen, P. H. (2021). Numerical impacts on tracer transport: Diagnosing the influence of dynamical core formulation and resolution on stratospheric transport. *Journal of the Atmospheric Sciences*, *78*, 3575–3592. https://doi.org/10.1175/JAS-D-21-0085.1

Gupta, A., Linz, M., Curbelo, J., Pauluis, O., Gerber, E. P., & Kinnison, D. E. (2023). Estimating the meridional extent of adiabatic mixing in the stratosphere using age-of-air. *Journal of Geophysical Research: Atmospheres*, *128*(4), e2022JD037712. https://doi.org/10.1029/2022JD037712

Haenel, F. J., Stiller, G. P., von Clarmann, T., Funke, B., Eckert, E., Glatthor, N., et al. (2015). Reassessment of MIPAS age of air trends and variability. *Atmospheric Chemistry and Physics*, *15*(22), 13161–13176. https://doi.org/10.5194/acp-15-13161-2015

Haine, T. W. N., & Hall, T. M. (2002). A generalized transport theory: Water-mass composition and age. *Journal of Physical Oceanography*, *32*(6), 1932–1946. https://doi.org/10.1175/1520-0485(2002)032<1932:agttwm>2.0.co;2

Hall, T. M. (2000). Path histories and timescales in stratospheric transport: Analysis of an idealized model. *Journal of Geophysical Research*, *105*(D18), 22811–22823. https://doi.org/10.1029/2000JD900329

Hall, T. M., & Plumb, R. A. (1994). Age as a diagnostic of stratospheric transport. *Journal of Geophysical Research*, *99*(D1), 1059–1070. https://doi.org/10.1029/93JD03192

Hall, T. M., & Prather, M. J. (1993). Simulations of the trend and annual cycle in stratospheric CO_2. *Journal of Geophysical Research*, *98*(D6), 10573–10581. https://doi.org/10.1029/93jd00325

Han, Y., Tian, W., Chipperfield, M. P., Zhang, J., Wang, F., Sang, W., et al. (2019). Attribution of the hemispheric asymmetries in trends of stratospheric trace gases inferred from Microwave Limb Sounder (MLS) measurements. *Journal of Geophysical Research*, *124*(12), 6283–6293. https://doi.org/10.1029/2018JD029723

Hassler, B., Young, P., Ball, W. T., Damadeo, R., Keeble, J., Barras, E. M., et al. (2022). Update on global ozone: Past, present and future. In WMO (Ed.), *Scientific assessment of ozone depletion: 2022, GAW report no. 278 (chapter 3). Geneva, Switzerland* (p. 509)

Hauck, M., Bönisch, H., Hoor, P., Keber, T., Ploeger, F., Schuck, T. J., & Engel, A. (2020). A convolution of observational and model data to estimate age of air spectra in the northern hemispheric lower stratosphere. *Atmospheric Chemistry and Physics*, *20*(14), 8763–8785. https://doi.org/10.5194/acp-20-8763-2020

Hauck, M., Fritsch, F., Garny, H., & Engel, A. (2019). Deriving stratospheric age of air spectra using an idealized set of chemically active trace gases. *Atmospheric Chemistry and Physics*, *19*(7), 5269–5291. https://doi.org/10.5194/acp-19-5269-2019

Haynes, P. H., McIntyre, M. E., Shepherd, T. G., Marks, C. J., & Shine, K. P. (1991). On the "downward control" of extratropical diabatic circulations by eddy-induced mean zonal forces. *Journal of the Atmospheric Sciences*, *48*(4), 651–678. https://doi.org/10.1175/1520-0469(1991)048⟨0651:OTCOED⟩2.0.CO;2

Haywood, J., Tilmes, S., Keutsch, F., Niemeier, U., Schmidt, A., Visioni, D., et al. (2022). Stratospheric aerosol injection and its potential effect on the stratospheric ozone layer. In WMO (Ed.), *Scientific assessment of ozone depletion: 2022, GAW report no. 278 (chapter 6), Geneva, Switzerland* (p. 509)

Hegglin, M. I., Plummer, D. A., Shepherd, T. G., Scinocca, J. F., Anderson, J., Froidevaux, L., et al. (2014). Vertical structure of stratospheric water vapour trends derived from merged satellite data. *Nature Geoscience*, *7*(10), 768–776. https://doi.org/10.1038/NGEO2236

Hegglin, M. I., & Shepherd, T. G. (2009). Large climate-induced changes in ultraviolet index and stratosphere-to-troposphere ozone flux. *Nature Geoscience*, *2*(10), 687–691. https://doi.org/10.1038/ngeo604

Hegglin, M. I., & Tegtmeier, S. (2017). The sparc data initiative: Assessment of stratospheric trace gas and aerosol climatologies from satellite limb sounders. In *SPARC report no. 8, WCRP-05/2017*. Retrieved from www.sparc-climate.org/publications/sparc-reports/10.3929/ethz-a-010863911

Hegglin, M. I., Tegtmeier, S., Anderson, J., Bourassa, A. E., Brohede, S., Degenstein, D., et al. (2021). Overview and update of the sparc data initiative: Comparison of stratospheric composition measurements from satellite limb sounders. *Earth System Science Data*, *13*(5), 1855–1903. https://doi.org/10.5194/essd-13-1855-2021

Hegglin, M. I., Tegtmeier, S., Anderson, J., Bourassa, A. E., Brohede, S., Degenstein, D., et al. (2020). SPARC Data Initiative monthly zonal mean composition measurements from stratospheric limb sounders (1978–2018). *Zenodo*. https://doi.org/10.5281/zenodo.4265393

Holton, J. R., Haynes, P., McIntyre, M. E., Douglass, A. R., Rood, R. B., & Pfister, L. (1995). Stratosphere-troposphere exchange. *Reviews of Geophysics*, *33*(4), 403–439. https://doi.org/10.1029/95rg02097

Holzer, M., & Hall, T. M. (2000). Transit-time and tracer-age distributions in geophysical flows. *Journal of the Atmospheric Sciences*, *57*(21), 3539–3558. https://doi.org/10.1175/1520-0469(2000)057<3539:ttatad>2.0.co;2

Holzer, M., & Hall, T. M. (2008). Tropospheric transport climate partitioned by surface origin and transit time. *Journal of Geophysical Research*, *113*(D8), D08104. https://doi.org/10.1029/2007JD009115

Holzer, M., & Waugh, D. W. (2015). Interhemispheric transit time distributions and path-dependent lifetimes constrained by measurements of SF_6, CFCS, and CFC replacements. *Geophysical Research Letters*, *42*(1), 1–9. https://doi.org/10.1002/2015GL064172

Hooghiem, J. J. D., Popa, M. E., Röckmann, T., Grooß, J.-U., Tritscher, I., Müller, R., et al. (2020). Wildfire smoke in the lower stratosphere identified by in situ co observations. *Atmospheric Chemistry and Physics*, *20*(22), 13985–14003. https://doi.org/10.5194/acp-20-13985-2020

Iglesias-Suarez, F., Wild, O., Kinnison, D. E., Garcia, R. R., Marsh, D. R., Lamarque, J.-F., et al. (2021). Tropical stratospheric circulation and ozone coupled to Pacific multi-decadal variability. *Geophysical Research Letters*, *48*(11), e2020GL092162. https://doi.org/10.1029/2020GL092162

Johnson, D. G., Jucks, W., Traub, W. A., Chance, K. V., Toon, G. C., Iii, J. M. R., & Mccormick, M. P. (1999). Stratospheric age spectra derived from observations of water vapor and methane. *Journal of Geophysical Research*, *104*(D17), 21595–21602. https://doi.org/10.1029/1999jd900363

Karion, A., Sweeney, C., Tans, P., & Newberger, T. (2010). AirCore: An innovative atmospheric sampling system. *Journal of Atmospheric and Oceanic Technology*, *27*(11), 1839–1853. https://doi.org/10.1175/2010JTECHA1448.1

Karpechko, A. Y., Afargan-Gerstman, H., Butler, A. H., Domeisen, D. I. V., Kretschmer, M., Lawrence, Z., et al. (2022). Northern hemisphere stratosphere-troposphere circulation change in CMIP6 models: 1. Inter-model spread and scenario sensitivity. *Journal of Geophysical Research: Atmospheres*, *127*(18), e2022JD036992. https://doi.org/10.1029/2022JD036992

Kida, H. (1983). General circulation of air parcels and transport characteristics derived from a hemispheric GCM. 2. Very long-term motions of air parcels in the troposphere and stratosphere. *Journal of the Meteorological Society of Japan*, *61*(4), 510–523. https://doi.org/10.2151/jmsj1965.61.4_510

Konopka, P., Grooß, J.-U., Günther, G., Ploeger, F., Pommrich, R., Müller, R., & Livesey, N. (2010). Annual cycle of ozone at and above the tropical tropopause: Observations versus simulations with the chemical Lagrangian model of the stratosphere (CLaMS). *Atmospheric Chemistry and Physics*, *10*(1), 121–132. https://doi.org/10.5194/acp-10-121-2010

Konopka, P., Ploeger, F., Tao, M., & Riese, M. (2016). Zonally resolved impact of ENSO on the stratospheric circulation and water vapor entry values. *Journal of Geophysical Research*, *121*(19), 11486–11501. https://doi.org/10.1002/2015JD024698

Kovács, T., Feng, W., Totterdill, A., Plane, J. M. C., Dhomse, S., Gómez-Martín, J. C., et al. (2017). Determination of the atmospheric lifetime and global warming potential of sulfur hexafluoride using a three-dimensional model. *Atmospheric Chemistry and Physics*, *17*(2), 883–898. https://doi.org/10.5194/acp-17-883-2017

Krause, J., Hoor, P., Engel, A., Plöger, F., Grooß, J.-U., Bönisch, H., et al. (2018). Mixing and ageing in the polar lower stratosphere in winter 2015–2016. *Atmospheric Chemistry and Physics*, *18*(8), 6057–6073. https://doi.org/10.5194/acp-18-6057-2018

Laube, J. C., Elvidge, E. C. L., Adcock, K. E., Baier, B., Brenninkmeijer, C. A. M., Chen, H., et al. (2020). Investigating stratospheric changes between 2009 and 2018 with halogenated trace gas data from aircraft, aircores, and a global model focusing on CFC-11. *Atmospheric Chemistry and Physics*, *20*(16), 9771–9782. https://doi.org/10.5194/acp-20-9771-2020

Laube, J. C., Engel, A., Bönisch, H., Möbius, T., Sturges, W. T., Braß, M., & Röckmann, T. (2010). Fractional release factors of long-lived halogenated organic compounds in the tropical stratosphere. *Atmospheric Chemistry and Physics*, *10*(3), 1093–1103. https://doi.org/10.5194/acp-10-1093-2010

Leedham Elvidge, E., Bönisch, H., Brenninkmeijer, C. A. M., Engel, A., Fraser, P. J., Gallacher, E., et al. (2018). Evaluation of stratospheric age of air from CF_4, C_2F_6, C_3F_8, CHF_3, HFC-125, HFC-227EA and SF_6; implications for the calculations of halocarbon lifetimes, fractional release factors and ozone depletion potentials. *Atmospheric Chemistry and Physics*, *18*(5), 3369–3385. https://doi.org/10.5194/acp-18-3369-2018

Li, F., Newman, P., Pawson, S., & Perlwitz, J. (2018). Effects of greenhouse gas increase and stratospheric ozone depletion on stratospheric mean age of air in 1960–2010. *Journal of Geophysical Research: Atmospheres*, *123*(4), 2098–2110. https://doi.org/10.1002/2017JD027562

Li, F., Waugh, D. W., Douglass, A. R., Newman, P. A., Strahan, S. E., Ma, J., et al. (2012). Long-term changes in stratospheric age spectra in the 21st century in the Goddard Earth observing system chemistry-climate model (GEOSCCM). *Journal of Geophysical Research*, *117*(D20), D20119. https://doi.org/10.1029/2012JD017905

Li, J., Baier, B. C., Moore, F., Newberger, T., Wolter, S., Higgs, J., et al. (2023). A novel, cost-effective analytical method for measuring high-resolution vertical profiles of stratospheric trace gases using a gas chromatograph coupled with an electron capture detector. *Atmospheric Measurement Techniques*, *16*(11), 2851–2863. https://doi.org/10.5194/amt-16-2851-2023

Lin, P., & Fu, Q. (2013). Changes in various branches of the Brewer–Dobson circulation from an ensemble of chemistry climate models. *Journal of Geophysical Research: Atmospheres*, *118*(1), 73–84. https://doi.org/10.1029/2012JD018813

Linz, M., Abalos, M., Glanville, A. S., Kinnison, D. E., Ming, A., & Neu, J. L. (2019). The global diabatic circulation of the stratosphere as a metric for the Brewer–Dobson circulation. *Atmospheric Chemistry and Physics*, *19*(7), 5069–5090. https://doi.org/10.5194/acp-19-5069-2019

Linz, M., Plumb, R. A., Gerber, E. P., Haenel, F. J., Stiller, G., Kinnison, D. E., et al. (2017). The strength of the meridional overturning circulation of the stratosphere. *Nature Geoscience*, *10*(663), 663–667. https://doi.org/10.1038/ngeo3013

Linz, M., Plumb, R. A., Gerber, E. P., & Sheshadri, A. (2016). The relationship between age of air and the diabatic circulation of the stratosphere. *Journal of the Atmospheric Sciences*, *73*(11), 4507–4518. https://doi.org/10.1175/JAS-D-16-0125.1

Linz, M., Plumb, R. A., Gupta, A., & Gerber, E. P. (2021). Stratospheric adiabatic mixing rates derived from the vertical gradient of age of air. *Journal of Geophysical Research*, *126*(21), e2021JD035199. https://doi.org/10.1029/2021JD035199

Loeffel, S., Eichinger, R., Garny, H., Reddmann, T., Fritsch, F., Versick, S., et al. (2022). The impact of sulfur hexafluoride (SF_6) sinks on age of air climatologies and trends. *Atmospheric Chemistry and Physics*, *22*(2), 1175–1193. https://doi.org/10.5194/acp-22-1175-2022

Luo, Z. J., Pan, L. L., Atlas, E. L., Chelpon, S. M., Honomichl, S. B., Apel, E. C., et al. (2018). Use of airborne in situ VOC measurements to estimate transit time spectrum: An observation-based diagnostic of convective transport. *Geophysical Research Letters*, *45*(1), 13150–13157. https://doi.org/10.1029/2018GL080424

McIntyre, M. E., & Palmer, T. N. (1984). The 'surf zone' in the stratosphere. *Journal of Atmospheric and Terrestrial Physics*, *46*(9), 825–849. https://doi.org/10.1016/0021-9169(84)90063-1

McLandress, C., Shepherd, T. G., Scinocca, J. F., Plummer, D. A., Sigmond, M., Jonsson, A. I., & Reader, M. C. (2011). Separating the dynamical effects of climate change and ozone depletion. Part II: Southern hemisphere troposphere. *Journal of Climate*, *24*(6), 1850–1868. https://doi.org/10.1175/2010JCLI3958.1

Membrive, O., Crevoisier, C., Sweeney, C., Danis, F., Hertzog, A., Engel, A., et al. (2017). Aircore-hr: A high-resolution column sampling to enhance the vertical description of CH_4 and CO_2. *Atmospheric Measurement Techniques*, *10*(6), 2163–2181. https://doi.org/10.5194/amt-10-2163-2017

Michelsen, H. A., Manney, G. L., Gunson, M. R., & Zander, R. (1998). Correlations of stratospheric abundances of NOY, O_3, N_2O and CH_4 derived from atmos measurements. *Journal of Geophysical Research*, *103*(D21), 28347–28359. https://doi.org/10.1029/98jd02850

Milz, M., Clarmann, T. V., Bernath, P., Boone, C., Buehler, S. A., Chauhan, S., et al. (2009). Validation of water vapour profiles (version 13) retrieved by the IMK/IAA scientific retrieval processor based on full resolution spectra measured by MIPAS on board Envisat. *Atmospheric Measurement Techniques*, *2*(2), 379–399. https://doi.org/10.5194/amt-2-379-2009

Mote, P. W., Rosenlof, K. H., McIntyre, M. E., Carr, E. S., Gille, J. C., Holton, J. R., et al. (1996). An atmospheric tape recorder: The imprint of tropical tropopause temperatures on stratospheric water vapor. *Journal of Geophysical Research*, *101*(D2), 3989–4006. https://doi.org/10.1029/95JD03422

Murcray, D. G., Bonomo, F. S., Brooks, J. N., Goldman, A., Murcray, F. H., & Williams, W. J. (1975). Detection of fluorocarbons in the stratosphere. *Geophysical Research Letters*, *2*(3), 109–112. https://doi.org/10.1029/GL002i003p00109

Muthers, S., Kuchar, A., Stenke, A., Schmitt, J., Anet, J. G., Raible, C. C., & Stocker, T. F. (2016). Stratospheric age of air variations between 1600 and 2100. *Geophysical Research Letters*, *43*(10), 5409–5418. https://doi.org/10.1002/2016GL068734

Nakajima, H., Sugita, T., Yokota, T., Ishigaki, T., Mogi, Y., Araki, N., et al. (2006). Characteristics and performance of the improved limb atmospheric spectrometer-II (ILAS-II) on board the ADEOS-II satellite. *Journal of Geophysical Research*, *111*(D11), 8213. https://doi.org/10.1029/2005JD006334

Neu, J. L., Glanville, A. S., & Kinnison, D. E. (2018). Decadal-scale variations in stratospheric circulation driven by seasonal timing of the Quasi-Biennial Oscillation. In *AGU Fall Meeting Abstracts*, A31A-07.

Neu, J. L., & Plumb, R. A. (1999). Age of air in a "leaky pipe" model of stratospheric transport. *Journal of Geophysical Research*, *104*(D16), 19243–19255. https://doi.org/10.1029/1999JD900251

Newman, P. A., Daniel, J. S., Waugh, D. W., & Nash, E. R. (2007). A new formulation of equivalent effective stratospheric chlorine (EESC). *Atmospheric Chemistry and Physics*, *7*(17), 4537–4552. https://doi.org/10.5194/acp-7-4537-2007

Newman, P. A., Nash, E. R., Kawa, S. R., Montzka, S. A., & Schauffler, S. M. (2006). When will the Antarctic ozone hole recover? *Geophysical Research Letters*, *33*(12), L12814. https://doi.org/10.1029/2005GL025232

Niwano, M., Yamazki, K., & Shiotani, M. (2003). Seasonal and QBO variations of ascent rate in the tropical lower stratosphere as inferred from UARS haloe trace gas data. *Journal of Geophysical Research*, *108*(D24), D18304. https://doi.org/10.1029/2003JD003871

Oberländer, S., Langematz, U., & Meul, S. (2013). Unraveling impact factors for future changes in the Brewer-Dobson circulation. *Journal of Geophysical Research: Atmospheres*, *118*(18), 10296–10312. https://doi.org/10.1002/jgrd.50775

Oman, L., Waugh, D. W., Pawson, S., Stolarski, R. S., & Newman, P. A. (2009). On the influence of anthropogenic forcings on changes in the stratospheric mean age. *Journal of Geophysical Research*, *114*(D3), D03105. https://doi.org/10.1029/2008JD010378

Orbe, C., Holzer, M., Polvani, L. M., & Waugh, D. (2013). Air-mass origin as a diagnostic of tropospheric transport. *Journal of Geophysical Research: Atmospheres*, *118*(3), 1459–1470. https://doi.org/10.1002/jgrd.50133

Orbe, C., Rind, D., Jonas, J., Nazarenko, L., Faluvegi, G., Murray, L. T., et al. (2020). Giss model e2.2: A climate model optimized for the middle atmosphere—2. Validation of large-scale transport and evaluation of climate response. *Journal of Geophysical Research: Atmospheres*, *125*(24), e2020JD033151. https://doi.org/10.1029/2020JD033151

Ostermöller, J., Bönisch, H., Jöckel, P., & Engel, A. (2017). A new time-independent formulation of fractional release. *Atmospheric Chemistry and Physics*, *17*(6), 3785–3797. https://doi.org/10.5194/acp-17-3785-2017

Palmeiro, F. M., Calvo, N., & Garcia, R. R. (2014). Future changes in the Brewer–Dobson circulation under different greenhouse gas concentrations in WACCM4. *Journal of the Atmospheric Sciences*, *71*(8), 2962–2975. https://doi.org/10.1175/JAS-D-13-0289.1

Park, S., Jim, R., Daube, B. C., Pfister, L., Conway, T. J., Gottlieb, E. W., et al. (2007). The CO_2 tracer clock for the tropical tropopause layer. *Atmospheric Chemistry and Physics*, *3*, 3989–4000.

Plieninger, J., Laeng, A., Lossow, S., von Clarmann, T., Stiller, G. P., Kellmann, S., et al. (2016). Validation of revised methane and nitrous oxide profiles from MIPAS-ENVISAT. *Atmospheric Measurement Techniques*, *9*(2), 765–779. https://doi.org/10.5194/amt-9-765-2016

Plieninger, J., von Clarmann, T., Stiller, G. P., Grabowski, U., Glatthor, N., Kellmann, S., et al. (2015). Methane and nitrous oxide retrievals from MIPAS-ENVISAT. *Atmospheric Measurement Techniques*, *8*(11), 4657–4670. https://doi.org/10.5194/amt-8-4657-2015

Ploeger, F., Abalos, M., Birner, T., Konopka, P., Legras, B., Müller, R., & Riese, M. (2015). Quantifying the effects of mixing and residual circulation on trends of stratospheric mean age of air. *Geophysical Research Letters*, *42*(6), 2047–2054. https://doi.org/10.1002/2014GL062927.1

Ploeger, F., & Birner, T. (2016). Seasonal and inter-annual variability of lower stratospheric age of air spectra. *Atmospheric Chemistry and Physics*, *2016*(15), 10195–10213. https://doi.org/10.5194/acp-16-10195-2016

Ploeger, F., Diallo, M., Charlesworth, E., Konopka, P., Legras, B., Laube, J. C., et al. (2021). The stratospheric Brewer–Dobson circulation inferred from age of air in the ERA5 reanalysis. *Atmospheric Chemistry and Physics*, *21*(11), 8393–8412. https://doi.org/10.5194/acp-21-8393-2021

Ploeger, F., & Garny, H. (2022). Hemispheric asymmetries in recent changes in the stratospheric circulation. *Atmospheric Chemistry and Physics*, *22*(8), 5559–5576. https://doi.org/10.5194/acp-22-5559-2022

Ploeger, F., Legras, B., Charlesworth, E., Yan, X., Diallo, M., Konopka, P., et al. (2019). How robust are stratospheric age of air trends from different reanalyses? *Atmospheric Chemistry and Physics*, *19*(9), 6085–6105. https://doi.org/10.5194/gmd-12-2441-2019

Plumb, R. A. (1996). A "tropical pipe" model of stratospheric transport. *Journal of Geophysical Research*, *101*(D2), 3957–3972. https://doi.org/10.1029/95JD03002

Plumb, R. A. (2002). Stratospheric transport. *Journal of the Meteorological Society of Japan*, *80*(4), 793–809. https://doi.org/10.2151/jmsj.80.793

Plumb, R. A. (2007). Tracer interrelationships in the stratosphere. *Reviews of Geophysics*, *45*(4), 1–33. https://doi.org/10.1029/2005RG000179

Plumb, R. A., & Ko, M. K. W. (1992). Interrelationships between mixing ratios of long-lived stratospheric constituents. *Journal of Geophysical Research*, *97*(D9), 10145–10156. https://doi.org/10.1029/92JD00450

Podglajen, A., & Ploeger, F. (2019). Retrieving the age of air spectrum from tracers: Principle and method. *Atmospheric Chemistry and Physics*, *19*(1), 1767–1783. https://doi.org/10.5194/acp-19-1767-2019

Polvani, L. M., Abalos, M., Garcia, R., Kinnison, D., & Randel, W. J. (2018). Significant weakening of Brewer-Dobson circulation trends over the 21st century as a consequence of the Montreal protocol. *Geophysical Research Letters*, *45*(1), 401–409. https://doi.org/10.1002/2017gl075345

Polvani, L. M., Wang, L., Abalos, M., Butchart, N., Chipperfield, M. P., Dameris, M., et al. (2019). Large impacts, past and future, of ozone-depleting substances on Brewer-Dobson circulation trends: A multimodel assessment. *Journal of Geophysical Research: Atmospheres*, *124*(13), 6669–6680. https://doi.org/10.1029/2018JD029516

Poshyvailo-Strube, L., Müller, R., Fueglistaler, S., Hegglin, M. I., Laube, J. C., Volk, C. M., & Ploeger, F. (2022). How can Brewer–Dobson circulation trends be estimated from changes in stratospheric water vapour and methane? *Atmospheric Chemistry and Physics*, *22*(15), 9895–9914. https://doi.org/10.5194/acp-22-9895-2022

Prather, M. J. (1996). Time scales in atmospheric chemistry: Theory, GWPs for CH_4 and CO, and runaway growth. *Geophysical Research Letters*, *23*(19), 2597–2600. https://doi.org/10.1029/96GL02371

Prather, M. J., Froidevaux, L., & Livesey, N. J. (2023). Observed changes in stratospheric circulation: Decreasing lifetime of N_2O, 2005–2021. *Atmospheric Chemistry and Physics*, *23*(2), 843–849. https://doi.org/10.5194/acp-23-843-2023

Raspollini, P., Arnone, E., Barbara, F., Bianchini, M., Carli, B., Ceccherini, S., et al. (2022). Level 2 processor and auxiliary data for ESA version 8 final full mission analysis of MIPAS measurements on ENVISAT. *Atmospheric Measurement Techniques*, *15*(6), 1871–1901. https://doi.org/10.5194/amt-15-1871-2022

Ray, E. A., Atlas, E. L., Schauffler, S., Chelpon, S. M., Pan, L. L., Boenisch, H., & Rosenlof, K. R. (2022). Age spectra and other transport diagnostics in the North American monsoon UTLS from SEAC4ES in situ trace gas measurements. *Atmospheric Chemistry and Physics*, *22*(1), 6539–6558. https://doi.org/10.5194/acp-22-6539-2022

Ray, E. A., Moore, F. L., Elkins, J. W., Dutton, G. S., Fahey, D. W., Vomel, H., et al. (1999). Transport into the northern hemisphere lowermost stratosphere revealed by in situ tracer measurements. *Journal of Geophysical Research*, *104*(D21), 26565–26580. https://doi.org/10.1029/1999jd900323

Ray, E. A., Moore, F. L., Elkins, J. W., Rosenlof, K. H., Laube, J. C., Röckmann, T., et al. (2017). Quantification of the SF_6 lifetime based on mesospheric loss measured in the stratospheric polar vortex. *Journal of Geophysical Research: Atmospheres*, *122*(8), 4626–4638. https://doi.org/10.1002/2016JD026198

Ray, E. A., Moore, F. L., Rosenlof, K. H., Davis, S. M., Sweeney, C., Tans, P., et al. (2014). Improving stratospheric transport trend analysis based on SF_6 and CO_2 measurements. *Journal of Geophysical Research: Atmospheres*, *119*(24), 14110–14128. https://doi.org/10.1002/2014JD021802

Ray, E. A., Moore, F. L., Rosenlof, K. H., Plummer, D. A., Kolonjari, F., & Walker, K. A. (2016). An idealized stratospheric model useful for understanding differences between long-lived trace gas measurements and global chemistry-climate model output. *Journal of Geophysical Research: Atmospheres*, *121*(10), 5356–5367. https://doi.org/10.1002/2015JD024447

Reddmann, T., Ruhnke, R., & Kouker, W. (2001). Three-dimensional model simulations of SF_6 with mesospheric chemistry. *Journal of Geophysical Research*, *106*(D13), 14525–14537. https://doi.org/10.1029/2000JD900700

Reithmeier, C., Sausen, R., & Grewe, V. (2008). Investigating lower stratospheric model transport: Lagrangian calculations of mean age and age spectra in the GCM ECHAM4. *Climate Dynamics*, *30*(2–3), 225–238. https://doi.org/10.1007/s00382-007-0294-1

Riese, M., Oelhaf, H., Preusse, P., Blank, J., Ern, M., Friedl-Vallon, F., et al. (2014). Gimballed limb observer for radiance imaging of the atmosphere (GLORIA) scientific objectives. *Atmospheric Measurement Techniques*, *7*, 1915–1928. https://doi.org/10.5194/amt-7-1915-2014

Riese, M., Ploeger, F., Rap, A., Vogel, B., Konopka, P., Dameris, M., & Forster, P. (2012). Impact of uncertainties in atmospheric mixing on simulated UTLS composition and related radiative effects. *Journal of Geophysical Research*, *117*(D16), D16305. https://doi.org/10.1029/2012JD017751

Rind, D., Suozzo, R., Balachandran, N. K., & Prather, M. J. (1990). Climate change and the middle atmosphere. Part I: The doubled CO_2 climate. *Journal of the Atmospheric Sciences*, *47*(4), 475–494. https://doi.org/10.1175/1520-0469(1990)047<0475:ccatma>2.0.co;2

Rinsland, C. P., Brown, L. R., & Farmer, C. B. (1990). Infrared spectroscopic detection of sulfur hexafluoride (SF_6) in the lower stratosphere and upper troposphere. *Journal of Geophysical Research*, *95*(D5), 5577–5585. https://doi.org/10.1029/89JD03413

Rinsland, C. P., Mahieu, E., Zander, R., Gunson, M. R., Salawitch, R. J., Chang, A. Y., et al. (1996). Trends of OCS, HCN, SF_6, CHClF2 (HCFC-22) in the lower stratosphere from 1985 and 1994 Atmospheric Trace Molecule Spectroscopy experiment measurements near 30°N latitude. *Geophysical Research Letters*, *23*(17), 2349–2352. https://doi.org/10.1029/96gl01234

Rivoire, L., Linz, M., & Li, J. (2024). Observational limitations to the emergence of climate signals. *Geophysical Research Letters*, *51*, e2024GL109638. https://doi.org/10.1029/2024GL109638

Rosenlof, K. H. (1995). Seasonal cycle of the residual mean meridional circulation in the stratosphere. *Journal of Geophysical Research*, *100*(D3), 5173–5191. https://doi.org/10.1029/94jd03122

Saunders, L. N., Walker, K. A., Stiller, G. P., von Clarmann, T., Haenel, F., Garny, H., et al. (2024). Age of air from ACE-FTS measurements of sulfur hexafluoride [preprint]. *EGUsphere*. https://doi.org/10.5194/egusphere-2024-2117

Scheele, M. P., Siegmund, P. C., & Velthoven, P. F. J. V. (2005). Stratospheric age of air computed with trajectories based on various 3D-Var and 4D-Var data sets. *Atmospheric Chemistry and Physics*, *5*, 1–7. https://doi.org/10.5194/acp-5-1-2005

Schmidt, U., Bauer, R., Khedim, A., Klein, E., Kulessa, G., & Schiller, C. (1991). Profile observations of long-lived trace gases in the Arctic vortex. *Geophysical Research Letters*, *4*, 767–770. https://doi.org/10.1029/91GL00552

Schoeberl, M. R., Douglass, A. R., Polansky, B., Boone, C., Walker, K. A., & Bernath, P. (2005). Estimation of stratospheric age spectrum from chemical tracers. *Journal of Geophysical Research*, *110*(D21), D21303. https://doi.org/10.1029/2005JD006125

Schoeberl, M. R., Douglass, A. R., Stolarski, R. S., Pawson, S., Strahan, S. E., & Read, W. (2008). Comparison of lower stratospheric tropical mean vertical velocities. *Journal of Geophysical Research*, *113*(D24), D24109. https://doi.org/10.1029/2008JD010221

Schoeberl, M. R., Sparling, L. C., Jackman, C. H., & Fleming, E. L. (2000). A Lagrangian view of stratospheric trace gas distributions. *Journal of Geophysical Research*, *105*(D1), 1537–1552. https://doi.org/10.1029/1999JD900787

Sheese, P. E., Walker, K. A., Boone, C. D., Bernath, P. F., Froidevaux, L., Funke, B., et al. (2017). ACE-FTS ozone, water vapour, nitrous oxide, nitric acid, and carbon monoxide profile comparisons with MIPAS and MLS. *Journal of Quantitative Spectroscopy and Radiative Transfer*, *186*, 63–80. https://doi.org/10.1016/j.jqsrt.2016.06.026

Shepherd, T. G., & McLandress, C. (2011). A robust mechanism for strengthening of the Brewer–Dobson circulation in response to climate change: Critical-layer control of subtropical wave breaking. *Journal of the Atmospheric Sciences*, *68*(4), 784–797. https://doi.org/10.1175/2010jas3608.1

Shindell, D. T., Fuglestvedt, J. S., & Collins, W. J. (2017). The social cost of methane: Theory and applications. *Faraday Discussions*, *200*, 429–451. https://doi.org/10.1039/c7fd00009j

Shuckburgh, E., d'Ovidio, F., & Legras, B. (2009). Local mixing events in the upper troposphere and lower stratosphere. Part II: Seasonal and interannual variability. *Journal of the Atmospheric Sciences*, *66*(12), 3695–3706. https://doi.org/10.1175/2009JAS2983.1

Solomon, S., Daniel, J. S., Neely, R. R., Vernier, J.-P., Dutton, E. G., & Thomason, L. W. (2011). The persistently variable "background" stratospheric aerosol layer and global climate change. *Science*, *333*(6044), 866–870. https://doi.org/10.1126/science.1206027

Solomon, S., Rosenlof, K. H., Portmann, R. W., Daniel, J. S., Davis, S. M., Sanford, T. J., & Plattner, G.-K. (2010). Contributions of stratospheric water vapor to decadal changes in the rate of global warming. *Science*, *327*(5970), 1219–1223. https://doi.org/10.1126/science.1182488

Stiller, G. P., Fierli, F., Ploeger, F., Cagnazzo, C., Funke, B., Haenel, F. J., et al. (2017). Shift of subtropical transport barriers explains observed hemispheric asymmetry of decadal trends of age of air. *Atmospheric Chemistry and Physics*, *17*(18), 11177–11192. https://doi.org/10.5194/acp-17-11177-2017

Stiller, G. P., von Clarmann, T., Glatthor, N., Grabowski, U., Kellmann, S., Kiefer, M., et al. (2023). Version 8 IMK/IAA MIPAS measurements of CFC-11, CFC-12, and HCFC-22. *Atmospheric Measurement Techniques Discussions*, *2023*, 1–48. https://doi.org/10.5194/amt-2023-172

Stiller, G. P., von Clarmann, T., Haenel, F., Funke, B., Glatthor, N., Grabowski, U., et al. (2012). Observed temporal evolution of global mean age of stratospheric air for the 2002 to 2010 period. *Atmospheric Chemistry and Physics*, *12*(7), 3311–3331. https://doi.org/10.5194/acp-12-3311-2012

Stiller, G. P., von Clarmann, T., Höpfner, M., Glatthor, N., Grabowski, U., Kellmann, S., et al. (2008). Global distribution of mean age of stratospheric air from MIPAS SF_6 measurements. *Atmospheric Chemistry and Physics*, *8*(3), 677–695. https://doi.org/10.5194/acp-8-677-2008

Strahan, S. E., Schoeberl, M. R., & Steenrod, S. D. (2009). The impact of tropical recirculation on polar composition. *Atmospheric Chemistry and Physics*, *9*(7), 2471–2480. https://doi.org/10.5194/acp-9-2471-2009

Strahan, S. E., Smale, D., Douglass, A. R., Blumenstock, T., Hannigan, J. W., Hase, F., et al. (2020). Observed hemispheric asymmetry in stratospheric transport trends from 1994 to 2018. *Geophysical Research Letters*, *47*(17), e2020GL088567. https://doi.org/10.1029/2020GL088567

Sugawara, S., Ishidoya, S., Aoki, S., Morimoto, S., Nakazawa, T., Toyoda, S., et al. (2018). Age and gravitational separation of the stratospheric air over Indonesia. *Atmospheric Chemistry and Physics*, *18*(3), 1819–1833. https://doi.org/10.5194/acp-18-1819-2018

Tegtmeier, S., Hegglin, M. I., Anderson, J., Funke, B., Gille, J., Jones, A., et al. (2016). The SPARC data initiative: Comparisons of CFC-11, CFC-12, HF and SF6 climatologies from international satellite limb sounders. *Earth System Science Data*, *8*(1), 61–78. https://doi.org/10.5194/essd-8-61-2016

Thompson, C. R., Wofsy, S. C., Prather, M. J., Newman, P. A., Hanisco, T. F., Ryerson, T. B., et al. (2022). The NASA atmospheric tomography (atom) mission: Imaging the chemistry of the global atmosphere. *Bulletin America Meteorology Social*, *103*(3), E761–E790. https://doi.org/10.1175/BAMS-D-20-0315.1

Toon, G. C. (1991). The JPL MkIV interferometer. *Optics & Photonics News*, *2*(10), 19–21. https://doi.org/10.1364/opn.2.10.000019

Umezawa, T., Matsueda, H., Sawa, Y., Niwa, Y., Machida, T., & Zhou, L. (2018). Seasonal evaluation of tropospheric CO_2 over the Asia-Pacific region observed by the contrail commercial airliner measurements. *Atmospheric Chemistry and Physics*, *18*(20), 14851–14866. https://doi.org/10.5194/acp-18-14851-2018

Urban, J., Lautié, N., Flochmoën, E. L., Jiménez, C., Eriksson, P., de La Noë, J., et al. (2005). Odin/SMR limb observations of stratospheric trace gases: Level 2 processing of CClO, N_2O, HNO_3, and O_3. *Journal of Geophysical Research*, *110*(D14), D14307. https://doi.org/10.1029/2004JD005741

Vernier, J.-P., Thomason, L. W., Pommereau, J.-P., Bourassa, A., Pelon, J., Garnier, A., et al. (2011). Major influence of tropical volcanic eruptions on the stratospheric aerosol layer during the last decade. *Geophysical Research Letters*, *38*(12), 389. https://doi.org/10.1029/2011GL047563

Vogel, B., Volk, C. M., Wintel, J., Lauther, V., Müller, R., Patra, P. K., et al. (2023). Reconstructing high-resolution in-situ vertical carbon dioxide profiles in the sparsely monitored Asian monsoon region. *Communications Earth & Environment*, *4*(1), 72. https://doi.org/10.1038/s43247-023-00725-5

Volk, C. M., Elkins, J. W., Fahey, D. W., Dutton, G. S., Gilligan, J. M., Loewenstein, M., et al. (1997). Evaluation of source gas lifetimes from stratospheric observations. *Journal of Geophysical Research*, *102*(D21), 25543–25564. https://doi.org/10.1029/97JD02215

von Clarmann, T., & Grabowski, U. (2016). Direct inversion of circulation and mixing from tracer measurements—Part 1: Method. *Atmospheric Chemistry and Physics*, *16*(22), 14563–14584. https://doi.org/10.5194/acp-16-14563-2016

von Clarmann, T., & Grabowski, U. (2021). Direct inversion of circulation from tracer measurements—Part 2: Sensitivity studies and model recovery tests. *Atmospheric Chemistry and Physics*, *21*(4), 2509–2526. https://doi.org/10.5194/acp-21-2509-2021

von Clarmann, T., Grabowski, U., Stiller, G. P., Monge-Sanz, B. M., Glatthor, N., & Kellmann, S. (2021). The middle atmospheric meridional circulation for 2002-2012 derived from MIPAS observations. *Atmospheric Chemistry and Physics*, *21*(11), 8823–8843. https://doi.org/10.5194/acp-21-8823-2021

von Clarmann, T., Höpfner, M., Kellmann, S., Linden, A., Chauhan, S., Funke, B., et al. (2009). Retrieval of temperature, H_2O, O_3, HNO_3, CH_4, N_2O, $ClONO_2$ and ClO from MIPAS reduced resolution nominal mode limb emission measurements. *Atmospheric Measurement Techniques*, *2*(1), 159–175.

von Clarmann, T., Oelhaf, H., & Fischer, H. (1993). Retrieval of atmospheric O_3, HNO_3, CFC–11, and CFC–12 profiles from MIPAS–B–89 limb emission spectra. *Applied Optics*, *32*(33), 6808–6817. https://doi.org/10.1364/AO.32.006808

Wagenhäuser, T., Engel, A., Bönisch, H., Ray, E., Garny, H., & Voet, F. (2024). AtmosphericAngels/AoA from convolution: Software version as used in Garny et al. 2024 (v1.0.0) [Dataset]. *Zenodo*. https://doi.org/10.5281/zenodo.11127613

Wagenhäuser, T., Engel, A., & Sitals, R. (2021). Testing the altitude attribution and vertical resolution of aircore measurements with a new spiking method. *Atmospheric Measurement Techniques*, *14*(5), 3923–3934. https://doi.org/10.5194/amt-14-3923-2021

Wagenhäuser, T., Jesswein, M., Keber, T., Schuck, T., & Engel, A. (2023). Mean age from observations in the lowermost stratosphere: An improved method and interhemispheric differences. *Atmospheric Chemistry and Physics*, *23*(7), 3887–3903. https://doi.org/10.5194/acp-23-3887-2023

Waters, J., Froidevaux, L., Harwood, R., Jarnot, R., Pickett, H., Read, W., et al. (2006). The Earth observing system microwave limb sounder (EOS MLS) on the aura satellite. *IEEE Transactions on Geoscience and Remote Sensing*, *44*(5), 1075–1092. https://doi.org/10.1029/2007JD008824

Waugh, D. (2009). The age of stratospheric air. *Nature Geoscience*, *2*(1), 14–16. https://doi.org/10.1038/ngeo397

Waugh, D., & Hall, T. M. (2002). Age of stratospheric air: Theory, observations, and models. *Reviews of Geophysics*, *40*(4), 1010. https://doi.org/10.1029/2000RG000101

Wofsy, S. C. (2011). Pole-to-pole observations (hippo): Fine-grained, global-scale measurements of climatically important atmospheric gases and aerosols. *Philosophical Transactions of the Royal Society A*, *369*(1943), 2073–2086. https://doi.org/10.1098/rsta.2010.0313

References From the Supporting Information

Etheridge, D. M., Steele, L. P., Francey, R. J., & Langenfelds, R. L. (1998). Atmospheric methane between 1000 a.d. and present: Evidence of anthropogenic emissions and climatic variability. *Journal of Geophysical Research*, *103*(D13), 15979–15993. https://doi.org/10.1029/98JD00923

Girard, A., Besson, J., Brard, D., Laurent, J., Lemaitre, M., Lippens, C., et al. (1988). Global results of grille spectrometer experiment on board spacelab 1. *Planetary and Space Science*, *36*(3), 291–300. https://doi.org/10.1016/0032-0633(88)90136-5

Grossmann, K., Gusev, O., Kaufmann, M., Kutepov, A., & Knieling, P. (2004). A review of the scientific results from the crista missions. *Advances in Space Research*, *34*(8), 1715–1721. https://doi.org/10.1016/j.asr.2003.02.041

Gunson, M. R., Farmer, C. B., Norton, R. H., Zander, R., Rinsland, C. P., Shaw, J. H., & Gao, B. C. (1990). Measurements of CH_4, N_2O, CO, H_2O, and O_3 in the middle atmosphere by the atmospheric trace molecule spectroscopy experiment on Spacelab 3. *Journal of Geophysical Research*, *95*(D9), 13867–13882. https://doi.org/10.1029/jd095id09p13867

Homan, C. D., Volk, C. M., Kuhn, A. C., Werner, A., Baehr, J., Viciani, S., et al. (2010). Tracer measurements in the tropical tropopause layer during the AMMA/SCOUT-O3 aircraft campaign. *Atmospheric Chemistry and Physics*, *10*(8), 3615–3627. https://doi.org/10.5194/acp-10-3615-2010

Hoor, P., Gurk, C., Brunner, D., Hegglin, M. I., Wernli, H., & Fischer, H. (2004). Seasonality and extent of extratropical TST derived from in-situ co measurements during spurt. *Atmospheric Chemistry and Physics*, *4*(5), 1427–1442. https://doi.org/10.5194/acp-4-1427-2004

Keeling, C. D., Piper, S. C., Bacastow, R. B., Wahlen, M., Whorf, T. P., Heimann, M., & Meijer, H. A. (2005). *Atmospheric CO_2 and $^{13}CO_2$ exchange with the terrestrial biosphere and oceans from 1978 to 2000: Observations and carbon cycle implications* (pp. 83–113). Springer.

Khosrawi, F., Müller, R., Irie, H., Engel, A., Toon, G. C., Sen, B., et al. (2004). Validation of CFC-12 measurements from the improved limb atmospheric spectrometer (ILAS) with the version 6.0 retrieval algorithm. *Journal of Geophysical Research*, *109*(D6), D06311. https://doi.org/10.1029/2003JD004325

Kikuchi, K.-I., Nishibori, T., Ochiai, S., Ozeki, H., Irimajiri, Y., Kasai, Y., et al. (2010). Overview and early results of the superconducting submillimeter-wave limb-emission sounder (smiles). *Journal of Geophysical Research*, *115*(D23), D23306. https://doi.org/10.1029/2010JD014379

Kloss, C., Tan, V., Leen, J. B., Madsen, G. L., Gardner, A., Du, X., et al. (2021). Airborne mid-infrared cavity enhanced absorption spectrometer (AMICA). *Atmospheric Measurement Techniques*, *14*(8), 5271–5297. https://doi.org/10.5194/amt-14-5271-2021

Meinshausen, M., Vogel, E., Nauels, A., Lorbacher, N., Meinshausen, K., Etheridge, D. M., et al. (2017). Historical greenhouse gas concentrations for climate modelling (CMIP6). *Geoscientific Model Development*, *10*(5), 2057–2116. https://doi.org/10.5194/gmd-10-2057-2017

National Aeronautics and Space Administration, & Roche, A. (2006). *Cryogenic limb array etalon spectrometer (class l3): Vertical temperature profiles and atmospheric particle concentration measurements, 15 September 2023*. NCAS British Atmospheric Data Centre. Retrieved from http://catalogue.ceda.ac.uk/uuid/1ae11ab1741c29c15ab58bbaeebc9550

Natural Environment Research Council, British National Space Centre, & National Aeronautics and Space Administration. (2013). *Hirdls: Level 2 version 7.00 atmospheric chemical and temperature measurements, 18 September 2023*. NCAS British Atmospheric Data Centre. Retrieved from https://catalogue.ceda.ac.uk/uuid/c547fe67f0e49bc3861b4369b921fb21

NASA Jet Propulsion Laboratory, National Aeronautics and Space Administration, Waters, J., Harwood, R., & Pumphrey, H. (2006). *Upper atmosphere research satellite (UARS) vertical profiles of atmospheric components from the microwave limb sounder (MLS L3) instrument and NERC microwave limb sounder (MLS) prototype water vapour data, 15 September 2023*. NCAS British Atmospheric Data Centre. Retrieved from http://catalogue.ceda.ac.uk/uuid/2e4c98d91a9237c128c0acbf3e11ce7f

NASA Langley Research Center, NASA Langley DAAC, Russell, J., & Harries, J. (2006). *Halogen occultation experiment (haloe): Global stratospheric and mesospheric profiles of pressure, temperature and chemical composition, 15 September 2023*. NCAS British Atmospheric Data Centre. Retrieved from http://catalogue.ceda.ac.uk/uuid/6297603d25100cc5e977b750c1a524f7

Offermann, D., Grossmann, K.-U., Barthol, P., Knieling, P., Riese, M., & Trant, R. (1999). Cryogenic infrared spectrometers and telescopes for the atmosphere (crista) experiment and middle atmosphere variability. *Journal of Geophysical Research*, *104*(D13), 16311–16325. https://doi.org/10.1029/1998JD100047

Papineau, N., Camy-Peyret, C., & Ackerman, M. (1989). Monitoring of the middle atmosphere: Grille spectrometer experiment results on board spacelab 1 and scientific program of atlas 1 mission. In *Advanced optical instrumentation for remote sensing of the earth's surface from space*. https://doi.org/10.1117/12.961483

Rinsland, C. P., Gunson, M. R., Abrams, M. C., Lowes, L. L., Zander, R., & Mahieu, E. (1993). ATMOS/ATLAS1 measurements of sulfur hexafluoride (SF_6) in the lower stratosphere and upper troposphere. *Journal of Geophysical Research*, *98*(D11), 20491–20494. https://doi.org/10.1029/93JD02258

Schuck, T. J., Brenninkmeijer, C. A. M., Baker, A. K., Slemr, F., von Velthoven, P. F. J., & Zahn, A. (2010). Greenhouse gas relationships in the Indian summer monsoon plume measured by the caribic passenger aircraft. *Atmospheric Chemistry and Physics*, *10*(8), 3965–3984. https://doi.org/10.5194/acp-10-3965-2010

Taylor, F., & Rogers, C. (2006). *Improved stratospheric and mesospheric sounder (ISAMS) vertical profiles of temperature and atmospheric constituents*. NCAS British Atmospheric Data Centre. Retrieved from http://catalogue.ceda.ac.uk/uuid/fb0a13f4a913daee7a93c393e6a67e79

Taylor, F. W., Rodgers, C. D., Nutter, S. T., & Oslik, N. (1989). *Nimbus-7 stratospheric and mesospheric sounder (SAMS) experiment data user's guide (NASA Reference Publication No. 1221)*. Goddard Space Flight Center, National Aeronautics and Space Administration.

Yokota, T., Nakajima, H., Sugita, T., Tsubaki, H., Itou, Y., Kaji, M., et al. (2002). Improved limb atmospheric spectrometer (ILAS) data retrieval algorithm for version 5.20 gas profile products. *Journal of Geophysical Research*, *107*(D24), 8216doi. https://doi.org/10.1029/2001JD000628